First Principles and Classical Molecular Dynamics of Oil-Quartz Interfacial Phenomena in Nanogeoscience

2012

Mia Ledyastuti

First Principles and Classical Molecular Dynamics of Oil-Quartz Interfacial Phenomena in Nanogeoscience

by

Mia Ledyastuti

A dissertation submitted in partial satisfaction of

the requirements for the degree of

Doctor of Engineering

in the

GRADUATE SCHOOL OF ENGINEERING

DEPARTMENT OF CIVIL AND EARTH RESOURCES ENGINEERING

of

KYOTO UNIVERSITY

ABSTRACT

As one of the main components of rock, quartz plays an important role in (Nano-) geosciences and oil industries. The interaction between quartz-water or oil component can be understood well if the structure information of its interface is known. In addition, the quartz bulk brings the geological interest due to the thermal and mechanical anomalies. In spite of many interests of quartz, this thesis only focused on three subjects, i.e. the investigation of heptane and toluene at binary solution on quartz surface, the reconstruction of the quartz surface in aqueous environment and the investigation of temperature effect on quartz structural and mechanical properties.

The molecular dynamics techniques are used as tool in this research. The first principles and classical molecular dynamics are employed dependent on the size of system and purpose of simulations. The first principles molecular dynamics, on the basis of plane waves in association with the use of pseudopotentials and density functional theory, provides accurate description for the atomic interaction, which is coming from the electronic structure of atom builder of system represented by the Kohn-Sham orbitals. However, the high cost of this calculation has limited the size of model, which is only reasonable for small system (~200 atoms) and a few tens of picoseconds. To overcome the limitation of the size and simulation time but still keep the accuracy, the Kohn-Sham orbitals can be expanded in Gaussian-type functions and an augmented-plane-waves. The other alternative is to develop a classical (many-body) potential with *ab initio* accuracy. For larger system (~50,000 atoms), the (semi-)empirical potential is used for the description of the atomic interaction in molecular dynamics.

The understanding of quartz-oil interface could give useful information for the oil recovery. The common hydrophilic quartz surface is believed to be alternated to hydrophobic by baking at high temperature or by chemical reactions, being more heavily populated with siloxane (-Si-O-Si-) bridges. Therefore, it is, of particular, interest to examine how these two types of quartz surfaces could generate systematically different interfacial structural properties and adsorption pattern of liquid component, e.g. water, aliphatic and aromatic hydrocarbon. Toluene and heptane are of importance because they are the most commonly used solvents for both

industrial and scientific applications, and their binary mixture is often chosen to simulate the aromatic/aliphatic content of the crude oil. In this thesis, we have been able to explain a recent experimental work by using Sum Frequency Generation, where they have found the toluene molecule is vertical to the silica surface with a tilted angle around 25^{o}*[Z. Yang, et al. J. Phys. Chem. C. 113, 20355 (2009)]*. The simulation results are indeed in support of the tilted angle: 1) the layering of the liquid molecules has been reproduced well; 2) only the molecule at second sub-layer presents the tilted angle, while first sub-layer in indeed lying flat on the surface. Further, by observing the density profile of mixture case, we have found that heptane can compete well only on hydrophobic quartz surface. Meanwhile, the presence of toluene molecule in the mixture, even in the small amount, has influenced the adsorption of heptane on the hydrophilic quartz surface as reflected by the decreasing of heptane first peak density on the interface. The strength of toluene adsorption on quartz surfaces in comparison to heptane can be explained thermodynamically in view of the relative free energy value. The driving force of the stronger interaction between toluene and hydrophilic quartz surface was indicated as weak hydrogen bonding π-electron of toluene (i.e. phenyl ring) -hydrogen atom of hydrophilic quartz interface (i.e. Si-OH).

While quartz surface usually represented as idealized surface whatever perfectly hydrophilic or hydrophobic as shown above, could be used in order to study the effect of the polarity of quartz surface. In the experiment, the surface of quartz is not always ideal. Some defects such as two-membered rings, peroxy links and double bonds may be present. In order to investigate the real structure of quartz surface, we have simulated the reaction between two different fresh quartz (0001) cleavages and liquid water by using first principles molecular dynamics. The first type of cleavage is terminated by $=Si(O)_2$ and =Si for two surfaces respectively, whereas the second type cleavage has the same termination on both surfaces that consists of =Si-O. In general, the aqueous environment has generated the hydrophilic quartz surface. The final configuration of quartz cleavages was found to be mostly covered by silanol groups~62.50% and ~83.33% for first type and the second type of cleavages, respectively. The other features such as siloxane bridge, peroxy link, peroxy radical, and unsaturated site are also observed in the first-type of cleavage, and siloxane bridge and unsaturated site in the second type of cleavage. In addition, it was found that the number of siloxane bridge could be increased by changing the environment to methane-rich environment. From energetic point of view, the

second quartz cleavage is more likely to be observed than the first one. However, the defects as observed in first quartz cleavage are definitely noteworthy.

The thermal and mechanical properties of quartz are different in low and high temperature (> 573°C). At low temperature (α-quartz), the volume expands at elevated temperature, namely positive thermal expansion. Meanwhile, at high temperature (β-quartz), the negative (zero) thermal expansion was observed. In contrast to other materials which are getting soft at elevated temperature, the bulk modulus of β-quartz at ambient pressure was found increasing at elevated temperature. According to our work, these anomalies can be explained by the different response of α and β-quartz structural parameter solely. In details, it was found that the thermal expansion was tightly connected with the changes of internal angle Si-O-Si and reflected by Si-Si distance. The negative thermal expansion of β-quartz is then simply explained by the decreasing of its Si-O-Si angle and Si-Si distance. Further, we have found that the different structural response with pressure for α- and β-quartz can be responsible for the anomalous high bulk modulus of β-quartz. For α-quartz, the response to pressure by bending of Si-O-Si angle, while for β-quartz, this response is through the compression of Si-O bond length. The harder Si-O bond compared with the Si-O-Si bond angle would implicitly explain the high bulk modulus of the β-quartz. The bulk modulus increases with temperature at ambient pressure can be explained by the shift of the pressure-induced α-β transition at elevated temperature.

Contents

List of Figures

List of Tables

Dedicated to my beloved husband Sastra Budi Rozie and my dearest son Muhammad Sabima Natsuhiko Al-Sas, my lovely parents, brothers and sisters, nephews and nieces

Acknowledgements

For three and a half years, I spend my life in beautiful city Kyoto to continue my study in Kyoto University. It is like a dream that I never imagine before. I am just an ordinary woman who wants to enjoy every single step of my life. But God give me His kindness by sending me to the great university and placed me to Katsura Campus Room C-1-118. Here, I met many great teachers and students who always keep spirit to reach they dream. They inspired me to do the same thing and always say “Yes, I can!!! Ganbarimasho!!!”. Therefore, I would like to express my gratitude to the inspiring people.

First of all, I would like to acknowledge my supervisor, Professor Toshifumi Matsuoka for his guidance and support throughout my period of study. He always gives me a brighter idea when the research did not go well and push me to keep on going.

Next, I also want to say my gratitude to Assistant Professor Yunfeng Liang for great guidance and amazing patience. He always burns my spirit to keep moving forward.

My deepest appreciation goes to Mr. Makoto Kunieda -my “Computational Master of MD”, who always helps me when I have trouble with my simulation. And also for all member of MD group who share their experiences in different system of simulation.

It is my pleasure to acknowledge all the member of Environmental and Resources System Engineering Laboratory especially Mr. Reona Masui and Mr. Seung Youl Yoo who helping me in Japanese-English translation. And also for Ms. Hisa Yasuda and Ms. Kana Moriyama who accompany me in every party since only three of us the female lab member.

I also want to thank my personal supervisor Professor Caetano R. Miranda and Professor Yasuhiro Fukunaka, who always support and keep my spirit.

Finally, I want to say my gratitude to my beloved family, especially for my beloved husband, Sastra Budi Rozie who always right beside me in happy and sadness, “This is for you, dear”.

CHAPTER 1

INTRODUCTION

Silica, one of important material in the earth, is found common as sand, gravel, gemstone, glass, etc. The application of silica was found widespread in some fields such as filter, raw material of ceramic and glass, jewelry, fiber optic for electronic industry and so on. The crystalline silica exists in several forms, i.e. α- and β-quartz, α- and β-cristobalite, tridymite, keatite, coesite and stishovite [Devine et al., 2000]. Most of these structures are composed of corner-sharing tetrahedral SiO_4 units with a fourfold-coordinated silicon at the centre and two-fold-coordinated oxygen atoms at the corners which differ only in the connectivity of the basic tetrahedral units.

As the main component of rock, silica cannot be separated from the oil exploration and production. Nowadays, enhanced oil recovery (EOR) is an indispensible tool for the energy security, since the oil reserves are limited [Lake, 1989]. As the oil coexists with the rock and clay minerals, the structure of liquid-rock interface should be better understood in order to determine fit condition of oil production. Sandstone reservoir minerals can be represented mainly by crystalline quartz with a small amount of clay minerals. The quartz and its poly(a)morphous, therefore, serve as a model system for those of the reservoirs. Since oil is the mixture of hydrocarbons, the competitive adsorption among its component most likely occurs.

Recently, Yang et al. (2009) reported the competitive adsorption of toluene and heptane at binary solution-silica interfaces by using sum frequency generation spectroscopy (SFG). Toluene and heptane are of particular importance because they are the most commonly used solvents for both industrial and scientific applications, and their binary mixture is often chosen to simulate the aromatic/aliphatic content of the crude oil [Yeung et al., 1998]. It was shown there that the SFG spectroscopy is quite sensitive probe, at a molecular level, to detect the toluene specie and its orientation. However, a quantitative interpretation of the reported spectra is not straightforward as the SFG is a coherent process. For example, it is not clear how the oscillation nature of liquid molecules in the vicinity of a solid surface [Horn and Israelachvili, 1981; Klein

and Kumacheva, 1998], interferes with the measured SFG spectra and how the orientation of molecules is accurately estimated [Zhuang et al., 1999; Yang et al., 2009]. Although it is well recognized that there is oscillation of both the density and the orientation of liquid molecules nearby the liquid-solid interface, it has not been considered in the analysis of the SFG spectra so far. To this end, molecular dynamics simulation will compensate the SFG experiment and help to entangle the observed spectra with a reliable molecular picture.

By employing a perfect hydrophilic or hydrophobic quartz surface, it is possible to gain insight on the effects of polarity of the quartz surface. But in the experiment the surface of quartz is not always ideal, some defects such as two-membered rings, peroxy links and double bonds may present. The reconstruction of quartz surface has been pursued in most of theoretical works. The formation of Si-O-Si bridges, two-membered rings, and three-membered rings are some features in the relaxation of fresh quartz surface [de Leeuw et al., 1999; Ceresoli et al., 2000; Murashov, 2005; Goumans et al., 2007; Adeagbo et al., 2008]. The relaxed fresh quartz surface was saturated into silanol groups by adding water molecule one by one with undercoordinated surface sites as initial structure. This method has not dealt with the full solid-liquid interaction, but rather individual water molecules with quartz surface.

The simulation of chemical reaction between fresh quartz surface and water should be, preferably, investigated by the first-principles approach. The first principles molecular dynamics simulation allows the bond breaking and formation, which is required in the chemical reaction. The disadvantage of first principles molecular dynamics (MD) is high cost or time consuming compared to the classical MD. Due to this reason, the investigation of full solid-liquid interface system by first-principles approach is in limited number. Very recently, Adeagbo et al. have investigated the transport processes at quartz-water interface which directly offers insight of the reliable structure of quartz surface under aqueous environment [Adeagbo et al., 2008]. The final structure resulted in 83% silanol coverage. However, only one trial quartz cleaved surface was employed in their study.

The fascination of quartz is not only coming from surface phase. The bulk phase of quartz also still keeps some long standing questions. In 1889, Le Chatelier observed the α-β quartz transition when studying the thermal expansion of quartz. He found that the two phases of quartz have different response to the change of temperature [Dolino, 1990]. The low temperature

phase, α-quartz with space group $P3_221$ or $P3_121$ (Fig. 1.1(a)), has a normal behavior material which expands at elevated temperature. Whereas the high temperature phase, β-quartz ($P6_222$ or $P6_422$) (Fig. 1.1(b)), shows contraction at elevated temperature. These two kinds of response have been indicated as the cause factor of cracking in quartz ceramics.

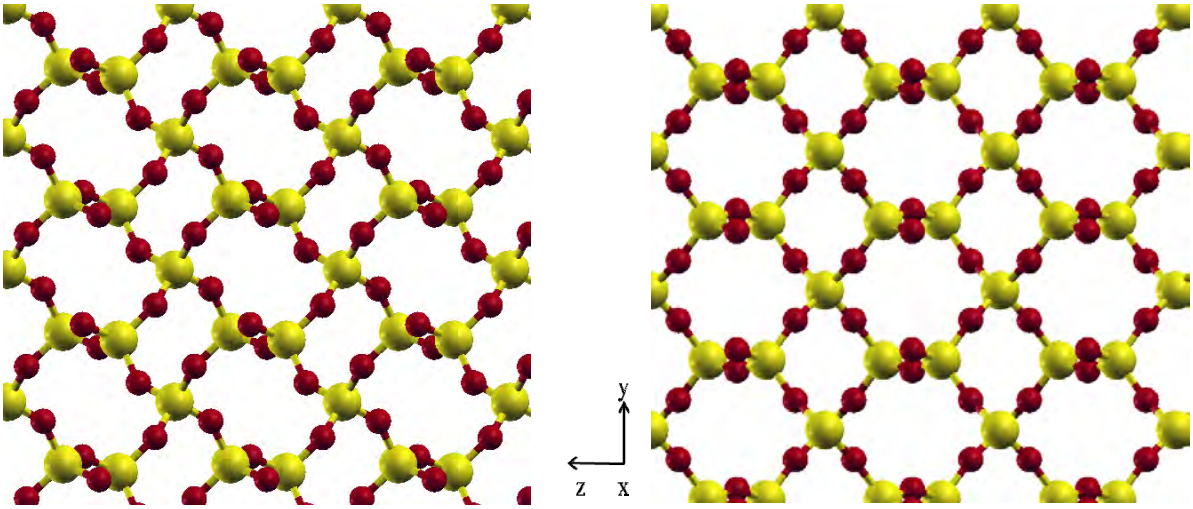

(a) (b)

Fig. 1.1 The structure of α-quartz (a) and β-quartz (b). The yellow and red balls represent silicon (Si) and oxygen (O), respectively.

The mechanical properties of β-quartz remain of interest to researchers due to its peculiar behavior. Usually, the bulk modulus of material decreases with temperature. As we know at ambient pressure, the low and high temperature phases are α-quartz and β-quartz, respectively. Consider to this statement, β-quartz should be less stiff than α-quartz, but in reality β-quartz has higher bulk modulus than the α-quartz [Kammer and Atanasoff, 1942; Ohno et al., 2006; Lakhstanov et al., 2007]. Moreover, the bulk modulus of β-quartz continues to increase with temperature up to at least 1520℃ [Lakhstanov et al., 2007]. This anomaly can in fact generate a measurable seismic signature [Mechie et al., 2004; Marini and Manzella, 2005] and therefore offers the possibility for precisely estimating temperature and pressure of the middle continental crust from the known phase diagram of quartz. However, the mechanism of such bulk modulus anomaly is still unclear. As the bulk modulus is defined by the pressure increase needed to cause a relative decrease in volume, it is interesting to jointly consider the bulk modulus anomalies and

the volume as function of temperature and pressure (namely, the zero or negative thermal expansion).

Molecular dynamics method is the computer simulation based on the motion of atom which can be used to determine the macroscopic thermodynamic properties of a system. The basic idea of first principles (*ab initio*) molecular dynamics is to compute the forces acting on the nuclei from electronic structure calculations that are performed "on-the-fly" as the molecular dynamics trajectory is generated [Grotendorst, 2000]. The first principles molecular dynamics is not tied to any particular approach. The strength and weakness of particular first principles molecular dynamics depends on the strength and weakness of the chosen electronic structure determination method. In classical simulation the object are most often described by point like centers which interact through pair-or multibody interaction potentials. In that way the highly complex description of electron dynamics is abandoned and an effective picture is adopted where the main features like the hard core of particle, electric multipoles or internal degrees of freedom of a molecules are modeled by a set of parameters and analytical functions which depend on the mutual position of particles in the configuration.

The accuracy of first principles molecular dynamics is higher than the classical. However, the first principles only reasonable for small system (~200 atoms) and short simulation time (~ps) on basis of plane waves and around 500 atoms on basis of Gaussian augmented plane waves. Whereas for larger system (~50,000 atoms) and long simulation time (~ns), the classical molecular dynamics is the suitable approach. The other molecular dynamics by using potential which is first principles parametrized can increase the size of system (~1000 atoms) and simulation time (~ns) with similar accuracy of first principles molecular dynamics. Therefore, different molecular dynamics approach will be chosen according to the size of system and the purpose of simulation.

This dissertation consists of six chapters. The highlight of each chapter is described as follows.

Chapter 1 introduces the brief description of quartz in (Nano-)geosciences and oil industry. The explicit problems of quartz are also included. In this chapter, we also describe the general

molecular dynamics approach which will be used as research methodology in this dissertation. Last, the structure of dissertation is shown.

Chapter 2 reviews some approaches of molecular dynamics. In this dissertation we will use the molecular dynamics approach which corresponds to the size and the purpose of simulation. The accurate first principles molecular dynamics will be used in the investigation of thermal and mechanical properties of quartz for low temperature. The GAPW basis set will be used in the case of mechanism of quartz surface and water reaction. The 'semi' first principles molecular dynamics, which employs the parameterized potential, will be performed to investigate the thermal and mechanical properties of quartz in wide range of temperature and pressure. Last, the classical molecular dynamics will be used in larger system for the studies on the interaction of quartz surface with liquid heptane and toluene.

Chapter 3 presents the molecular dynamics of binary mixture heptane-toluene on top of hydrophilic and hydrophobic quartz surfaces. The binary mixture heptane-toluene in various compositions was placed on top of two different quartz surfaces. Our main purpose is to investigate the competitive adsorption of crude oil component with different polarity on quartz surfaces. In this thesis, we have been able to explain a recent experimental work by using Sum Frequency Generation, where they have found the toluene molecule is vertical to the silica surface with a tilted angle around 25^{o}. The simulation results are indeed in support of the tilted angle: 1) the layering of the liquid molecules has been reproduced well; 2) only the molecule at second sub-layer presents the tilted angle, while first sub-layer in indeed lying flat on the surface.

Chapter 4 investigates the reaction mechanism of quartz surface and water. The ambiguities of quartz surface structure necessitate us to perform the first principles molecular dynamics of fresh quartz surface in aqueous and non-aqueous environment. This study was particularly motivated by the limited information of the formation silanol group or other structure that might feature the quartz surface. Some snapshots of simulation will be presented to describe the mechanism and study the final configuration. Our main findings are that (1) the reaction pathways for silanols and the types of silanols (triple, germinal and single) were identified from the trajectories; (2) the unsaturated SiO and siloxane were found coexisting with various silanol groups which is in consistent with the recent X-Ray photoelectron spectroscopy experiments; (3) the formation mechanism of peroxy defects were revealed. In addition, we have also analyzed the detailed ring

statistics for the silica slab with the new formed Si-O-Si bridge and found that the newly formed rings at surface are from 4- to 7- member ring for both surfaces, and therefore 2- and 3-member rings are ruled out at least within the total time of our calculation for the two different fresh silica cleavages (in aqueous environment) employed in this study.

Chapter 5 describes the effect of temperature on structure of quartz. It is well-known that quartz presents the anomalous thermal and mechanical properties at high temperature. We will perform the molecular dynamics by using α-quartz as initial structure. The simulation will be done in the wide range of temperature (0-1650K) and pressure (-10 to 10 GPa). Then, the trajectory of simulation will be analyzed from the structural parameter to see the response of heating process. It was found that the negative thermal expansion (NTE) of β-quartz is tightly connected with the changes of internal angle Si-O-Si and reflected by Si-Si distance.

Chapter 6 summarizes all chapters in this dissertation and suggests the future research based on our finding.

References

Adeagbo, W. A., Doltsinis, N. L., Klevakina, K. and Renner, J. Transport processes at α-quartz-water interfaces: Insights from first-principles molecular dynamics simulations. Chem. Phys. Chem. **9**, 994-1002 (2008).

Ceresoli, D., Bernasconi, M., Iarlori, S., Parrinello, M., and Tosatti, E. Two-membered silicon rings on the dehydroxylated surface of silica. Phys. Rev. Lett. **84**, 3887-3890 (2000).

De Leeuw, N. H., Higgins, F. M. and Parker, S. C. Modeling the surface structure and stability of α-quartz. J. Phys. Chem. B **103**, 1270-1277 (1999).

Devine, R. A. B., Duraud, J. P. and Dooryhée, E. Structure and Imperfections in Amorphous and Crystalline Silicon Dioxide. John Willey, Chicester (2000).

Dolino, G. The α-inc-β transitions of quartz, a century of research on the displacive phase transitions. Phase Transitions. **21**, 59-72 (1990).

Goumans, T. P. M. Wander, A., Brown, W. A. and Catlow, C. R. A. Structure and stability of the (001) α-quartz surface. Phys. Chem. Chem. Phys.**9**, 2146-2152 (2007).

Horn, R. G. and Israelachvili, J. N. Direct measurement of structural forces between two surfaces in a nonpolar liquid.J. Chem. Phys.**75**, 1400-1412 (1981).

Kammer, E. W. and Atanasoff, J. V.A determination of the elastic constants of beta-quartz.J. Appl. Phys. **19**, 265-270 (1942).

Klein, J. and Kumacheva, E. Simple liquids confined to molecularly thin layers. I. confinement-induced liquid-to-solid phase transitions. J. Chem. Phys.**108**, 6996-7010 (1998). Detailed solvation force as a function of gap distance for toluene was not reported in this paper. However, it was reported that the sharp liquid-to-solid phase transition on increasing confinement between films of the thickness corresponds four layers for toluene and six or seven layers for cyclohexane.

Lake, L. W. Enhanced Oil Recovery. Prentice Hall, New Jersey (1989).

Lakhstanov, D. L., Sinoigeikin, S. V. and Bass, J. D. High-temperature phase transitions and elasticity of silica polymorphs.Phys. Chem. Minerals **34**, 11-22 (2007).

Marini, L. and Manzella, A. Possible seismic signature of the α-β quartz transition in the lithosphere of Southern Tuscany (Italy). J. Vol. Geo. Res. **148**, 81-97 (2005).

Mechie, J. Sobolev, S. V., Ratschbacher, L., Babeyko, A. Y., Bock, G., Jones, A. G., Nelson, K. D., Solon, K. D., Brown, L. D., and Zhao, W. Precise temperature estimationin the Tibetan crust from seismic detection of the α-β transition. Geology **32**, 601-604 (2004).

Murashov, V. V. Reconstruction of pristine and hydrolyzed quartz surface.J. Phys. Chem. B **109**, 4144-4151 (2005).

Ohno, I., Harada, K. and Yoshitomi, C. Temperature variation of elastic constants of quartz acrossthe α-β transition.Phys. Chem. Minerals **33**, 1-9 (2006).

Yang, Z., Li, Q., Hua, R., Gray, M. R. and Chou, K. C. Competitive adsorption of toluene and *n*-alkanes at binary solution/silica interfaces. J. Phys. Chem. C**113**, 20355 (2009).

Yeung, A., Dabros, T. and Maliyah, J. Does equilibrium interfacial tension depend on method of measurement? J. Colloid & Interface Sci. **208**, 241-247 (1998).

Zhuang, X., Miranda, P. B., Kim, D. and Shen, Y. R. Mapping molecular orientation and conformation at interfaces by surface nonlinear optics. Phys. Rev. B **59**, 12632 (1999).

CHAPTER 2

Molecular Dynamics Simulation

In this chapter, we will review the molecular dynamics simulation technique which is the interaction potential models as the central part ranging from first principles approach to additive non-polarizable potential. We also describe the computational approaches in this research.

2.1 First Principles Approach

The basic idea of first principles (*ab initio*) molecular dynamics is to compute the forces acting on the nuclei from electronic structure calculations that are performed "on-the-fly" as the molecular dynamics trajectory is generated [Grotendorst, 2000]. The first principles molecular dynamics is not tied to any particular approach. The strength and weakness of particular first principles molecular dynamics depends on the strength and weakness of the chosen electronic structure determination method. In this research we use the density functional function (DFT) method to obtain the electronic structure, which is well established to perform the electronic structure calculations. DFT defines the ground state properties, particularly the total energy *E*, of a system of interacting particles could be related to the density distribution [Hohenberg and Kohn, 1964]. In order to solve the self-consistent Kohn-Sham equation numerically, we have to choose the basis set to represent the orbitals in terms of simple analytic functions with well-known properties.

2.1.1 Gaussian Basis Set

The Slater or Gaussian basis functions are in general centered at the positions of the nuclei, which leads to the linear combination of atomic orbitals (LCAO) to solve differential equations algebraically [Grotendorst, 2000]. Furthermore, their derivatives as well as the resulting matrix elements are efficiently obtained by differentiation and integration in real-space.

The disadvantage of this basis set is the Pulay forces may appear if the fixed atoms are allowed to move, either in geometry optimization or molecular dynamics schemes.

2.1.2 Plane Wave

Plane wave (PW) also can be used as the basis set of DFT. PWs are atomic position independent, totally unbiased and do not lead to basis set superposition errors. However, PW is not the natural language of chemistry. The interpretation of results is not straightforward and need to be projected into a localized basis set in order to extract the relevant chemistry [Lippert et al., 1997]. Furthermore, a large number of PWs is needed to reproduce the rapid variations of the wavefunctions close to the nuclei. The empty space is also represented by the same way of atom-filled region. This makes PW based algorithm very demanding in terms of memory.

2.1.3 Gaussian Augmented Plane Wave

As mentioned above, Gaussian and PW have their own advantages and disadvantages. In order to keep the advantages of Gaussian and PW, the Gaussian augmented plane wave (GAPW) combine both basis sets [Krack and Parrinello, 2000; VandeVondele et al., 2005]. PW is used as the auxiliary basis set in which to represent the full charge density. This will simplify the calculation of the Hartree and exchange correlation potentials. This also reduces the number of Gaussians needed to represent the wavefunctions and has a beneficial effect on the basis set superposition error. The resulting algorithm is accurate and efficient and holds a great promise for large scale computations and *ab* initio molecular dynamics.

The principle of GAPW is described as follows. The electronic energy functional for a molecular or crystalline system in the framework of the GAPW method was define as

$$E^{e1}[n] = E^{T}[n] + E^{V}[n] + E^{H}[n + n^{Z}] + E^{XC}[n] \tag{2.17}$$

where $E^{T}[n]$ is the kinetic energy, $E^{V}[n]$ is the electronic interaction with the ionic cores, $E^{H}[n]$ is the electronic Hartree (Coulomb) energy and $E^{XC}[n]$ is the exchange-correlation energy, n^{Z} is the charge density of the ionic cores. The GAPW method is applied two representations of the electron density. The first representations is based on an expansion in atom centred, contracted Gaussian functions

$$n(r) = \sum_{\mu v} P^{\mu v} \varphi_{\mu}(r) \varphi_{v}(r) \tag{2.18}$$

where $P^{\mu v}$ is a density matrix element, and $\varphi_\mu(r) = \sum_i d_{i\mu}\, g_i(r)$ with primitive Gaussian functions $g_i(r)$ and corresponding contraction coefficient $d_{i\mu}$. The second representation employs an auxiliary basis of plane waves given by,

$$\tilde{n}(r) = \frac{1}{\Omega}\sum_G \tilde{n}(G) exp(iG.r) \tag{2.19}$$

The $E^V[n]$ is described by norm conserving pseudopotentials with a potential split in a local part and a fully non-local part. Pseudopotential is needed to minimize the size of PW and to represent the long order interactions of the core. Pseudopotential is also required to produce pseudo-wavefunction solution that approaches the full wavefunction outside the core radius. Inside this radius the pseudopotential and the wavefunction should be as smooth as possible, in order to allow for a small plane wave cut off.

2.2 Classical Approach

In classical simulation the object are most often described by point like centers which interact through pair-or multibody interaction potentials. In that way the highly complex description of electron dynamics is abandoned and an effective picture is adopted where the main features like the hard core of particle, electric multipoles or internal degrees of freedom of a molecules are modeled by a set of parameters and analytical functions which depend on the mutual position of particles in the configuration. Since the parameters and functions give complete information of the system's energy as well as the force acting on each particle through$\mathrm{F} = -\nabla U$, the combination of parameters and functions is also called a force field (potential).

The potential can be classified to pair and multibody potential. In systems with no constraints, the interaction is most often described by pair potentials, which is simple to implement into a program. In the case where multibody potentials come into play, the counting of interaction partners become increasingly more complex and dramatically slows down the execution of the program. Only for the case where interaction partners are known in advance, e.g. in the case of torsional or bending motions of a molecule the interaction can be calculated efficiently by using neighbor lists or by an intelligent way of indexing the molecule site.

The potential also can be differentiated by the sort and long range interactions. The sort range interactions offer the possibility to take into account only neighbored particles up to a certain distance for the calculation of interactions. In that way a cutoff radius is introduced beyond of which mutual interactions between particles are neglected. Two common forms of short range interaction are the Buckingham potential and Lennard-Jones potential. In the case of long range potentials, e.g. Coulomb potential, interactions between all particles in the system must be taken into account, if treated without any approximation. This leads to an $\mathcal{O}(N^2)$ problem, which increases considerably the execution time of a program for larger systems. In the case of periodic boundary conditions are applied, not only the interactions with particles in the central cell but also with all periodic images must be taken into account and formally a lattice sum has to be evaluated.

Some existing potentials do not account for electronic polarization of the environment. They described the electronic static interactions in terms of fixed charge. However, in real system the charge could change depends on the environment of the substance, especially when placed in water or other high-dielectric medium. This polarization will strongly affect the geometry and energetic of molecules. Therefore, the polarizable potential was developed to solve the polarization effect.

2.2.1 Polarizable Potential

The specific polarizable potential for silica was developed by Tangney and Scandolo (2002). The Tangney-Scandolo (TS) potential was parametrized by fitting to first principles calculations. This potential is using three approaches to construct more realistic potentials [Tangney and Scandolo, 2002].

(i) The flexible form of potential which incorporates the effects of dipole polarization of the oxygen ions including the effective dipoles induced by the short range forces between ions was used.
(ii) Since the force field is to be designed for use in bulk silica, the *ab initio* calculation from which the force field is parametrized are performed on a relatively large unit cell under periodic boundary conditions to minimize the finite size and surface effects which may be present in cluster calculations.

(iii) The potential was applied for silica at low pressures and so fit to *ab initio* calculations at low pressures.

The TS potential treat carefully the electrostatic effect (polarizability and compressibility/distorability of the oxygen ions) which are the most important factor for structure determining. The potential of Morse-Stretch form was used to describe the pairwise interactions between ions.

$$U_{ij} = \frac{q_i q_j}{r_{ij}} + D_{ij}\left[e^{\gamma_{ij}\left[1-\left(r_{ij}/r_{ij}^0\right)\right]} - 2e^{(\gamma_{ij}/2)\left[1-\left(r_{ij}/r_{ij}^0\right)\right]}\right] \quad (2.1)$$

where the interaction between an atom of type i and an atom of type j is defined by the parameter q_i, q_j, D_{ij}, γ_{ij}, r_{ij}^0 and the distance between them r_{ij}. This form was proven to be more transferable between phases. In addition, the effects of dipole polarization of the oxygen ions were included to this pair potential, represented by α. The short-range contribution to the dipole moments is given by

$$\mathbf{p}_i^{\mathrm{SR}} = \alpha \sum_{j\neq i} \frac{q_j \mathbf{r}_{ij}}{r_{ij}^3} f_{ij}\left(r_{ij}\right) \quad (2.2)$$

where $f_{ij}\left(r_{ij}\right) = c\sum_{k=0}^{4} \frac{\left(br_{ij}\right)^k}{k!} e^{-br_{ij}}$ (2.3)

and$\mathbf{r}_{ij} = \mathbf{r}_i - \mathbf{r}_j$ and b and c are parameters of the model.

The parametrization begins with molecular dynamics simulation of liquid silica using BKS potential [van Beest et al., 1990]. Then, the trajectory of molecular dynamics is generated for the system of interest. From this trajectory a number of atomic configurations (10-15) are chosen which are well separated from one another in time such that correlation between configurations is minimized. *Ab initio* calculations of total energies, forces, and stress are performed on these configurations. From these calculations, the potential is parametrized by minimizing the function

$$\Gamma(\{\eta_i\}) = w_f \Delta F + w_s \Delta S + w_e \Delta E \quad (2.4)$$

where

$$\Delta F = \frac{\sqrt{\sum_{k=1}^{n_c}\sum_{I=1}^{N}\sum_{\alpha}\left|F_{c1,I}^{\alpha}(\{\eta_i\})F_{ai,I}^{\alpha}\right|^2}}{\sqrt{\sum_{k=1}^{\eta_c}\sum_{I=1}^{N}\sum_{\alpha}\left(F_{ai,I}^{\alpha}\right)^2}}, \tag{2.5}$$

$$\Delta \mathrm{S} = \frac{\sqrt{\sum_{k=1}^{n_c}\sum_{\alpha,\beta}\left|S_{c1}^{\alpha\beta}(\{\eta_i\})-S_{ai}^{\alpha\beta}\right|^2}}{3B\sqrt{n_c}}, \tag{2.6}$$

$$\Delta \mathrm{E} = \frac{\sqrt{\sum_{k,l}^{n_c}\left(\left(U_k^{c1}-U_l^{c1}\right)-\left(U_k^{ai}-U_l^{ai}\right)\right)^2}}{\sqrt{\sum_{k,l}^{\eta_c}\left(U_k^{ai}-U_l^{ai}\right)^2}}. \tag{2.7}$$

Here $F_{c1,I}^{\alpha}$ is the αth component of the force on atom I as calculated with the classical potential, $F_{ai,I}^{\alpha}$ is the force component as calculated *ab initio*, $S_{c1}^{\alpha\beta}$ is the stress tensor component as calculated with the classical potential and $S_{ai}^{\alpha\beta}$ is the stress tensor component as calculated *ab initio*, B is the bulk modulus, (U_k^{c1} and U_k^{ai} are the potential energy of configuration k as calculated classically and *ab initio*, respectively, n_c are the number of atomic configurations for which *ab initio* calculations have been performed. Once a parameter set has been found, a new set of configurations are extracted. *Ab initio* calculations are performed on these configurations and a new parameter set obtained from these calculations. This process is repeated until the difference in the values of $\Gamma(\{\eta_i\})$ from successive minimization converges to a small enough value. The force field parameter is presented in Table 2.1.

Table 2.1 Force field parameter (atomic units) [Tangney and Scandolo, 2002]

q_O	q_{Si}	α	b	c
-1.382 57	2.765 14	8.893 78	2.029 89	-1.504 35
D_{O-O}		D_{Si-O}		D_{Si-Si}
2.4748x10^{-4}		1.9033x10^{-3}		-2.084 60x10^{-3}
γ_{O-O}		γ_{Si-O}		γ_{Si-Si}
12.070 92		11.152 30		10.455 17
r_{O-O}^0		r_{Si-O}^0		r_{Si-Si}^0
7.170 05		4.637 10		5.750 38

This interatomic force field has already been used in various studies and shown a very good agreement with first principles calculations as well as experiments. The experimental crystal parameters and densities of quartz, cristobalite and coesite are reproduced well. This accuracy is important to learn the structural respond of crystal at elevated temperature. In addition, the temperature dependence of the volume per unit cell at the α-β transition, TS potential showed the best agreement with the experiment compared to other potential such as TTAM [Tsuneyuki et al., 1990] and BKS [van Beest et al., 1990]. This potential also matches the *c/a* ratio of α-β transition which is not shown by other potential [Herzbach et al., 2005]. Thus, we will adopt the advantages of TS potential to model the α-quartz in our simulation.

2.2.2 Non-Polarizable Potential

The polarizable potential is more accurate than non-polarizable potential. However, the molecular dynamics using polarizable potential will take longer time. The time will increase when applied on larger system (~50,000 atoms). In this case the non-polarizable potential will be more preferable. According to our system which needs the larger system, the CLAYFF and CHARMM27 are the most suitable potentials to describe the interface system of silica (quartz) and hydrocarbon (heptane-toluene).

The Potential for Mineral Systems

CLAYFF is a general force field which suitable for the simulation of hydrated and multicomponent mineral systems and their interfaces with fluid phases [Cygan, et al., 2004]. CLAYFF is based on an ionic (nonbonded) description of the metal-oxygen interactions associated with hydrated phases. All atoms are represented as point charges and are allowed complete translational freedom within this force field framework.

The total energy in a molecular mechanics simulation is determined by the evaluation of the appropriate energy term for every atom-atom interaction in the system such as Columbic (electrostatic) interactions, the short-range interactions (van der Waals), and the bonded interactions. Generally, formulation of total energy is given by

$$E_{total} = E_{Coul} + E_{VDW} + E_{bond\ stretch} + E_{angle\ bend} \tag{2.8}$$

The Columbic energy is inversely proportional to the distance of separation r_{ij}, as represented in eq. 2.9.

$$E_{Coul} = \frac{e^2}{4\pi\epsilon_0}\sum_{i\neq j}\frac{q_i q_j}{r_{ij}} \tag{2.9}$$

The partial charges q_i and q_j are derived from quantum mechanics calculations, e is the charge of the electron, and ϵ_0 is the dielectric permittivity of vacuum (8.85419x10^{-12} F/m). The van der Waals energy is represented by the conventional Lennard-Jones (12-6) function includes the short range repulsion associated with the increase in energy as two atoms approach each other and the attractive dispersion energy, as represented in eq. 2.10.

$$E_{VDW} = \sum_{i\neq j} D_{0,ij}\left[\left(\frac{R_{0.ij}}{r_{ij}}\right)^{12} - 2\left(\frac{R_{0,ij}}{r_{ij}}\right)^{6}\right] \tag{2.10}$$

$D_{0,ij}$ and $R_{0.ij}$ are empirical parameters derived from the fitting of the model to observed structural and physical property data. The large number of experimental structures for simple oxides, hydroxides, and oxyhydroxides is used to derive the optimal values for these parameters. The interaction parameters between the unlike atoms are calculated according to the arithmetic mean rule for the distance parameter, R_0, and the geometric mean rule for the energy parameter, D_0:

$$R_{0,ij} = \frac{1}{2}\left(R_{0,i} + R_{0,j}\right) \tag{2.11}$$

$$D_{0,ij} = \sqrt{D_{0,i}D_{0,j}} \tag{2.12}$$

The parameterization procedure involves the evaluation of the total energy for each of the observed structures used in the fitting process based on some initial guess for the unknown metal-oxygen Lennard-Jones parameter. Phases containing hydroxyl groups require the evaluation of the stretch energy associated with each of the O-H bonds. The bond stretch energy of the hydroxyl bond, like the O-H bond in SPC water, is described by a simple harmonic term:

$$E_{bond\ stretch\ ij} = k_1\left(r_{ij} - r_0\right)^2 \tag{2.13}$$

where k_1 is a force constant and r_0 represents the equilibrium bond length, both values taken from the flexible version of the SPC water model [Teleman et al., 1987]. The bonded hydrogen associated with the hydroxyl group, like the hydrogen of SPC water, does not require any nonbonded Lennard-Jones component; only Columbic interactions involving hydrogen charges are required. Intramolecular nonbonded interactions between oxygen and hydrogen in hydroxyl groups and water molecules are excluded due to the incorporation of the bonded term.

An additional enhancement of CLAYFF that was incorporated to better describe metal sorption on hydrated surfaces, and to improve the vibrational (librational) behavior of hydroxyl groups, is the inclusion of an angle bend (three-body) term for describing hydroxyl groups. The energy of the angle bend term can be described by a simple harmonic relationship:

$$E_{angle\ bend\ ijk} = k_2\left(\theta_{ijk} - \theta_0\right)^2 \tag{2.14}$$

where k_2 is a force constant, θ_{ijk} is the bond angle for the metal-oxygen-hydrogen, and θ_0 represents the equilibrium bond angle. This equation is equivalent to the flexible bond angle component associated with the modified SPC water model. The nonbond and bond parameters for the CLAYFF force field for silica surface are represented in Table 2.2 and 2.3.

Table 2.2 Non-bond parameter for the CLAYFF of silica surface [Cygan et al., 2004]

Species	Symbol	Charge (e)	D_0 (kcal/mol)	R_0 (Å)
Tetrahedral silicon	St	2.1000	1.8405×10^{-6}	3.7064
Bridging oxygen	Ob	-1.0500	0.1554	3.5532

Table 2.3 Bond parameter for the CLAYFF of hydrophilic silica surface [Cygan et al., 2004]

Bond Stretch			k_1 (kcal/mol Å^2)	r_0 (Å)
Species i	Species j			
o*	h*		554.1349	1.0000
Angle Bend			k_2 (kcal/mol rad^2)	θ_0 (Å)
Species i	Species j	Species k		
h*	o*	h*	45.7696	109.47

The CLAYFF was used to investigate the quartz $(10\bar{1}0)$/water interface [Skelton et al., 2011]. The result has a good agreement with experiment in describe the interfacial water structure more accurately. The hydrogen bond of hydroxyl silica (silanol) and water was observed. The CLAYFF also has shown the weak hydrogen bonding at the oil-water interface which implied to the self accumulation of aromatics compound [Kunieda et al., 2010].

The Potential for Oil Molecules

CHARMM27 is the improved CHARMM force field by refining the torsional potential of alkanes based on the *ab initio* calculation [Klauda et al., 2005]. The energy function of CHARMM force field includes internal (bonding) terms for bond stretching, angle bending, Urey-Bradley 1, 3 interaction, torsional rotation, and out-of-plane (improper) motion while the external (nonbonded) interactions are presented by a Lennard-Jones 6-12 term for the van der Waals repulsion and dispersion interaction and a Coulomb term for the charge-charge interactions; in the latter both partial and full charges are included [Mackerrel et al., 1995]. The form of energy function is given by

$$U(\vec{R}) = \sum_{bonds} K_b(b-b_0)^2 + \sum_{angle} K_\theta(\theta-\theta_0)^2 + \sum_{UB} K_{UB}(S-S_0)^2 + \sum_{dihedrals} K_\chi\big(1 + cos(n\chi-\delta)\big) + \sum_{impropers} K_{imp}(\varphi-\varphi_0)^2 + \sum_{nonbond} \epsilon\left[\left(\frac{R_{min,ij}}{r_{ij}}\right)^{12} - 2\left(\frac{R_{min,ij}}{r_{ij}}\right)^{6}\right] + \frac{q_i q_j}{4\pi e r_{ij}} \quad (2.15)$$

where K_b, K_θ, K_{UB}, K_χ, and K_{imp} are the bond, bond angle, Urey-Bradley, dihedral angle, and improper dihedral angle force constants, respectively; b, θ, S, χ, and φ are the bond length, bond angle, Urey-Bradley 1,3 distance, dihedral torsion angle, and improper dihedral angle, respectively, with the subscript zero representing the equilibrium values for the individual terms. Coulomb and Lennard-Jones 6-12 terms contribute to the external or nonbonded interactions.

The refinement force field begins with the *ab initio* calculations to obtain the conformational energy. The following functional form for the dihedral terms of the CHARMM27 force field was used in potential fitting to *ab initio* conformational energies.

$$V_{dihedral} = \sum_{\forall\ dihedrals} \sum_{j=1}^{no.of\ sets} K_{\chi,j}\big[1 + cos\big(n_j\chi - \delta_j\big)\big] \quad (2.16)$$

where $K_{\chi,j}$, n_j, and δ_j are fitted parameters with 2-4 sets, j, per dihedral type and summed over all the dihedral angles in the molecule. Conformational energies of alkanes with empirical forces were obtained in an identical manner compared to *ab initio* calculation, i.e. the dihedral angle of interest was restrained and the other degrees of freedom were minimized in CHARMM. Simulations of neat alkanes and a DPPC lipid bilayer were run to verify the modified force field parameter, and the results have good agreement with experimental data [Klauda et al., 2005].

2.3 The Computational Approaches in This Work

In this thesis, we have used the non-polarizable potential for the oil-quartz interface (Chapter 3), which is too large to be addressed by first principles molecular dynamics. In Chapter 4, we have used the first principle molecular dynamics, on the basis of the Gaussian Augmented plane wave method, in the study of the quartz surface chemistry in aqueous and non-aqueous environment, as the interface system is relative large ~ 500 atoms. The many body polarizable potential with *ab initio* accuracy, as it was fitted to first principles molecular dynamics, has been employed in the study of the effect of the temperature on quartz structure and the mechanical properties in Chapter 5. The classical potential with *ab initio* accuracy has enabled us to employ many pressure and temperature points, which, otherwise, will not be possible in this research. In addition, the first principles molecular dynamics, on basis of the plane waves, was employed to verify the accuracy for two selected points. This special design of the work has given us confidence that simulation results of that thesis are predictive.

References

Cygan, R. T., Liang, J. J. and Kalinichev, A.G. Molecular models of hydroxide, oxyhydroxide, and clay phases and the development of a general force field. J. Phys. Chem. B **108**, 1255(2004).

Grotendorst, J. Modern Methods and Algorithms of Quantum Chemistry, NIC series, vol. 1, pp. 301-449 (2000).

Grotendorst, J., Marx, D. and Muramatsu, A. Quantum Simulations of Complex Many-Body Systems: from Theory to Algorithms, Lecture Notes, NIC Series, vol. 10, pp. 211-254 (2002).

Herzbach, D., Binder, K. and Müser, M. H. Comparison of model potentials for molecular-dynamics simulations of silica. J. Chem. Phys. **123**. 124711 (2005).

Hohenberg, P. and Kohn, W. Inhomogeneous electron gas. Phys. Rev. **136**, B864-B871 (1964).

Klauda, J. B., Brooks, B. R., Mackerrel Jr., A. D., Venable, R. M. and Pastor, R. W. An *ab initio* study on the torsional surface of alkanes and its effect on the molecular simulations of alkanes and a DPPC bilayer. J. Phys. Chem. B **109**, 5300(2005).

Krack, M. and Parrinello, M. All-electron *ab initio* molecular dynamics.Phys. Chem. Chem. Phys. **2**, 2105-2112 (2000).

Kunieda, M., Nakaoka, K., Liang, Y., Miranda, C. R., Ueda, A., Takahashi, S., Okabe, H. and Matsuoka, T. Self-accumulation of aromatics at the oil-water interface through weak hydrogen bonding. J. Am. Chem. Soc. **132**, 18281-18286 (2010).

Lippert, G., Hutter, J. and Parrinello, M., A hybrid Gaussian and plane wave density functional scheme. Mol. Phys. **92**, 477-487 (1997).

MacKerrel, Jr., A. D., Wiórkiewicz-Kuczera, J. and Karplus, M. An all atom empirical energy function for the simulation of nucleic acids. J. Am. Chem. Soc. **117**, 11946-11975 (1995).

Skelton, A. A., Wesolowski, D. J. and Cummings, P. T. Investigating the quartz (10-10)/water interface using classical and *ab initio* molecular dynamics. Langmuir **27**, 8700-8709 (2011).

Tangney, P. & Scandolo, S. An *ab initio* parametrized interatomic force field for silica. J. Chem. Phys. **117**. 8898-8904 (2002).

Teleman, O., Jönsson, B. and Engström, S. A molecular dynamics simulation of a water model with intra molecular degrees of freedom. Mol. Phys. **60**, 193-203 (1987).

Tsuneyuki, S., Aoki, H., Tsukada, M. and Matsui, Y. Molecular-dynamics study of the α to β structural transition of quartz. Phys. Rev. Lett. **64**. 776-779 (1990).

Van Beest, B. W. H., Kramer, G. J. and Van Santen, R. A. Force field for silicas and aluminophosphate based on ab initio calculations. Phys. Rev. Lett. **64**. 1955-1958 (1990).

VandeVondele, J., Krack, M., Mohamed, F., Parrinello, M., Chassaing, T. and Hutter, J. QUICKSTEP: Fast and accurate density functional calculations using mixed Gaussian and plane waves approach. Comp. Phys. Comm. **167**, 103-128 (2005).

CHAPTER 3

The Quartz-Heptane/Toluene Interfacial Structure

In this chapter, we discuss the interfacial structure of toluene and heptane at binary solution-quartz. By analyzing the trajectories of classical molecular dynamics, we able to explain a recent experimental work by using Sum Frequency Generation, where they have found the toluene molecule is vertical to the quartz surface with a tilted angle around 25° [Yang et al., 2009]. The simulation results are indeed in support of the tilted angle: 1) the layering of the liquid molecules has been reproduced well; 2) only the molecule at second sub-layer presents the tilted angle, while first sub-layer in indeed lying flat on the surface.

3.1 Introduction

As the main component of rock, silica cannot be overlooked from the oil exploration and production. Nowadays, enhanced oil recovery (EOR) is an indispensable tool for the energy security, since the oil reserves are limited [Lake, 1989]. As the oil coexists with the rock and clay minerals, the structure of liquid-rock interface should be better understood in order to optimize the oil production from natural reservoir. Sandstone reservoir minerals can be represented mainly by crystalline quartz with a small amount of clay minerals. Therefore, quartz and it various surface, serve as a zeroth model for rocks at sandstone reservoirs.

Like the other inorganic oxides and its poly(a)morphous, quartz owes its inherent hydrophilicity to surface hydroxyl groups (Si-OH), which can be removed by baking at high temperature or by chemical reactions, being more heavily populated by siloxane (–Si-O-Si-) bridges [Liu and Shen, 2008; Lamb and Furlong, 1982; Zhuravlev, 2000]. The HNO_3/H_2SO_4 solution was employed in the pretreatment for different experiment including spectrum measurement [Yang et al., 2009] and some other wettability measurements etc. It is not clear, however, how such chemical treatments could potentially affect the silica surface, i.e. the ratio between surface hydroxyl groups and the siloxane bridges and how much these different surfaces

will eventually affect the adsorption and the orientation of the adsorbed molecules as reflected by measurements. Therefore, it is of particular interest to examine, at first, how two types of quartz surfaces (one is extremely hydrophilic, and another is extremely hydrophobic) could reproduce systematically different interfacial structural properties and adsorption pattern of liquid component, e.g. water, aliphatic and aromatic hydrocarbon.

Toluene and heptane are of particular importance because they are the most commonly used solvents for both industrial and scientific applications, and their binary mixture is often chosen to simulate the aromatic/aliphatic content of the crude oil [Yeung et al., 1998]. The competitive adsorption of toluene and heptane at binary solution — silica interfaces has been studied by using SFG spectroscopy, where they reported the surface coverage over a complete mole fraction from 0 to 1 [Yang et al., 2009]. Once again, it was shown there that the SFG spectroscopy is quite sensitive probe on a molecular level to detect the toluene specie and its orientation. However, a quantitative interpretation of the reported spectra is not straightforward as the SFG is a coherent process. For example, it is not clear how the oscillation nature of liquid molecules in the vicinity of a solid surface, interferes with the measured SFG spectra, how the molecular vibrational spectrum mode corresponds to the structure [Ostroverkhov et al., 2004] and how the orientation of molecules is accurately estimated [Zhuang et al., 1999; Yang et al., 2009]. Although it is well recognized that there is oscillation of both the density and the orientation of liquid molecules nearby the liquid-solid interface, it has not been considered in the analysis of the SFG spectra so far. To this end, molecular dynamics simulation will compensate the SFG experiment and help to entangle the observed spectra with a reliable molecular picture.

The theoretical investigation, by using either molecular dynamics or Monte Carlo calculations, has developed rapidly and offered us a molecular-level understanding of packing structures, adsorption and other details of liquid-solid, liquid-liquid and liquid-vapor interfaces, that cannot easily be achieved through experiment solely. The pioneering simulation work, by using Lennard-Jones potential, has clearly demonstrated how the attractive interactions between the solid wall and the fluid atoms significantly influence the interfacial fluid density profile to present an oscillatory feature [Abraham, 1978; Rao et al., 1979]. The simple Lennard-Jones potential has also been employed very recently in grand-canonical molecular dynamics simulations to calculate the solvation force and show the oscillation [Gao et al.,1997a; Camara

and Bresme, 2004], which is pertinent to the surface force apparatus measurement [Horn and Israelachvili, 1981; Christenson, 1983 and 1985; Christenson and Horn, 1983; Christenson et al., 1987; Gee et al., 1990; Klein and Kumacheva, 1998]. With a help of the full atom potential, it is possible to study the detailed structure of the interface. A recent molecular dynamics study has shown that even CCl_4 molecules, close to a spherical shape with high symmetry, form a fascinating structure with alternating layered mixture of face and corner contacts of the CCl_4tetrahedra at a CCl_4-water interface [Hore et al., 2007]. The explicit full atomic models of different hydrocarbon molecules have been investigated by using molecular simulations and shown some unique behavior of liquid behavior in contact with solid surface, such as metal [Gaoet al., 1997b and 1997c; Wang and Fichthorn, 1997; Kalyanasundaram et al., 2009] or mineral surface [Jin et al., 2000; Docherty and Cummings, 2010; Matsubara et al., 2011].

Molecular dynamics simulations have been carried out on several linear alkane systems of different chain lengths, confined between alumina to investigate the structural properties of the liquid film [Jin et al., 2000]. It has been shown, in their studies, that the width of oscillation density by means of the maxima to maxima distance is equal to the width of liquid molecule, which is in excellent agreement with the surface force apparatus measurements reported earlier [Christenson et al., 1987]. Comparison studies between straight-chain alkane and branched has also been performed in details to investigate how the shape and size of molecules could affect the oscillation behavior [Gao et al., 1997b and 1997c; Wang and Fitchtorn, 1997]. On one hand, the branch of alkane will affect the oscillation pattern, like in the case of squalane (2,6,10,1519,23-hexamethyl-tetracosane) which has different feature compared to hexadecane density profile, by the irregularity that derive from it [Gao et al., 1997b and 1997c]. On the other hand, the single branch of methyl would not have sufficient effect to the irregularity of alkane, which not alternates the properties of the straight chain alkane of its isomer that found on decane isomers [Wang and Fichthorn, 1997]. The competitive adsorption has been studied for n-hexadecane and n-hexane on gold surface [Xia and Landman, 1993] and heptane-toluene at oil-water interface [Kunieda et al., 2010]. However, no attempts have been pursued toward an understanding of the competitive adsorption of toluene and heptane at binary solution/silica interfaces as revealed by the recent SFG spectroscopy [Yang et al., 2009].

The goal of this study is three fold. First, we study how the heptane and toluene behaves differently at liquid-solid (quartz) interface at molecular scale in terms of their oscillations and the orientations. Second, we present how the orientation oscillation will be reflected by the SFG spectroscopy. Third, we determine the competitive adsorption heptane/toluene on top of hydrophilic/hydrophobic quartz surface. In next Section, we present the model of quartz surface used in this work and briefly discuss the details of molecular dynamics simulations. In Section 3.3, we report the simulation results on the density profile (3.3.1), detailed orientation profile (3.3.2) and the competitive adsorption (3.3.3). A conclusion is given Section 3.4.

3.2 Computational Detail

3.2.1 Quartz surface

Each silica polymorph has specific surface structure, for example, the fully hydroxylated α-quartz (001) interface contains vicinal silanol which has zigzag hydrogen bonded network with short and long hydrogen bonds [Murashov, 2005; Yang and Wang, 2006; Goumans et al., 2007]. The hydrophilic quartz in this study was modeled by cleaving the bulk crystal of α-quartz (space group $P3_121$) along <001> direction. The fresh quartz surface, which is terminated by O atoms, was saturated by adding H atoms manually to create the hydrophilic interface. We performed the first principles calculation using the plane-wave DFT based Vienna ab initio simulation package (VASP) [Kresse and Furtmuller, 1996] step by step similar to what has been described by the previous simulations [Yang and Wang, 2006] to optimize the hydrophilic quartz surface. Our final hydrophilic surface structure has good agreement with the previous as shown in Fig. 3.1. For hydrophobic quartz surface, we used the reconstructed structure which was reported by Rignanese et al [Rignanese et al., 2000], which has three-membered and six-membered rings after the reconstruction of newly cleaved surface with siloxane bridge. The surface area (x,y) of hydrophilic and hydrophobic quartz surface are 5.9172 x 6.8400 nm^2 and 5.8920 x 6.8032 nm^2, respectively, with both thickness of quartz slab (z) is about ~2 nm.

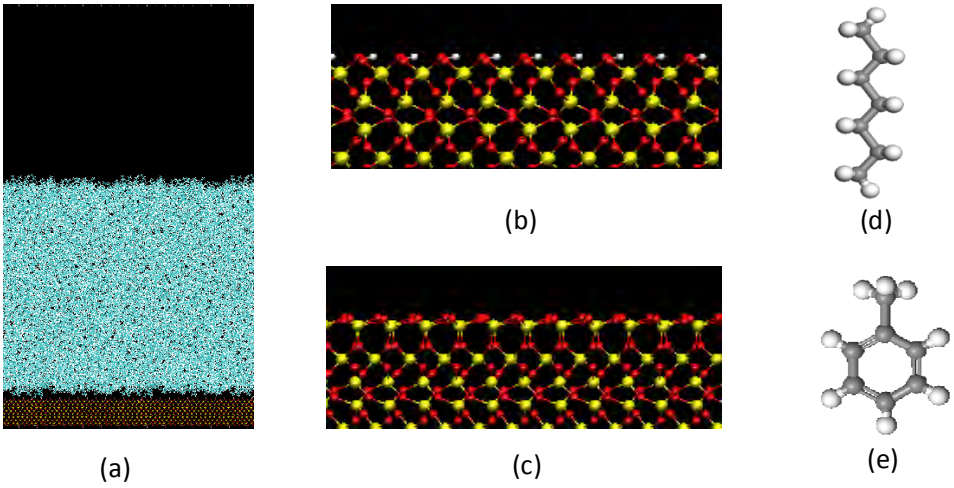

Fig. 3.1 The snapshot of heptane/toluene-quartz interface system (a): the liquid (in blue) is placed on top of quartz slab, which is either hydrophilic quartz surface (b), or hydrophobic quartz surface (c). Red: oxygen, yellow: silicon, white: hydrogen. The snapshot was repeated twice along the horizontal direction. The molecule structure of heptane and toluene are shown in (d) and (e), respectively. Note: the hydrophilic quartz surface structure is terminated with geminal $Si(OH)_2$ and the hydrophobic quartz surface is terminated with the siloxane Si-O-Si bridge.

3.2.2 Details of Molecular Dynamics

The GROMACS package was used to perform the molecular dynamics of binary liquid heptane-toluene mixture on top of quartz surface [Hess et al., 2008]. Hydrocarbon compound (heptane and toluene) was modeled by CHARMM27 force field [Klauda et al., 2005]. The CLAYFF was chosen for both hydrophilic and hydrophobic silica slabs [Cygan et al., 2004, Skelton et al., 2011]. The pure liquid heptane and toluene were generated by compressing the vapor phase at constant temperature 298K and pressure 1 bar for 3.0 ns. After the liquid formed, the mixture of heptane and toluene were composed in three variations of mole fraction (1:3, 1:1 and 3:1). The equilibrated density of mixture has a good agreement with experiment [Bromiley and Quiggle, 1933]. All liquid contains same number of molecules (2064 molecules) which were placed on hydrophilic and hydrophobic silica surface, respectively. The interface system consists of three phases i.e. solid (quartz slab), liquid (heptane and toluene) and vapor (or vacuum) with the vertical size (z) of box same for all calculations (25 nm). The simulation was performed at constant temperature 300K by using Nose-Hoover thermostat [Nose, 1984] for 3.0 ns and 4.0 ns in case of pure and mixture liquid, respectively. The structural properties of the interface system

were analyzed by using the last 2.0 ns and every 1.0 ps of trajectory. The snapshot was prepared by Visual Molecular Dynamics (VMD) software [Humphrey et al., 1996].

3.2.3 Order Parameter

For the orientation preference of the heptane and toluene near the interface, we calculated the order parameter [van Buuren et al., 1993],

$$S(z) = \frac{3}{2} < cos^2\theta(z) > -\frac{1}{2} \tag{3.1}$$

where θ is the angle between the molecular axis and the interface normal (z axis) and <···> implies the averaging over time and molecules. *z* is the *z*-component of the Cartesian coordinate of the center of the mass for any given molecule and the vapor side of quartz slab (i.e. the bottom in Fig. 3.1(a)) is chosen as origin. S(z) ranges from -1/2 to 1, where -1/2 indicates perfectly perpendicular between two axes and 1 indicates parallel. It is zero if there is no preferred orientation. The molecular axis of heptane is defined as the vector from the head carbon site C_1 to the tail carbon site C_7, where the head and tail are chosen randomly. The molecular axis of toluene is defined by two different methods: (i) the vector from the *para*-carbon of the phenyl ring to the carbon of the methyl group; (ii) the normal direction of the phenyl ring plane. Only by combination with two different vectors, it is possible to explicitly describe the orientation of toluene on top of quartz surface.

3.2.4 Everett isotherm

We adopted the Everett isotherm [Everett, 1964] to describe the adsorption on quartz surface from the binary mixture with component 1 (toluene) and component 2 (heptane), as it had been employed in the experimental study [Yang et al., 2009]. According to Everett, the surface mole fraction of component 1 can be written as

$$x_1^S = \frac{K_1 x_1^B}{1+(K_1-1)x_1^B} \tag{3.2}$$

with K_1 is determined by the adsorption free energy difference between two components

$$K_1 = exp\left\{-\frac{(\mu_1^{oS}-\mu_1^{oB})-(\mu_2^{oS}-\mu_2^{oB})}{RT}\right\} = exp\left\{-\frac{\Delta\mu_1^o-\Delta\mu_2^o}{RT}\right\} \tag{3.3}$$

x_1^S and x_2^S are the surface mole fractions for component 1 (toluene) and component 2 (heptane), respectively. x_1^B and x_2^B are the bulk mole fractions for components 1 and 2, respectively. μ_1^{oS} and μ_2^{oS} are the chemical potential for component 1 and 2 at surface, respectively. μ_1^{oB} and μ_2^{oB} are the chemical potential for component 1 and 2 for bulk in its standard state, respectively. $\Delta\mu_1^o$ and $\Delta\mu_2^o$ are the chemical potential change associated with the adsorption of components 1 and 2, respectively. R is the gas constant. T is the temperature. Since the amplitude of SFG peaks measures the surface number density n^S, instead of the surface mole fraction x_1^S, a modified Everett isotherm equation was used by Yang (2009) on the basis of the surface coverage.

$$\theta_c = \frac{n_1^S}{n_{max,1}^S} = \frac{\beta K_1 x_1^B}{1+(\beta K_1 - 1)x_1^B} \tag{3.4}$$

with $\beta = \frac{n_{max,2}^S}{n_{max,1}^S}$ (3.5)

where β describes the relative footprint on the quartz surface for component 1 (toluene) and component 2 (heptane), which can be easily measured from molecular dynamics simulations by integrating the first adsorption peaks of toluene and heptane, respectively. Therefore, the same equation was employed in our simulation study.

3.2.5 Angular dependent radial distribution

Similar to our previous study on benzene-water interface and benzene aqueous solutions [Kunieda et al, 2010], we calculated the angular dependent radial distribution function of Si-OH from hydrophilic quartz surface and the center of phenyl ring of toluene as follows:

$$g_{AB}(r,\Theta) = \frac{\langle \rho_B(r,\Theta) \rangle}{\langle \rho_B \rangle_{local,\Theta}} = \frac{1}{\langle \rho_B \rangle_{local,\Theta}} \frac{1}{N_A} \sum_{i \in A}^{N_A} \sum_{j \in B}^{N_B} \frac{\delta(r_{ij} - r)\delta(\Theta_{ij} - \Theta)}{2\pi r^2 \sin\Theta} \tag{3.6}$$

where $\langle \rho_B(r,\Theta) \rangle$ is the particle density of atom ***B*** at a distance r and angle Θ around atom ***A***. $\delta(\cdots)$ is the delta function. The distribution function described here have been shown very successfully to describe the interplay between hydrogen site of water and the center of the benzene ring via a "weak hydrogen bonding" [Kunieda et al., 2010]. Therefore it is interesting to

verify whether a “weak hydrogen bonding” is formed between the Si-OH and phenyl ring of toluene.

3.3 Results and Discussions

3.3.1 Density Profile

Segmental density profiles for pure heptane, toluene and their binary mixture on top of hydrophilic and hydrophobic quartz surfaces are shown in Fig. 3.2. The oscillation pattern was observed ~2 nm from the origin of z in all composition. The highest intensity presents in the nearest liquid-solid interface, then followed by several peak with lower intensity until the bulk phase. The first peak in the density profile implies a strong anisotropic interaction between liquid molecules and quartz slab. This strong peak can be employed to investigate the liquid adsorption into solid surface (as will be discussed in Section 3.3.3).

The similar trend also occurred on the center of mass density profiles (Fig. 3.3). There are some different features between segmental and center of mass density profiles. We observed the appearance of shoulder and shifted maximum-minimum in the center of mass density profiles. The center of mass density profile is based on molecule position in the system, which includes the orientation of molecules. Meanwhile, the segmental density profile is based on atom position in the system.

The oscillation feature in the liquid-solid interface also can be found in some experiments such as X-ray scattering [Doerr et al., 1998; Yu et al., 2000] and surface force measurement [Horn and Israelachvili, 1981; Christenson, 1983 and 1985; Christenson and Horn, 1983; Christenson et al., 1987; Gee et al., 1990; Klein and Kumacheva, 1998]. Moving away from the solid surface, the solvation force oscillation will show a damped feature up to 2-10 molecular layers, dependent on the shape, the size and the internal rigidity of the molecules, the water activity and the temperatures [Horn and Israelachvili, 1981; Christenson, 1983 and 1985; Christenson and Horn, 1983; Christenson et al., 1987; Gee et al., 1990; Klein and Kumacheva, 1998]. Heptane and toluene have different pattern of oscillation because their geometry is different. Heptane has shown four peaks similar to the oscillation pattern of *n*-octane between hydroxylated α-Al_2O_3 (0001) surfaces at 300K [Jin et al., 2000]. On the other hand, toluene

shows less number of peaks which is two clear peaks in the density profile. Our simulation has good agreement with shear force experiment which the linear molecule like heptane and octane usually shows more oscillation than the planar molecule, e.g aromatic and cyclic molecule [Christenson et al., 1987; Klein and Kumacheva, 1998].

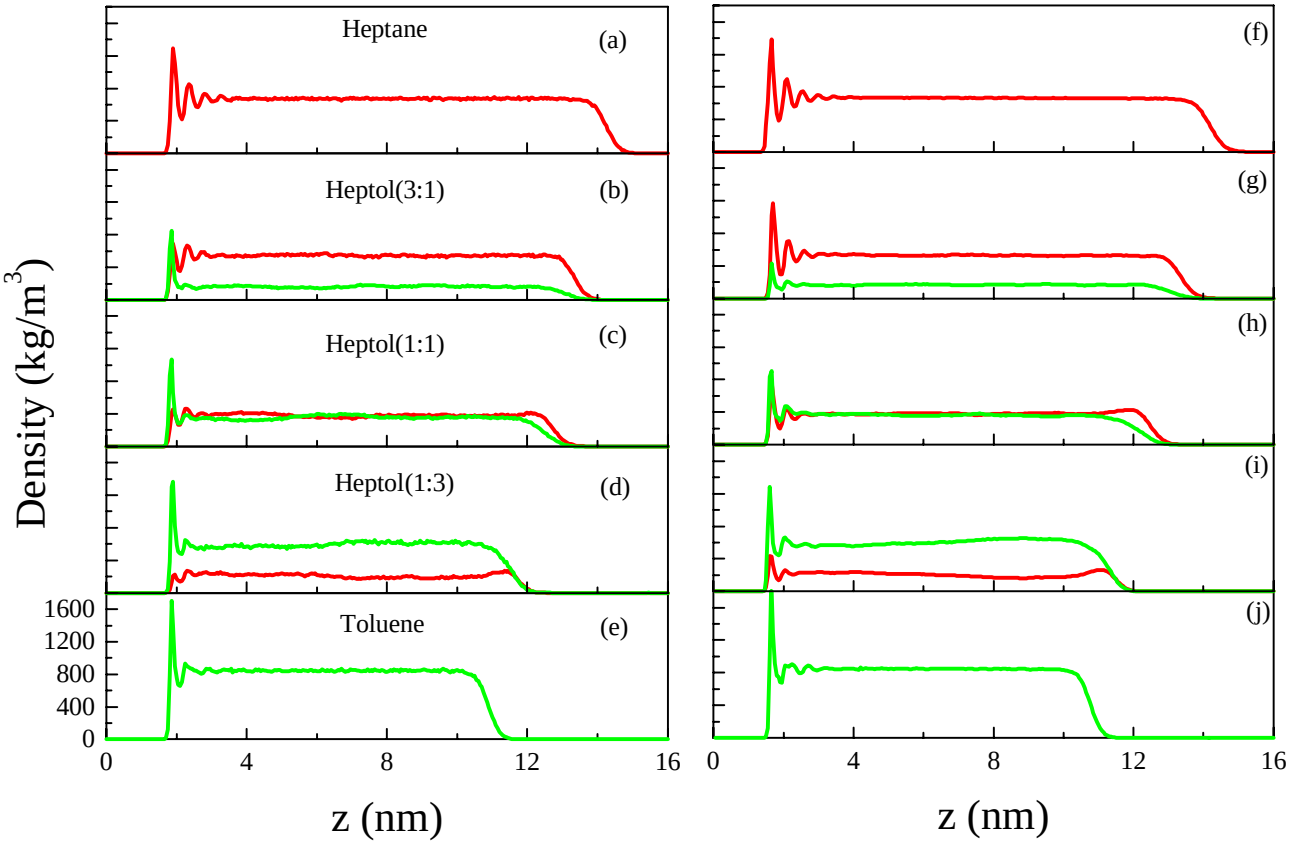

Fig. 3.2 The segmental density profiles along the normal direction of the interface (z) of heptane (in red), toluene (in green) and their mixture on top of hydrophilic (a-e) and hydrophobic surface (f-j). Heptol refers to heptane-toluene mixture. Note: pure heptane (a) and (f) has more oscillation than pure toluene (e) and (j).

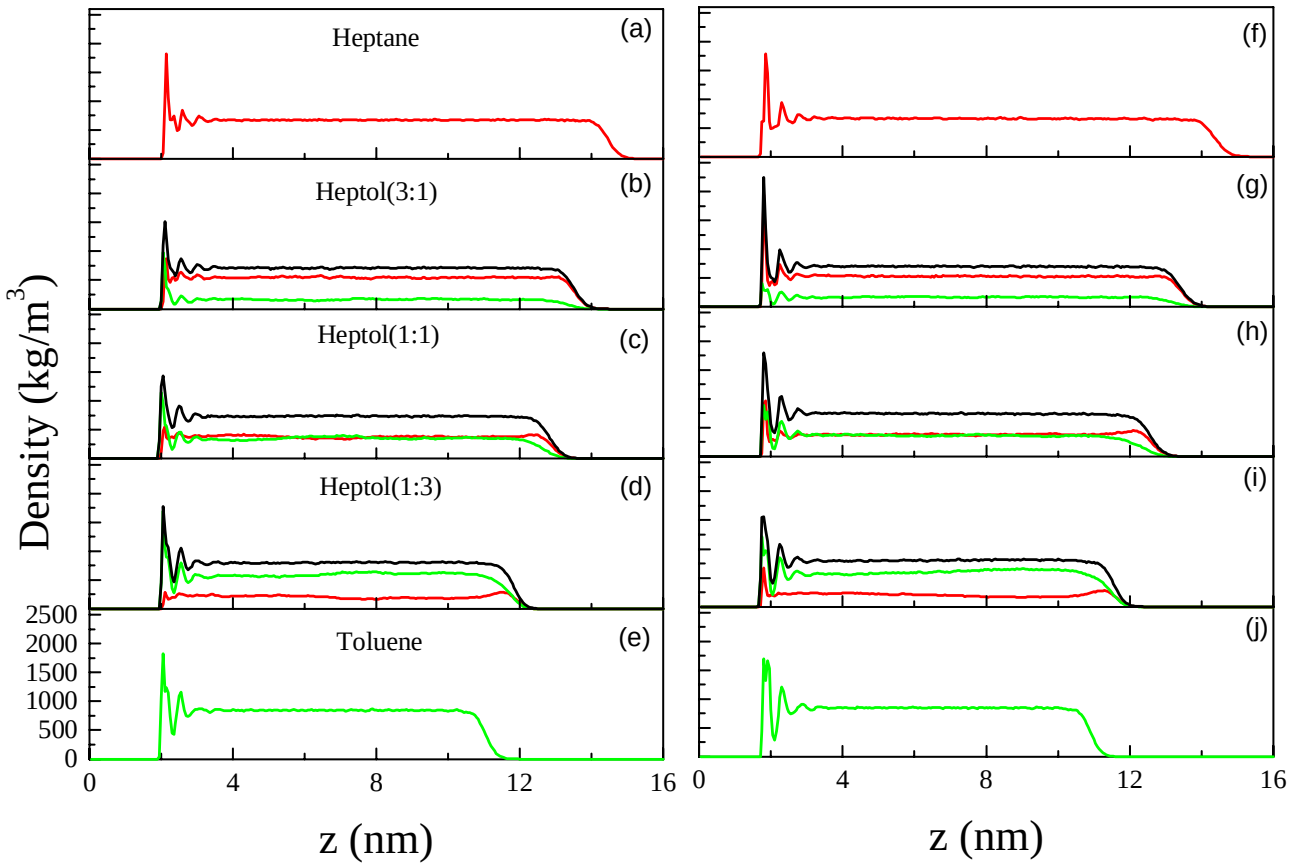

Fig. 3.3 The center of mass density profiles along the normal direction of the interface (z) of heptane (in red), toluene (in green) and their mixture on top of hydrophilic (a-e) and hydrophobic surface (f-j). Heptol refers to heptane-toluene mixture. Note: pure heptane (a) and (f) has more oscillation than pure toluene (e) and (j).

In the case of mixture, we assumed toluene act as the “impurity” of heptane. On the hydrophilic quartz surface, we have observed that the oscillation pattern of heptane was varied and the first peak was decreased significantly, even in the small amount of toluene. At the higher concentration of toluene, the first peak of heptane could not be observed. This means that toluene is more adsorbed than heptane on the hydrophilic quartz surface. A detectable difference was observed on the hydrophobic quartz surface. As shown in Fig. 3.2(i), the first peak of heptane can still be observed in the mixture case, though the intensity decreases with the increasing of toluene concentration. The different response of heptane upon the addition of toluene on

hydrophilic and hydrophobic quartz surfaces results from the different polarity of two different quartz surfaces. The polarity of quartz surface is increased by the density of silanol group. The surface with high polarity would be more attractive for the polar adsorbate like aromatic or other polar compound. A similar behavior was observed in the system of benzene on top of silica surface with various polarities. The higher density of silanol groups (7-8 OH per nm^2) was found to attract more benzene molecules in the interface than the lower density (2 OH per nm^2), as reported in a recent Monte Carlo simulation [Coasne et al., 2009].

3.3.2 Orientation

The strong interaction of solid and liquid in the interface has influenced the packing of liquid molecules with certain orientation with respect to the solid surface. The liquid molecules which usually have random orientation in the bulk become well-ordered in the interface. Moving away from the solid surface, the interaction getting weaker and slowly disappear at bulk liquid. The orientation of molecules near the surface has implemented in the order parameter (See 3.2.3 for the definition). The normal direction of the surface (*z*) towards to the liquid phase has been chosen as the surface axis, meanwhile the axis of heptane and toluene are along the chain from head to tail carbon and from *para*-carbon to the methyl group, respectively. Therefore, if heptane or toluene has orientation parallel to surface, the *S* value will equal to -1/2. As shown in Fig. 3.4, both heptane and toluene molecules nearly lie parallel to hydrophilic and hydrophobic quartz surface at the first layer (the first minimum in Fig. 3.4). The fact that the heptane nearly lies on top of quartz surface, is similar to other linear chain alkanes [Wang and Fichthorn, 1997] also in excellent agreement with the SFG measurement [Yang et al., 2009]. In case of toluene, however, another possibility of axis is the normal of phenyl ring which may be parallel to the quartz surface, namely, the phenyl plane is vertical to the quartz surface. Thus, we have defined another vector by using the normal of phenyl ring, where “up” and “down” are randomly chosen and the reference direction is still normal direction of the quartz surface. We have found the *S* of first layer is almost around 1. This indicates that the phenyl ring does indeed lie on top of quartz surface. This finding is apparently in contrast to the recent SFG measurement, where the toluene of the first contact layer adopts an upright geometry with a tilted angle ~25^o.

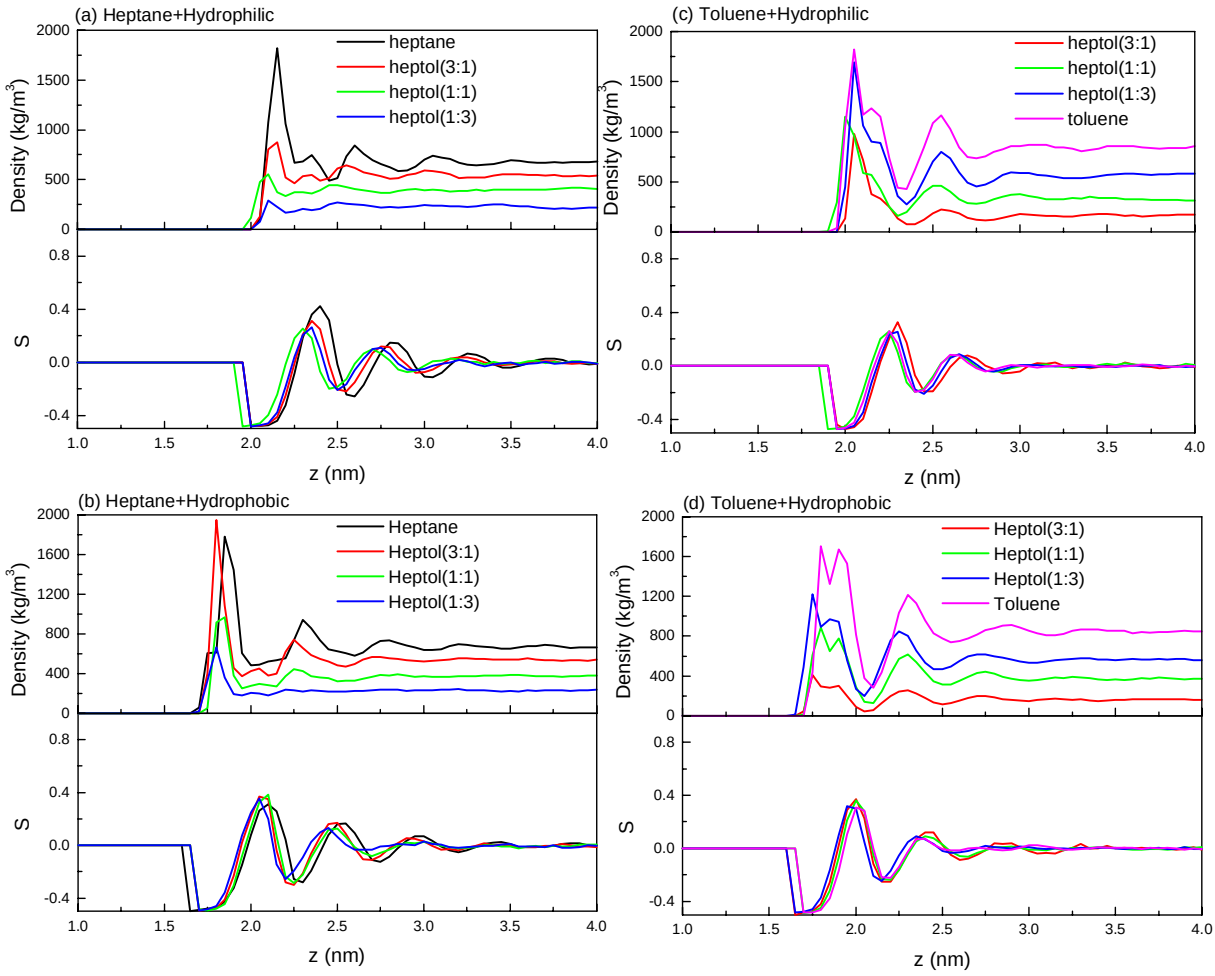

Fig. 3.4 The preferred orientation of heptane and toluene on hydrophilic (a) and (b) and hydrophobic quartz surface (c) and (d) as reflected by the order parameter defined in Eq. (3.1), the center-of-mass density profile correspond to the orientation of molecules.

Toluene as the derivative of benzene has different behavior in first layer of toluene-quartz interface. In the case of benzene, the orientation is influenced by the polarity of quartz surface. The benzene molecules have perpendicular orientation to the surface in the first layer of fully hydroxylated (larger density) [Coasne et al., 2009]. But the partially hydroxylated (smaller density) provides two kinds of orientation, perpendicular and nonperpendicular. We have obtained the similar results in case of the benzene – quartz interface and found the portion of

benzene, which is first-contact and perpendicular to the quartz surface, is very small. Instead, the benzene at the maximum by using the density profile of the benzene does lie on quartz surface. In case of the toluene, such small portion of perpendicular molecules is undetectable, even in the low polarity (hydrophobic) quartz surface.

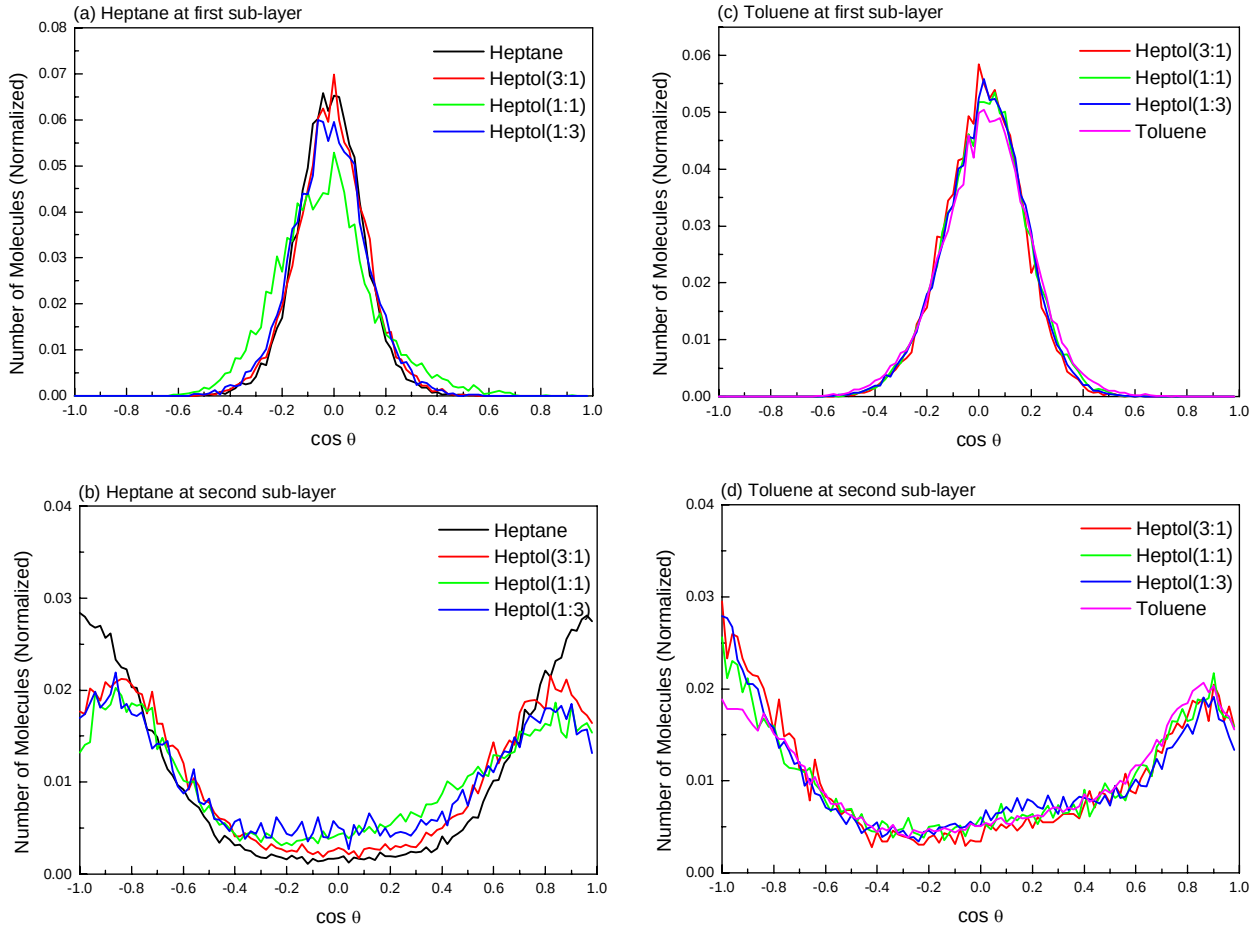

Fig. 3.5 The angle distribution of heptane and toluene on top of hydrophilic quartz surface. No detectable changes of the first sub-layer of heptane and toluene were observed. But clearly some varies for the second layer at the angle with cosθ around -0.9 and 0.9, when the concentration of heptane is varied.

In the mixture case, we only found a slightly different pattern of oscillation for heptane molecules on the hydrophilic quartz surface. As observed on density profile (Fig. 3.2 and Fig. 3.3), the heptane molecules cannot compete well with toluene on hydrophilic quartz surface. This

situation has affected the orientation of heptane molecules near the heptane-toluene-hydrophilic quartz interface (Fig. 3.4). Because we notice the different orientation between minimum and maximum on orientation profile, then we call the first minimum and maximum as first and second sub-layer of the first layer, respectively. Generally the first sub-layer does not influence by the concentration, but the different *S* value observes in the second sub-layer that moves to negative direction. Consider to this change, we notice that the packing of heptane molecules slightly changing by the present of toluene, within the preferential adsorption.

In order to gain more detailed information on the first and second sub-layer of the orientation, we have calculated the angle distribution of heptane and toluene on top of hydrophilic surface (Fig. 3.5) which located on the first minimum and maximum of orientation profile. In the first sub-layer of heptane, the pattern of angle distribution is similar for pure and mixture case, but in the second sub-layer we observed the highest intensity shifted to cos θ -0.75 and 0.75 when the heptane is diluted. This will explain the small changes as depicted in Fig. 3.4(a). The fact that toluene doesn't adopt an upright geometry on top of quartz surface is different from what they have derived from the SFG spectroscopy. Surprisingly, we have found the answer on the second contact layer. As shown in Fig. 3.5(d) and 3.6(d), toluene does have preferred orientation perpendicular to the surface in the second layer, which shows a maximum of 0.8-0.9 for cosθ, i.e. with an angle 25-35°.

We only focused on the pure heptane and toluene to avoid the influence from other compound in the mixture case. Regarding the structure of toluene, it is interesting to verify the direction of methyl group whether up (away from the surface) or down (facing the surface). As shown in Fig. 3.7, the methyl up was found more dominated than methyl down. Although, at one point of toluene on hydrophobic surface, the methyl down more dominated than methyl down, but in general the polarity of quartz surface did not influence the methyl orientation. More detail of methyl orientation can be seen from the orientation map (Fig. 3.7 (b) and (d)). The asymmetric orientation of toluene molecule also presented in these figures especially at second sub layer interface. The oscillation pattern of toluene density profile can be confirmed by the orientation map. In this figure, we found two clear patterns repeated every ~0.5 nm as observed on the density profiles.

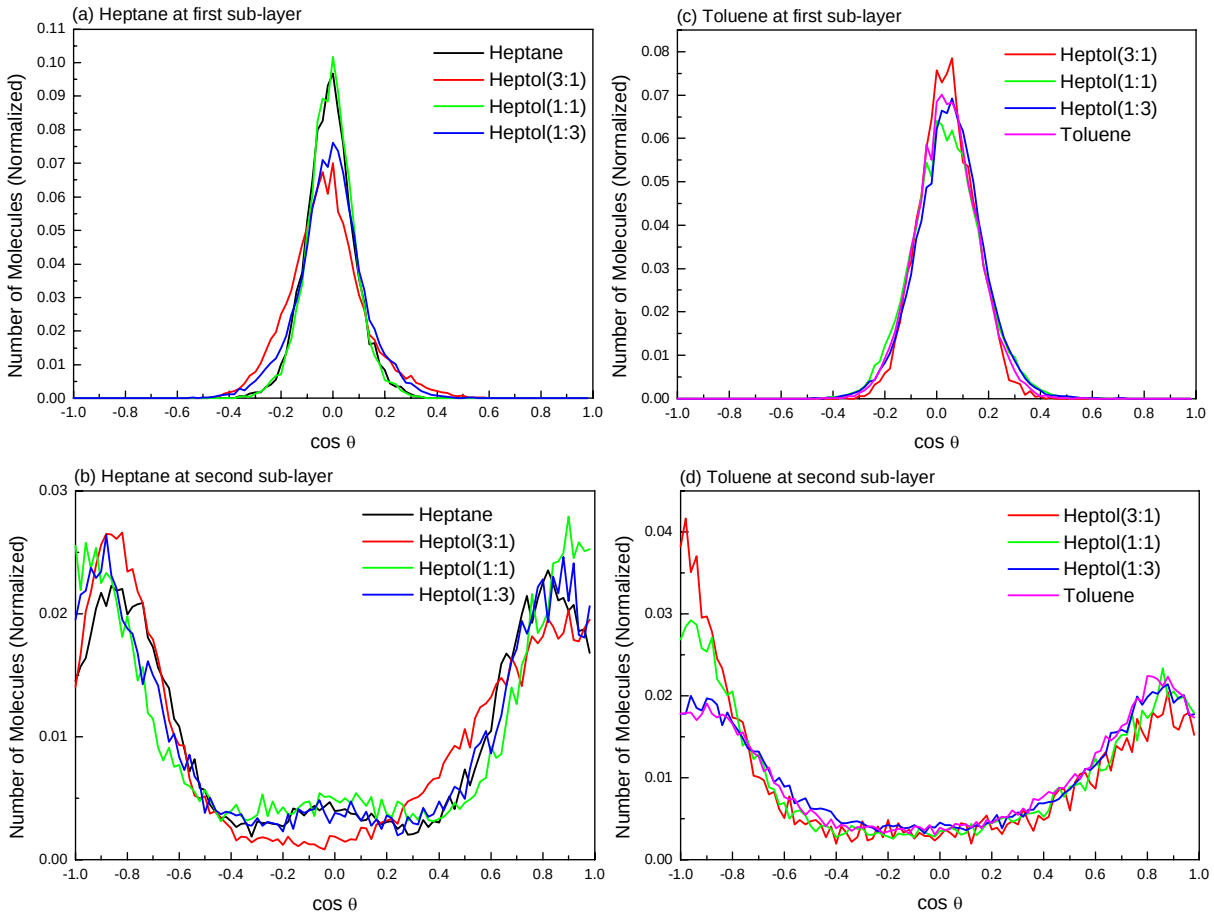

Fig. 3.6 The angle distribution of heptane and toluene on top of hydrophobic quartz surface. No detectable changes of the first contact and second layers of heptane and toluene were observed. Similar to the case for hydrophilic surface, the toluene presents a preferred orientation perpendicular to the surface in the second layer with tilting angle ~25-35^{o}, as was suggested by the SFG measurements [Yang et al., 2009]. The 'perfectly' perpendicular orientation also was observed.

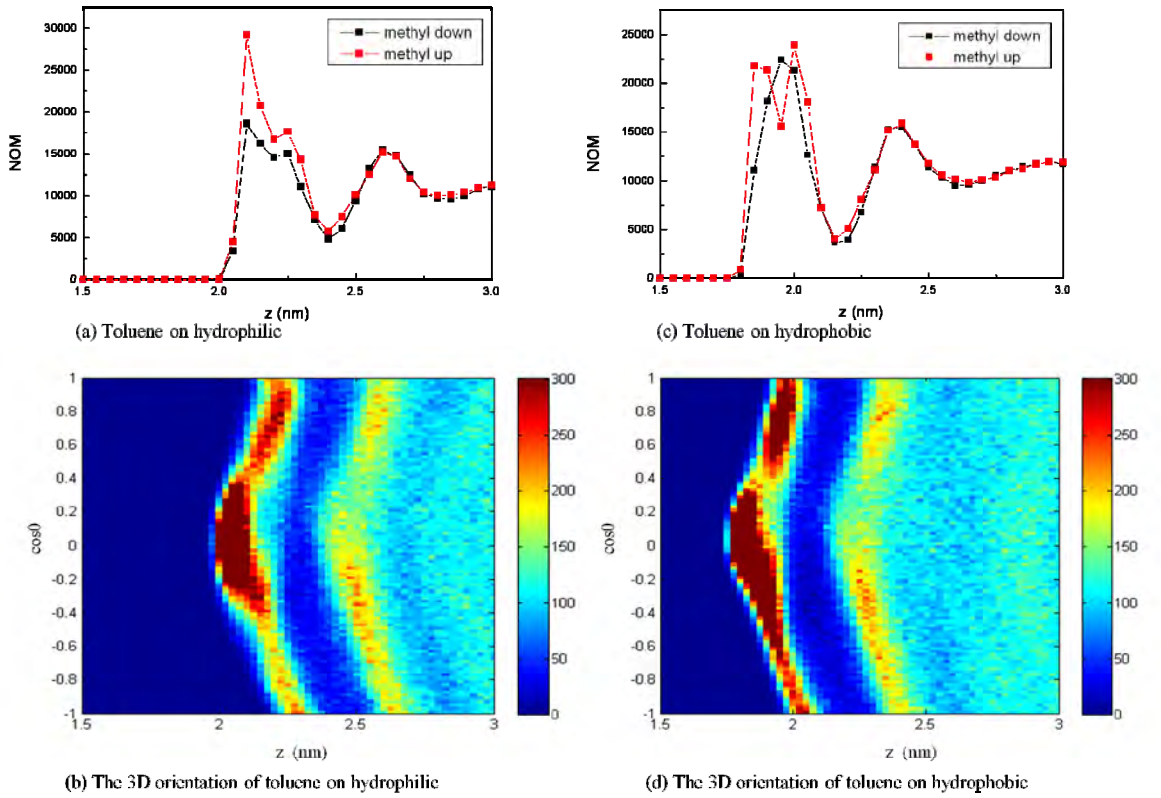

Fig. 3.7 The orientation of toluene's methyl group. (a) Toluene on hydrophilic quartz surface. (b) The orientation of toluene on hydrophilic quartz surface with x, y and z direction represent z(nm), cos θ and number of molecules (NOM). (c) Toluene on hydrophobic quartz surface. (d) The orientation of toluene on hydrophobic quartz surface with x, y and z direction represent z(nm), cos θ and number of molecules (NOM).

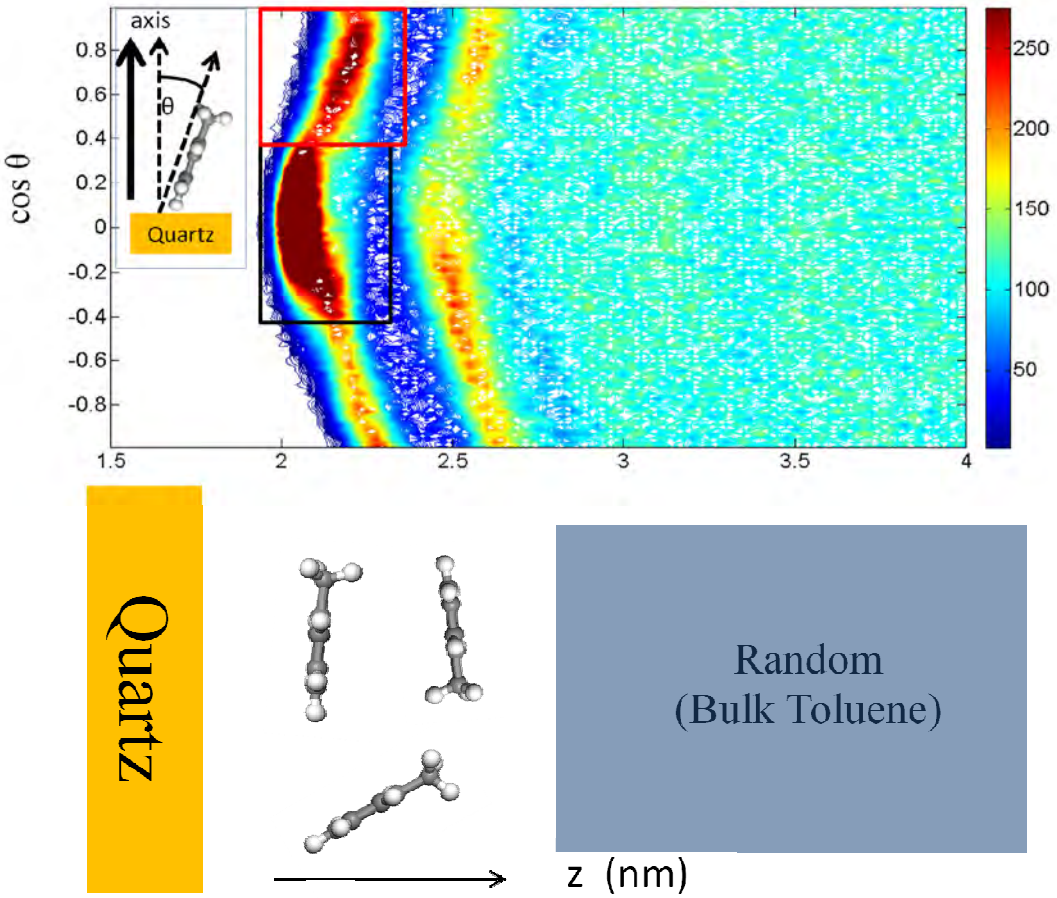

Fig. 3.8. The layering of toluene molecules on hydrophilic quartz surface. The same behavior was found on the hydrophobic quartz surface.

The orientation map can give the description of toluene molecule at the interface. The toluene might be illustrated mostly lying flat at the first sub layer with the methyl group slightly away from the surface. At the second sub layer, toluene has orientation perpendicular ~30° with methyl group away from the quartz surface. The 'thickness' of first and second sub layer is around ~0.5 nm which is similar to the 'thickness' of oscillation at the surface force measurement. The layering of toluene molecules can be seen in Fig. 3.8. Like toluene, heptane also has well-ordered packing in the interface with orientation lying flat and perpendicular, simultaneously. The orientation map illustrates that heptane has more layer than toluene as well

as the oscillation trend in density profile. The layering of heptane molecules can be seen in Fig. 3.9.

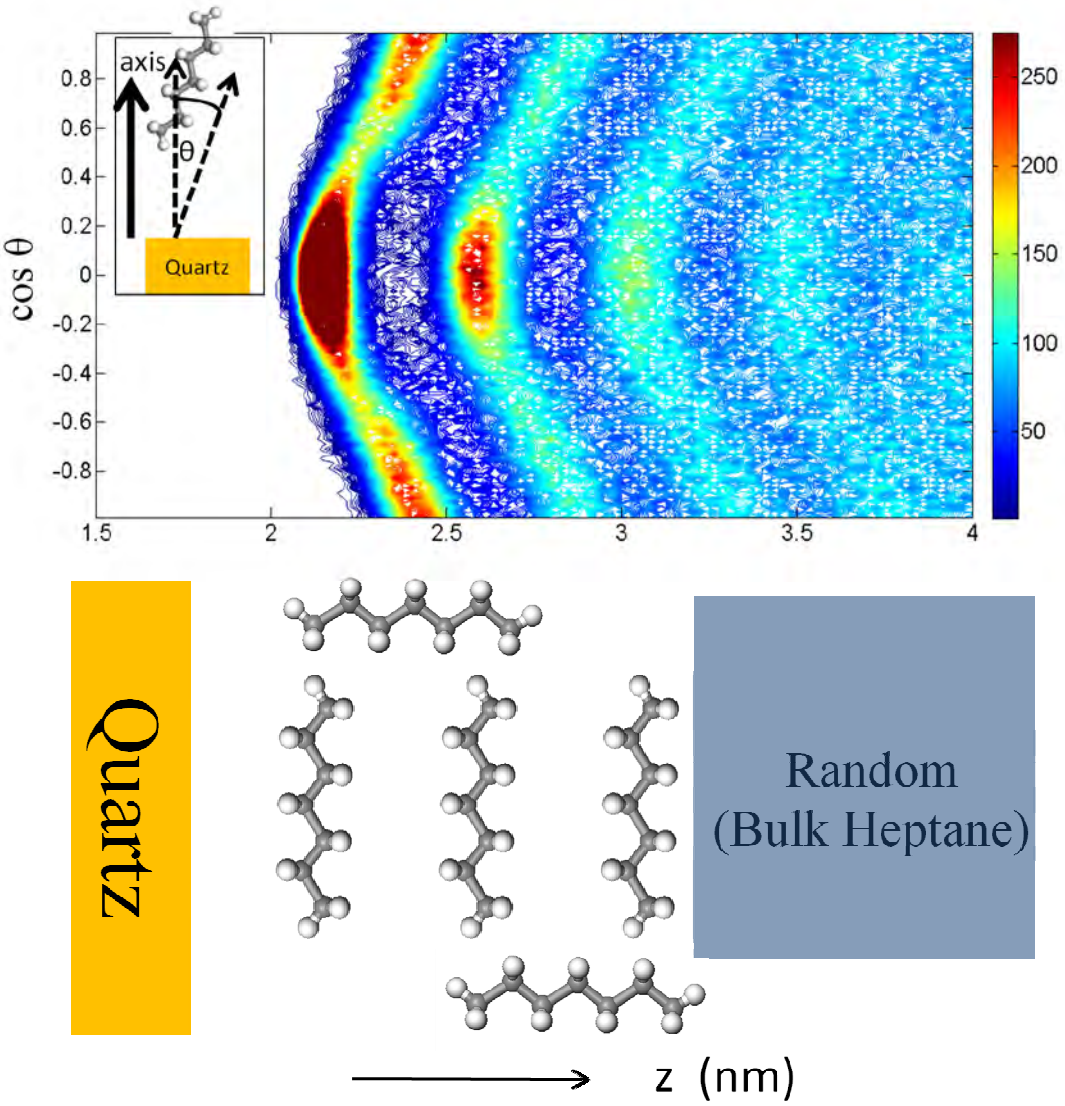

Fig. 3.9. The layering of heptane molecules on hydrophilic quartz surface.

3.3.3 Competitive Adsorption

The competitive adsorption can be detected by the density profiles as shown in the previous section. The thermodynamic parameter like free energy also can be the proof of competitive adsorption. If the relative adsorption free energy of one component to the other component in the mixture equal to zero, the components in the mixture are adsorbed to the surface in equilibrium state. If the relative adsorption free energy equal to positive or negative

value, then one component of mixture less or more adsorbed than the other. The Everett isotherm was used to determine the adsorption free energy as described in section 3.2.4. The adsorption isotherm of toluene relative to heptane is presented in Fig. 3.10. In this figure, we only show data from center of mass density profile. From this curve, the relative adsorption free energy of toluene in hydrophilic quartz interface is indicated more negative than in hydrophobic because of the positive deviation shape of trend. We calculate the relative free energy of toluene to heptane on hydrophilic and hydrophobic by fitting the data point to the Eq.3.4, which value are -1.25 kJ/mol and -0.67 kJ/mol, respectively, as shown in Table 3.1. The experimental data on basis of the silica glass also show the relative free energy in the same order [Yang et al., 2009].

It is shown here that π-electron of toluene can act as electron donor to form weak hydrogen bond with electron acceptor H. Fig. 3.11 shows the radial distribution function of O and H atom of hydrophilic quartz interface to the normal ring of toluene with angle dependent. In this figure, we see ~0.3 nm distance as the highest intensity to found O atom of hydrophilic quartz interface with angle 0 degree to the normal ring of toluene. The highest intensity to found H atom of hydrophilic quartz interface located ~0.2 nm from normal ring of toluene with angle less than 20°. Considering two orientations of toluene in the first layer, we have particularly investigated the first and second sub-layer regions which are discussed above and defined by the highest population on certain position (z) and orientation ($\cos\Theta$) range as marked in Fig. 3.8. It is shown that the maximum intensity to find O and H atom of hydrophilic silica from normal ring of toluene corresponds to the molecules at the first sub-layer only (Fig. 3.11(a)-(f)). This indicates that the toluene of the second sub-layer adopts an upright geometry simply stems from a geometry constrain of the toluene molecules by the first sub-layer and the second layer.

Table 3.1The free energy of toluene adsorption relative to heptane at hydrophilic and hydrophobic quartz interface

Interface	β	K_1	$\Delta\mu$(kJ/mol)
Hydrophilic	0.98	2.30	-1.25
Hydrophobic	0.77	1.05	-0.67

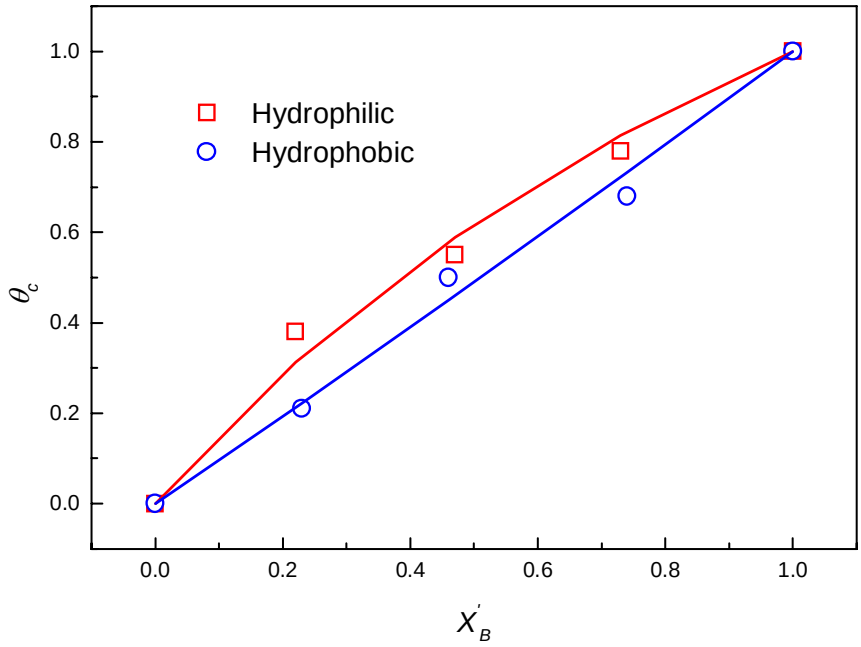

Fig. 3.10 The toluene adsorption on quartz interface (hydrophilic and hydrophobic). The toluene and heptane surface coverage (θ_c) was calculated from the integration of first peak in density profile. The X'_B is the toluene bulk mole fraction after 3 ns of simulation.

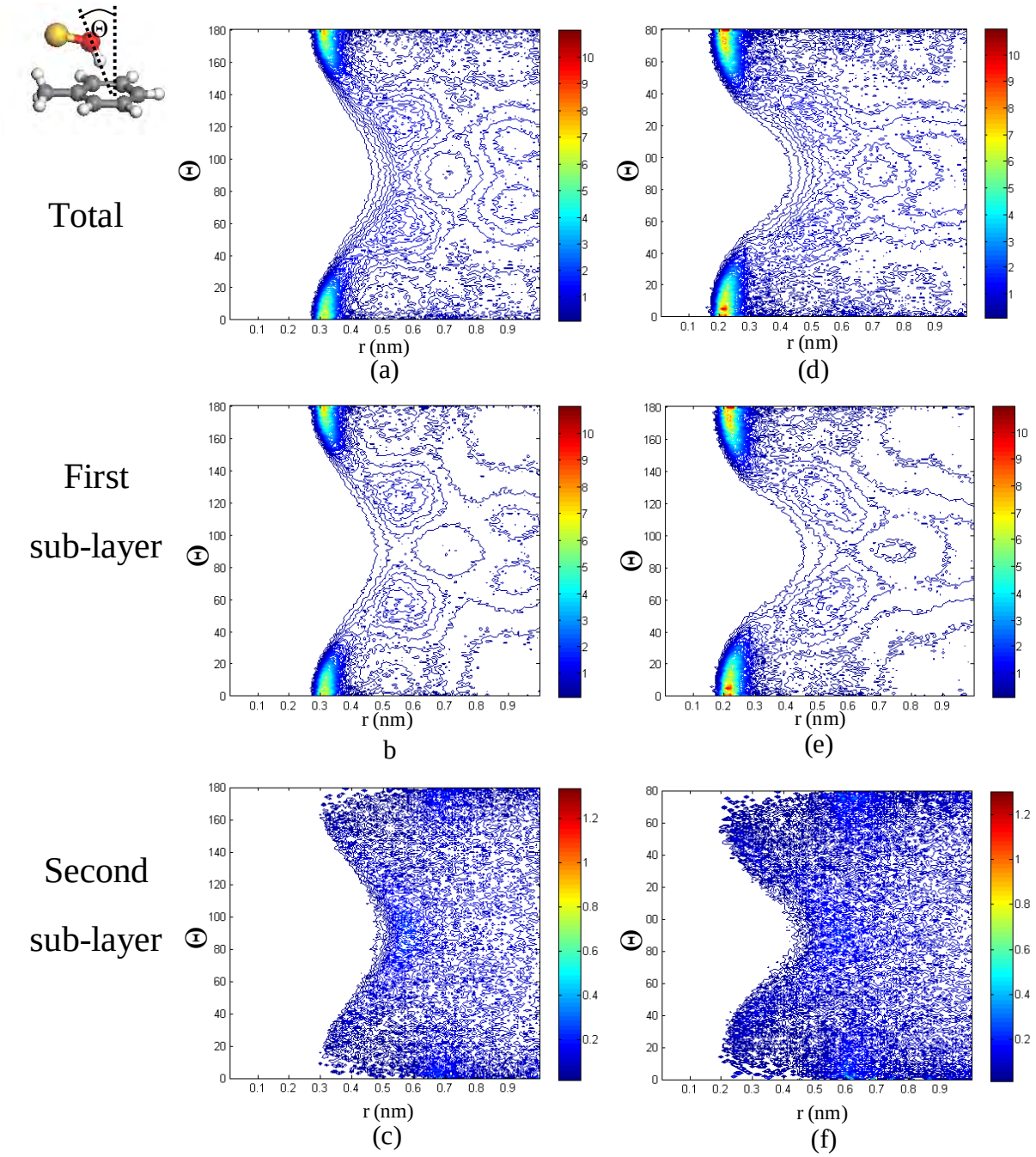

Fig. 3.11 The angular dependent radial distribution functions from the center of the phenyl ring of toluene to the oxygen (a-c) and hydrogen atoms(d-f) of Si-OH on the hydrophilic quartz surface. (a) and (d) are for total system. (b) and (e) consider only the toluene molecules at the first sub-layer, while (c) and (f) are those at the second sub-layer.

3.4 Conclusion

Our simulation has shown that heptane mostly lie flat and perpendicular in the first and second sub-layer, respectively. This result is in excellent agreement with the recent sum frequency generation spectrum measurement. The toluene molecule, which is perpendicular to the quartz surface with a tilted angle ~25° as detected in a recent sum frequency generation experiment, was found to be located in the second sub layer. The presence of methyl group in toluene molecule has generated the asymmetric pattern of orientation with methyl group pointed away from the quartz surface. The knowledge obtained from our simulation study will, no doubt, advance the understanding on the interfacial structure in combination with the modern sum frequency generation spectrum measurement.

In addition, we have shown the adsorption of heptane and toluene on hydrophilic and hydrophobic quartz surface on the basis of density profile normal to the interface. By observing the density profile of mixture case, we have found that heptane compete well only on hydrophobic quartz surface. Meanwhile, the presence of toluene molecule in the mixture, even in the small amount, has influenced the adsorption of heptane on the hydrophilic quartz surface as reflected by the decreasing of first peak density of heptane at the interface. The strength of toluene adsorption on the hydrophilic quartz surface compared to heptane can also be explained thermodynamically by the relative free energy value. By integrating the first peak density profiles each system and fitting to the Everett isotherm equation, we have found the difference free energy between toluene and heptane. The negative value means toluene adsorbed on the surface stronger than heptane. The driving force of the stronger interaction between toluene and hydrophilic quartz surface was rationalized as “weak hydrogen bonding” between the phenyl ring of toluene and hydrogen atom of hydrophilic quartz surface. The “net” absorption of toluene on the hydrophobic quartz surface might only come from the fact that the density of pure toluene is higher than that of heptane, thus the stronger van der Waals interaction.

References

Abraham, F. F. The interfacial density profile of a Lennard-Jones fluid in contact with a (100) Lennard-Jones wall and its relationship to idealized fluid/wall systems: A Monte Carlo simulation. J. Chem. Phys. **68**, 3713-3717 (1978).

Bromiley, E. C. and Quiggle, D. Vapor-liquid equilibria of hydrocarbon mixtures.Ind.Eng. Chem. **25**, 1136-1138 (1933).

Camara, L. G. and Bresme, F. Liquids confined in wedge shaped pores: Nonuniform pressure induced by pure geometry. J. Chem. Phys. **120**, 11355-11359 (2004).

Christenson, H. K. and Horn, R. G. Direct measurement of the force between solid surfaces in a polar liquid. Chem. Phys. Lett. **98**, 45-48 (1983).

Christenson, H. K. Forces between solid surfaces in a binary mixture of a non-polar liquids. Chem. Phys. Lett.**118**, 455-458 (1985).

Christenson, H. K., Gruen, D. W. R., Horn, R. G. and Israelachvili, J. N. Structuring in liquid alkanes between solid surfaces: Forces measurements and mean-field theory. J. Chem. Phys.**87**, 1834-1842 (1987).

Christenson, H. K. Experimental measurements of solvation forces in nonpolar liquids. J. Chem. Phys. **78**, 6906-6914 (1983).

Coasne, B., Alba-Simionesco, C., Audonnet, F., Dosseh, G. and Gubbins, K. E. Adsorption and structure of benzene on silica surfaces and in nanopores. Langmuir **25**, 10648-10659 (2009).

Cygan, R. T., Liang J. J. and Kalinichev, A. G. Molecular models of hydroxide, oxyhydroxide, and clay phases and the development of a general force field. J. Phys. Chem. B **108**, 1255-1266 (2004).

Docherty, H. and Cummings, P. T. Direct evidence for fluid-solid transition of nanoconfined fluids. Soft Matter **6**, 1640-1643 (2010).

Doerr, A. K., Tolan, M., Seydel, T. and Press, W. The interface structure of thin liquid hexane films. Physica B **248**, 263-268 (1998).

Everett, D. H. Thermodynamics of adsorption from solution. Part 1. Perfect system. Trans. Faraday Soc. **60**, 1803-1813 (1964).

Gao, J., Luedtke, W. D. and Landman, U. Layering transition and dynamics of confined liquid films. Phys. Rev. Lett. **79**, 705-708 (1997a).

Gao, J., Luedtke, W. D. and Landman, U. Structure and solvation forces in confined films: linear and branched alkanes. J. Chem. Phys. **106**, 4309-4319 (1997b).

Gao, J., Luedtke, W. D. and Landman, U. Origin of solvation forces in confined films J. Phys. Chem. B **101**, 4013-4023 (1997b).

Gee, M. L., McGuiggan, P. M. and Israelachvili, J.N. Liquid to solidlike transitions of molecularly thin films under shear. J. Chem. Phys. **93**, 1895-1907 (1990).

Goumans, T. P. M., Wander, A., Brown, W. A. and Catlow, C. R. A. Structure and stability of the (001) α-quartz surface. Phys. Chem. Chem. Phys. **9**, 2146-2152 (2007).

Harris, J. G. Liquid-vapor interfaces of alkane oligomers. Structure and thermodynamics from molecular dynamics simulations of chemically realistic models. J. Phys. Chem. **96**, 5077-5086 (1992).

Hess, B., Kutzner, C., van der Spoel, D. and Lindahl, E. GROMACS 4: Algorithms for highly efficient, load-balanced, and scalable molecular simulation. J. Chem. Theory Comput. **4**, 435-447 (2008).

Hore, D. K., Walker, D. S. and Richmond, G. L. Layered organic structure at the carbon tetrachloride-water interface. J. Am. Chem. Soc. **129**, 752-753 (2007).

Horn, R. G. and Israelachvili, J. N. Direct measurement of structural forces between two surfaces in a nonpolar liquid. J. Chem. Phys.**75**, 1400-1412 (1981).

Humphrey, W., Dalke, A., Schulten, K. VMD: visual molecular dynamics. J. Molec. Graph. **14**, 33-38 (1996).

Jin, R. Y., Song, K. and Hase, W. L. Molecular dynamics simulations of the structures of alkane/hydroxylated α-Al_2O_3(0001) interfaces. J. Phys. Chem. B **104**, 2692-2701 (2000).

Kalyanasundaram, V., Spearot D. E. and Malshe, A. P. Molecular dynamics simulation of nanoconfinement induced organization of *n*-decane. Langmuir **25**, 7553-7560 (2009).

Kawamata, M. and Yamamoto, T. Molecular dynamics simulation of surface ordering in liquid n-alkanes. J. Phys. Soc. Jpn. **66**, 2350-2354 (1997).

Klauda, J. B., Brooks, B. R., Mackerrel Jr., A. D., Venable, R. M. and Pastor, R.W. An *ab initio* study on the torsional surface of alkanes and its effect on the molecular simulations of alkanes and a DPPC bilayer. J. Phys. Chem. B **109**, 5300-5311 (2005).

Klein, J. and Kumacheva, E. Simple liquids confined to molecularly thin layers. I. confinement-induced liquid-to-solid phase transitions. J. Chem. Phys.**108**, 6996-7010 (1998). Detailed solvation force as a function of gap distance for toluene was not reported in this paper. However, it was reported that the sharp liquid-to-solid phase transition on increasing confinement between films of the thickness corresponds four layers for toluene and six or seven layers for cyclohexane.

Kresse, G. and Furthmuller, G. Efficient iterative schemes for *ab initio* total-energy calculations using a plane-wave basis set. Phys. Rev. B **54**, 11169-11186 (1996).

Kunieda, M., Nakaoka, K., Liang, Y., Miranda, C. R., Ueda, A., Takahashi, S., Okabe, H. and Matsuoka, T. Self-accumulation of aromatics at the oil-water interface through weak hydrogen bonding. J. Am. Chem. Soc.**132**, 18281-18286 (2010).

Lake, L. W. Enhanced Oil Recovery. Prentice Hall, New Jersy (1989).

Lamb, R. N. and Furlong, D. N. Controlled wettability of quartz surfaces. J. Chem. Soc. Faraday Trans. I **78**, 61-73 (1982).

Liu, W.-T. and Shen, Y. R. Surface vibrational modes of α-quartz (0001) probed by sum-frequency spectroscopy. Phys. Rev. Lett. **101**, 016101 (2008).

Matsubara, H., Pichierri, F. and Kurihara, K. Unraveling the properties of octamethylcyclotetrasiloxane under nanoscale confinement: atomistic view of the liquidlike state from molecular dynamics simulation. J. Chem. Phys. **134**, 044536-(2011).

Murashov, V. V. Reconstruction of pristine and hydrolyzed quartz surfaces. J. Phys. Chem. B **109**, 4144-4151 (2005).

Nose, S. A molecular dynamics method for simulations in the canonical ensemble. Mol. Phys. **52**, 255-268 (1984).

Ostroverkhov, V., Waychunas, G. A. and Shen, Y. R. Vibrational spectra of water at water/α-quartz (0001) interface. *Chem. Phys. Lett.* **386**, 144-148(2004).

Rao, M., Berne, B. J., Percus, J. K. and Kalos, M. H. Structure of a liquid-vapor interface in the presence of a hard wall in the transition region. J. Chem. Phys. **71**, 3802-3806 (1979).

Rignanese, G. M.,Vita, A. D., Charlier, J. C., Gonze, X. and Car, R. First principles molecular-dynamics study of the (0001) α-quartz surface. Phys. Rev. B **61**, 13250-13255 (2000).

Shen, Y. R. Surface properties probed by second-harmonic and sum-frequency generation. Nature **337**, 519-525 (1989).

Skelton, A. A., Wesolowski, D. J. and Cummings, P. T. Investigating the quartz (10-10)/water interface using classical and ab initio molecular dynamics. Langmuir **27**, 8700-8709 (2011).

Van Buuren, A. R., Marrink, S.-J. and Berendsen, H. J. C. A molecular dynamics study of the decane/water interface. J. Phys. Chem. **97**, 9206-9212 (1993).

Wang, J. C. and Fichthorn, K. A. Effects of chain branching on the structure of interfacial films of decane isomers. J. Chem. Phys. **108**, 1653-1663 (1997).

Xia, T. K. and Landman, U. Molecular dynamics of adsorption and segregation from alkane mixture. Science **261**, 1310-1312 (1993).

Yang J. and Wang, E. G. Water adsorption on hydroxylated α-quartz (0001) surfaces: From monomer to flat bilayer. Phys. Rev. B **73**, 035406(2006).

Yang, Z., Li, Q., Hua, R., Gray, M. R. and Chou, K. C. Competitive adsorption of toluene and *n*-alkanes at binary solution/silica interfaces. J. Phys. Chem. C **113**, 20355-20359 (2009).

Yeung, A., Dabros, T., and Maliyah, J. Does equilibrium interfacial tension depend on method of measurement? J. Colloid & Interface Sci. **208**, 241-247 (1998).

Yu, C.-J., Richter, A. G., Kmetko, J., Datta, A. and Dutta, P. X-ray diffraction evidence of ordering in a normal liquid near the solid-liquid interface. Europhys. Lett. **50**, 487-493 (2000).

Zhuang, X., Miranda, P. B., Kim, D. and Shen, Y. R. Mapping molecular orientation and conformation at interfaces by surface nonlinear optics. Phys. Rev. B **59**, 12632-12640 (1999).

Zhuravlev, L. T. The surface chemistry of amourphous silica.Zhuravlev model. Colloids and Surfaces A: Physicochem. Eng. Aspects **173**, 1-38 (2000).

CHAPTER 4

The Investigation of Quartz Surface Chemistry

In this chapter, we investigate the quartz (0001) surface structure immersed in liquid for two different fresh quartz cleavages by using first principles molecular dynamics. For the first type of cleavage, the final structure contains of geminal, triple and single silanols together with peroxy –Si-O-O-Si and Si-O-O-H defects. For the second type of cleavage, the final structure contains of geminal silanol, single silanol and siloxane bridge. A small amount of unsaturated sites were also found on both surfaces.

4.1 Introduction

Quartz is a ubiquitous chemical compound in the Earth's crust. The interaction with water becomes crucial due to the role in many environmental and geochemical processes. The rapid hydroxylation of fresh silica surface, refer to quartz, by water has already been observed in the experiment [Parks, 1984; Klaus et al., 1997; Schlegel et al., 2002; Du et al., 1994; Ostroverkhov et al., 2004; Liu and Shen, 2008; Duval et al., 2002] and simulations [de Leeuw et al., 1999, Rignanese et al., 2004; Murashov, 2005; Mischler et al., 2005; Goumans et al., 2007; Bandura et al., 2011; Adeagbo et al., 2008]. The experimental information of quartz surface structure is limited and still in debate [Schlegel et al., 2002; Ostroverkhov et al., 2004; Duval et al., 1994]. The structure of quartz $(10\bar{1}0)$ and $(10\bar{1}1)$-water interface were investigated by X-ray reflectivity indicates that quartz surface is likely fully hydroxylated [Schlegel et al., 2002]. The two modes at 880 and 980 cm^{-1} were identified as Si-O-Si and Si-OH vibration of quartz (0001) surface which observed using sum-frequency spectroscopy [Ostroverkhov et al., 2004]. The surface composition of a quartz surface reacted with various electrolyte solutions was evaluated by using X-Ray photoelectron spectroscopy (XPS), where three different surface species have been quantitatively verified [Duval et al., 2002]. A deeper insight into the quartz-water interface, towards a consistent interpretation on experiment data, is therefore desirable.

The reconstruction of quartz surface has been pursued in most of theoretical works. The formation of Si-O-Si bridges, two-membered rings, and three-membered rings are some features in the relaxation of fresh quartz surface [de Leeuw et al., 1999; Ceresoli et al., 2000; Murashov, 2005; Goumans et al., 2007; Adeagbo et al., 2008]. The other defect also may occur on the silica surface or bulk which has been detected by experiment. The two-membered rings, peroxy links and double bonds were the surface defects that have been observed by infrared spectroscopy [Bunker et al., 1989; Friebele et al., 1979; Edwards and Fowler, 1982; Griscom, 1991; Skuja et al., 1984]. The two-membered ring silica surface has been detected when silica was dehydroxylated at temperatures above ~800K [Bunker et al., 1989]. The presence of peroxy link =Si-O-O-Si= has been identified as the defect in silica glass via electron spin resonance (ESR) measurement [Friebele et al., 1979]. This defect is believed to be the precursor for other defect formation such as E' centers (≡Si·), nonbridging-oxygen hole centers (≡Si-O·), peroxy radicals (≡Si-O-O·), and self-trapped holes [Edwards and Fowler, 1982]. The two coordinated Si atom was also supposed as defect of silica surface which reported by the Luminescence polarization [Griscom, 1991; Skuja et al., 1984]. In the Earth science, peroxy link is indicated as the non-seismic pre-earthquake signal [Freund, 2010]. Every igneous and high-grade metamorphic rock in the Earth's crust carries a non-zero complement of peroxy, which can be activated to generate electric current when rocks are subjected to mechanical stress. This electric current is detectable and has been regarded as one pre-earthquake signal [Freund, 2010; Freund et al., 2006, 2007; Balk et al., 2009; Takeuchi, 2009]. If the electromagnetic signals that are 'reported' by the earth can be understood well, we would be able to predict the major earthquake. It is, therefore, interesting to understand the formation mechanism at molecular scale for all relevant defects in crystalline and amorphous silica.

Previously, the relaxed fresh quartz surface was saturated into silanol groups by adding water molecule one by one with undercoordinated surface sites as initial structure [De Leeuw et al., 1999; Rignanese et al., 2004; Murashov, 2005; Mischler et al., 2005; Goumans et al., 2007; Bandura et al., 2011]. This method has not dealt with the full solid-liquid interaction, but rather individual water molecules with quartz surface. The other simulation presents the quartz surface as fully hydroxylated structure with higher density (~10 silanol groups per nm^2) [Yang and Wang, 2006; Skelton et al., 2011]. In comparison, the experimental average surface density of Si-OH of the various silica surfaces is around 4.5-6.2 silanol groups per nm^2 under ambient

condition [Iler, 1955; Zhuravlev, 2000] under ambient condition. To examine the effect of the polarity of quartz surface, different degrees of hydroxylation of a crystalline silica surface have also been employed [Argyris et al., 2009; Chen et al., 2011]. However, the above simulation work could not answer the real structure of silica surface as revealed by the XPS measurements, i.e. with a significant amount of SiO [Duval et al., 2002].

The simulation of chemical reaction between fresh quartz surface and water should be, preferably, investigated by the first-principles approach. The first principles molecular dynamics simulation allows the bond breaking and formation, which is required in the chemical reaction. The disadvantage of first principles molecular dynamics (MD) is high cost or time consuming compared to the classical MD. Due to this reason, the investigation of full solid-liquid interface system by first-principles approach is in limited number. Very recently, Adeagbo et al. have investigated the transport processes at quartz-water interface which indirectly offers insight of the reliable structure of quartz surface under aqueous environment [Adeagbo et al., 2008]. The initial structure was modeled as Si and O terminated surfaces in the (0001) direction. The water molecules were put between the terminals then the chemical reaction, namely hydroxylation, occurred within femto seconds. The final structure was resulting in 83% silanol coverage. However, only one trial quartz cleaved surface was employed in their study.

Here, we have investigated the structure of quartz-water interface by comparing two different cleaved quartz surfaces with first-principles molecular dynamics simulations. Our main findings are that (1) the reaction pathways for silanols and the types of silanols (triple, geminal and single) were identified from the trajectories; (2) the unsaturated SiO and siloxane were found coexisting with various silanol groups which is in consistent with the recent XPS experiments [Duval et al., 2002]; (3) the formation mechanism of peroxy defects were revealed. Other defects like two-coordinated silicons were also detected. Of particular, we studied the “formation” of the unsaturated site and detailed local environmental atom varies along the trajectories. As the two-membered ring quartz surface was believed with high local stress field and favors hydroxylation at a relatively high temperature [Mischler et al., 2005], we have also analyzed the detailed ring statistics for the quartz slab and found that the newly formed rings at surface are from 4- to 7-member ring. As a comparison, we replaced the water by methane molecules in one of fresh quartz surface. The final configuration was found to be the hydrophobic quartz surface which is

dominated by siloxane bridge feature. We present the detailed comparison on two different quartz surfaces including the thermodynamic stabilities of two different surfaces.

4.2 Computational Detail

The fresh quartz surface was obtained by cleaving the unit cell of bulk quartz, which consists of 72 Si atoms and 144 O atoms, along the (0001) direction. Both surfaces, i.e. top and bottom, which is terminated by single Si-O was reconstructed by moving manually the O atom in the bottom surface to the top surface. After the reconstruction, the final structure of fresh quartz surface is similar to the initial structure of previous work [Adeagbo et al., 2008]. We named this fresh quartz surface as system A. We also employed another fresh quartz surface which is similar to the initial structure in some previous simulations [de Leeuw et al., 1999; Goumans et al., 2007], namely system B. The quartz surface size (for both A and B systems) is 14.74 and 17.02 Å in x and y direction, respectively. The size of empty space between top and bottom surface including the quartz slab is 18.48 Å and 18.88 Å for system A and B, respectively. The additional simulation was performed by substituting water to methane molecules and employed 21.51 Å as the size of z direction.

The Quickstep as integrated on the open source CP2K was employed to perform the first-principles molecular dynamics based on density functional theory within the Born-Oppenheimer framework [Lippert et al., 1997; Vande Vondele et al., 2005]. This code uses an atom-centered Gaussian-type basis to describe the wave function, but uses an auxiliary plane wave basis to describe the density. The Becke, Lee, Yang and Parr (BLYP) gradient-corrected functional [Becke, 1988; Lee et al., 1988] were employed in our study for the exchange and correlation terms in combination with Goedecker-Teter-Hutter (GTH) pseudopotentials [Goedecker et al., 1996] and large Gaussian basis sets double-ζ valence plus 1 set of polarization functions (DZVP) [Vande Vondele et al., 2005]. The molecular dynamics was performed in constant temperature and volume (NVT ensemble) and the temperature was controlled by means of a Nosé thermostat [Nosé, 1984]. The high temperature (1000 K) was chosen to accelerate the chemical reaction due to the expensive calculation. The simulation was run using 0.5 fs as the time step for 6 ps. The initial liquid water was prepared by simulation of 64 water molecules at standard condition. The

36 methane molecules were also prepared in the similar procedure for the additional simulation. The snapshot of simulation in this study was visualized by XCrySDen [Kokalj, 2003] to see the mechanism of chemical reaction and the final structure. It has been shown that we can understand the structure of quartz in terms of the indecomposable rings of network, i.e. the closed paths in the network. Closed paths, or rings are defined here by the shortest-path criterion [Marlans et al., 1988; Liang et al., 2008] and a Si-O pair is considered connected if the interatomic distance is less than 2.0 Å, which is well located in the first minimum regime of Si-O pair correlation function.

4.3 Quartz Surface in Aqueous Environment

The simulation was started by using the clean surface of quartz and the liquid water in between as shown in Fig. 4.1(a) and (c) for system A and system B, respectively. The hydroxylation process occurred immediately after the simulation started. During the simulation, some water molecules were found dissociated into H^+ and OH^- quickly (~ 20 fs for System A and ~200 fs for System B). Most of these molecules have initial position near the quartz-water interface. The water molecules with initial position in the bulk keep steady as H_2O specie and move around the bulk area. After dissociation, the H^+ and OH^- species attached to the quartz surface spontaneously. As anticipated, the simulation of fresh silica surface and liquid water has revealed the formation of the silanol group on both surfaces. Within 4 ps of simulation, the hydroxylation of quartz surface has reached the equilibrium state. At the end of simulation, we found both surfaces mostly covered by silanol group with a small amount of unsaturated sites (Fig. 4.1.(b) and (d)). We have also found some defects on the quartz surfaces, such as peroxy link and peroxy Si-O-O-H. In the next subsection we described some detailed features of quartz surfaces in aqueous environment.

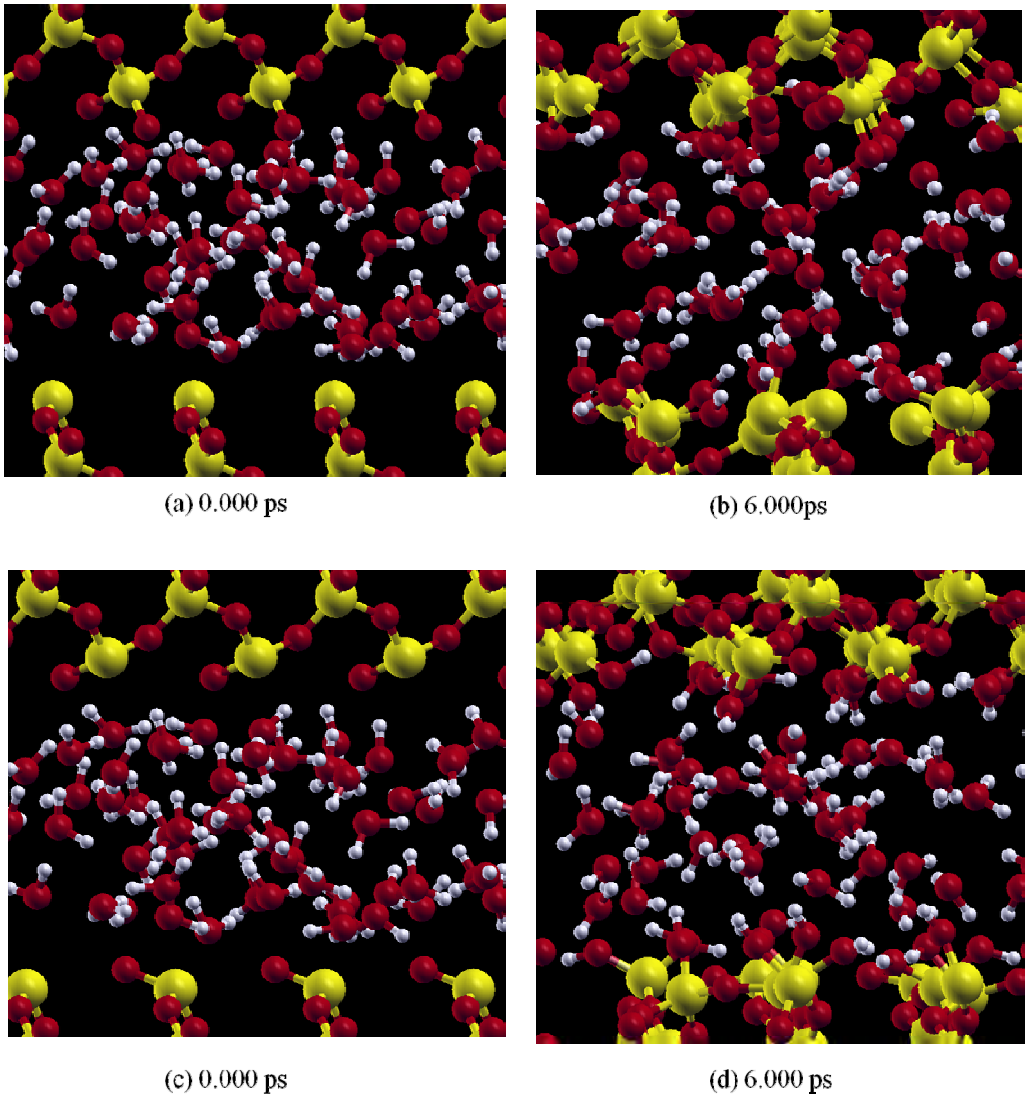

Fig. 4.1.The snapshot of first-principles molecular dynamics of fresh quartz system A and system B in aqueous environment at 1000K NVT ensemble. (a) The initial structure of system A (t=0.0000 ps). (b) The last configuration of system A after 6.0000 ps of simulation. (c) The initial structure of system B (t= 0.0000 ps). (d) The last configuration after 6.0000ps of simulation. Color legend: O: red, Si: yellow, H: white.

4.3.1 Surface Hydroxylation: Formation of Silanols and Unsaturated Sites

The silanol formation was begun by the attachment of water molecule to the O-terminated of system A at 0.0025 ps (Fig. 4.2(a)). In the next step (0.0040 ps), a second water molecule, bound to this intermediate specie, formed “dimer” water molecules. Then, the first

silanol group and $[O_2H_3]^-$ were formed at 0.0050 ps, simultaneously. The side product $[O_2H_3]^-$ was found unstable and dissociated to $H_2O$and OH^- at 0.0060 ps. We observed different formation mechanism occurred at the opposite site. The first silanol in the Si terminal was observed at 0.0220 ps via the formation of H^+ and OH^- intermediate species (Fig. 4.2(b)). Dissociation of two water molecules was observed for the first time at 0.0195 ps. Then, the specie OH^- immediately attached to Si terminal as the silanol group. At the very beginning of simulation, the O terminal is more reactive than the Si terminal, but in the end the number of silanol group is similar. As shown in Fig. 4.2(c), 16 and 14 silanol groups were observed at O terminal and Si terminal after 6.0000 ps of simulation, respectively.

We found some differences on the mechanism of hydroxylation fresh quartz system A with previous simulation [Adeabgo et al., 2008]. The previous simulation did not report the formation of "dimer" water as the intermediate specie. Instead, they only showed OH^- and H_3O^+ as the intermediate species. The OH^- bind directly to the Si-terminated surface then the proton (H^+) diffuse through the water film before attaching to the O-terminated surface. The difference may come from slightly different initial structures employed in two different studies, which indicates a slightly different local stress field on the surfaces, and the exchange correlation functional. Although we found some differences in the beginning of simulation, the last configuration of surface was mostly hydroxylated similar to the previous simulation [Adeagbo et al., 2008].

Although, rather slower than the formation of first silanol group on system A, system B also formed the first silanol group less than 0.200 ps. The attachment of OH^- to the Si atom in the bottom system B was observed at 0.020 ps as shown in Fig. 4.3. The first silanol group in the O site occurred at 0.148 ps. The dissociation of water molecule into OH^- and H^+ was started before the hydroxylation process of Si atom on the system B (Fig. 4.3(a)). Those two species were moved into different directions. The H^+ moves close to other water molecules, in the meanwhile the OH^- binds to Si atom on the surface. The water molecule also can bind to Si atom then one of H atom of water molecule attach to the neighbor O atom on surface and form two silanol groups directly as shown in Fig. 4.3(c) and d. At the end of simulation, the fresh quartz system B was generally covered by silanol groups.

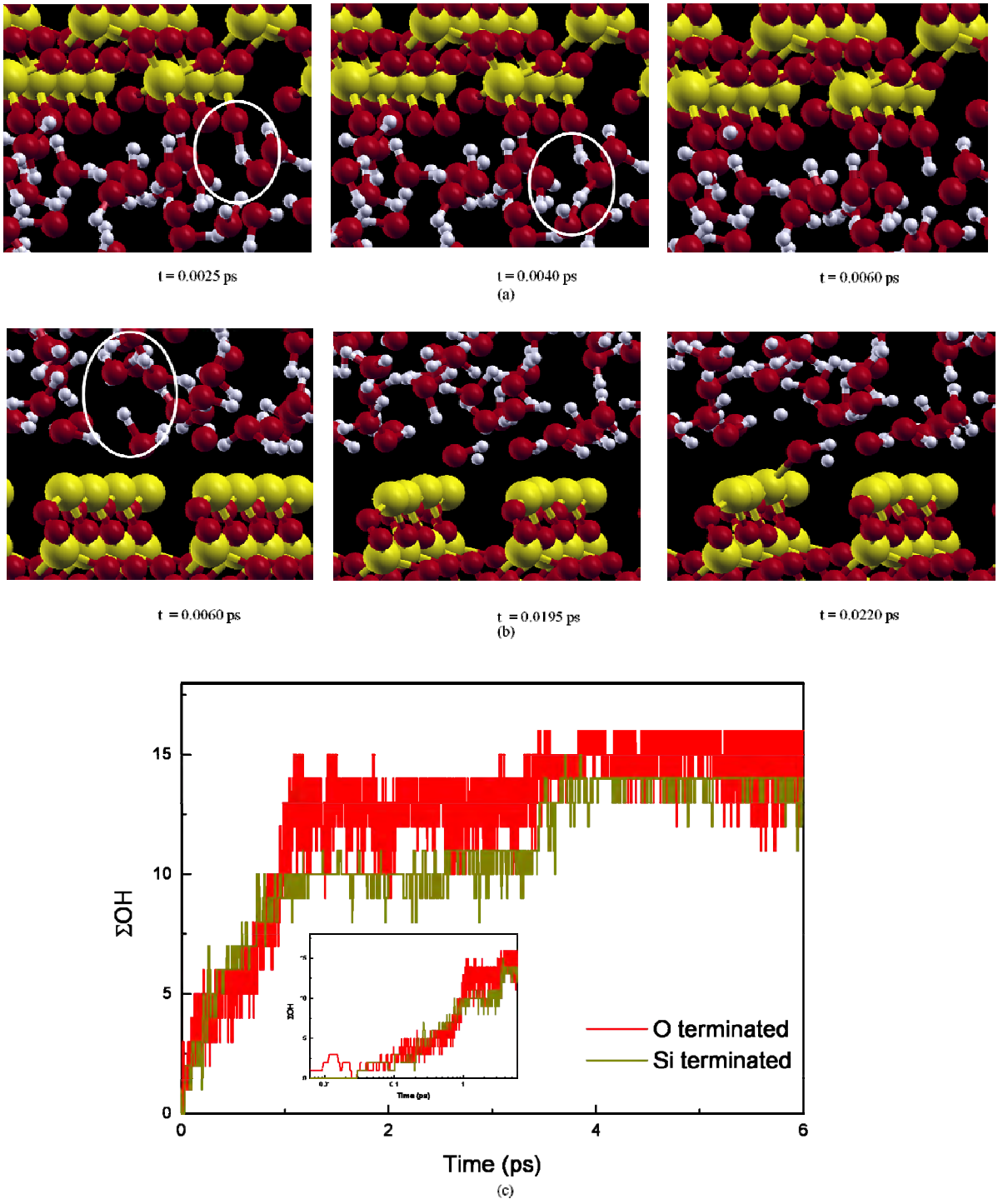

Fig. 4.2. (a) The mechanism of first silanol formation at O terminal (b) The mechanism of first silanol formation at Si terminal. (c) The number of silanol groups at O and Si terminal as function of simulation time. Inset: the formation of silanol at less than 1.0000 ps. See the text for detail mechanism.

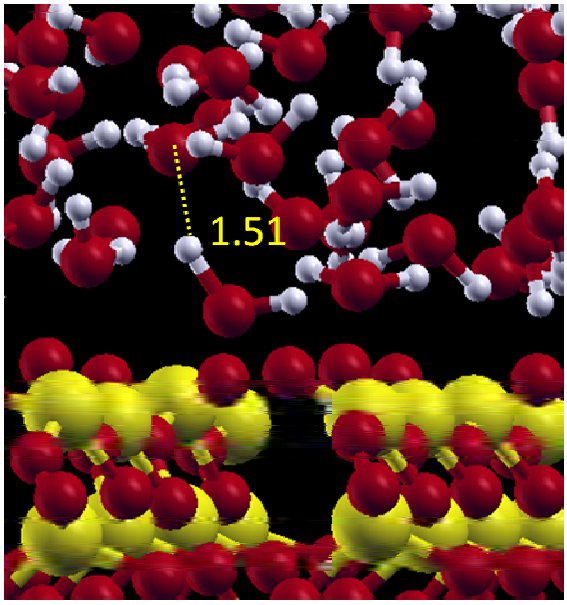

(a) 0.0195 ps

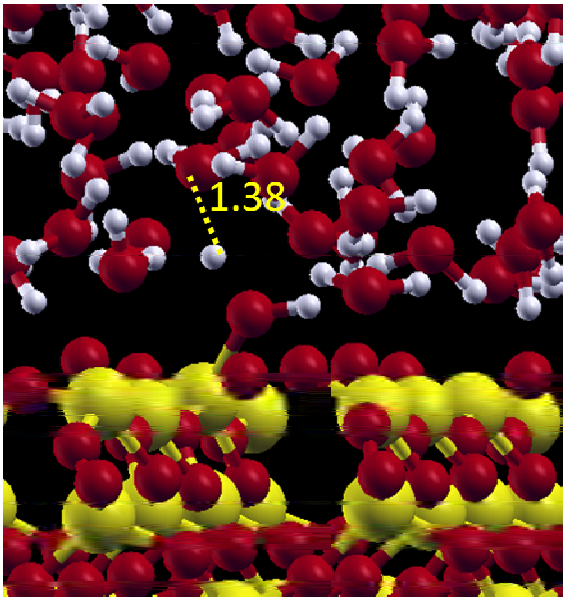

(b) 0.0200 ps

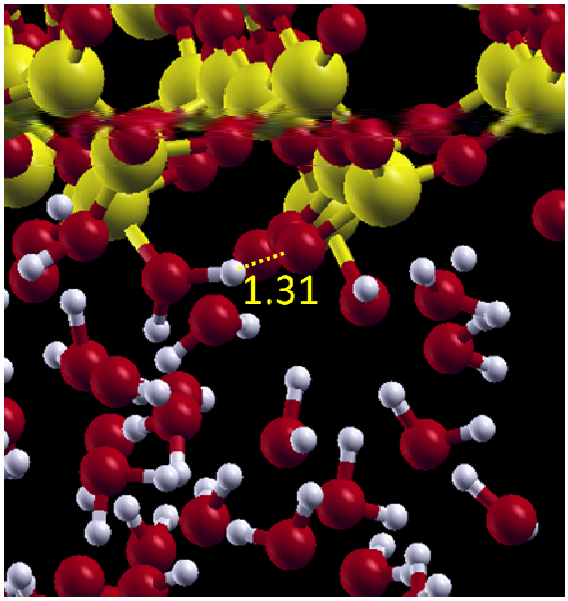

(c) 0.1475 ps

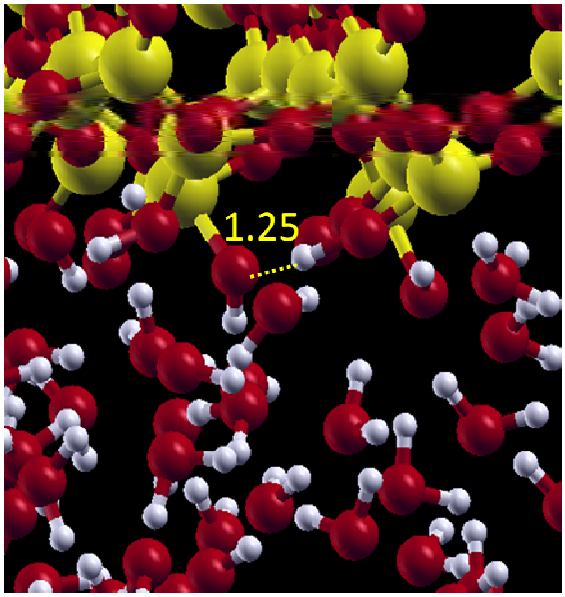

(d) 0.1480 ps

Fig. 4.3.The hydroxylation mechanism of system B in aqueous environment. (a) The two water molecules which are connected by dot line will dissociate into OH^- and H^+ near the Si atom on the surface. (b) The OH^- specie directly binds to Si atom on the surface form silanol group. (c) The water molecule attach to O atom on the surface act as the intermediate specie. (d) The H atom of intermediate specie bind to the Si atom neighbor on the surface, two silanol groups form simultaneously.

We found that the system B was 83.33% covered by silanol groups, which is higher than system A of 62.50%. The previous simulation also cannot reach 100% silanol coverage, after time span 2 ps the coverage is 83% [Adeagbo et al., 2008]. The history of silanol formation by the time function is shown in Fig. 4.4. We assumed the water molecules is always dissociated into OH^- and H^+ then bind to Si and O atom on the surface, respectively. The silanol group was defined as Si atom on surface with O atom of water molecules within 1.85 Å of distance. Meanwhile, O atom on surface with H atom of water molecules within distance 1.3 Å was defined as silanol group on O surface. At the beginning of simulation, no silanol groups were detected then the silanol groups were formed rapidly with time. The total number of silanol groups increase with simulation time until reaching roughly a constant level at 4 ps – 6ps for both quartz surfaces. The constant number of silanol groups indicates that the surface has already been saturated.

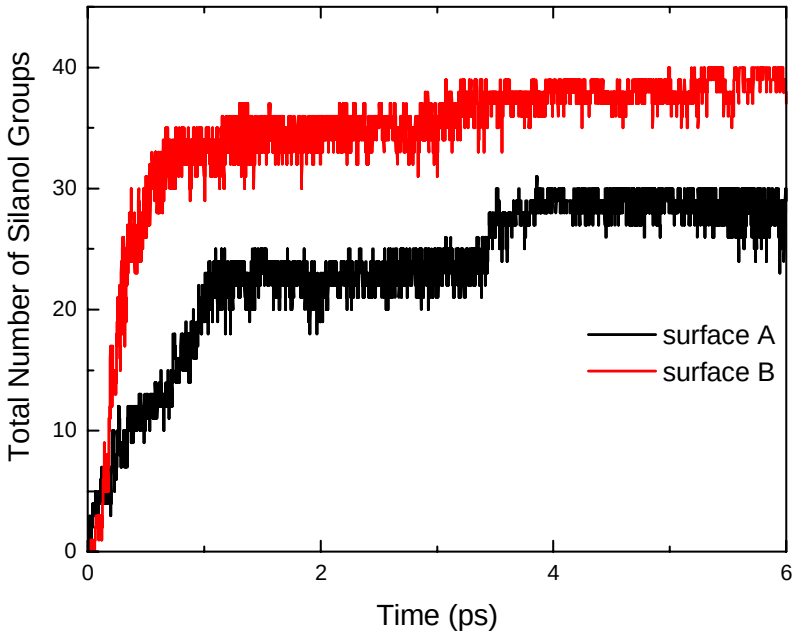

Fig. 4.4. The total number of silanol groups as function of time. At the beginning of simulation, no silanol group was detected. The silanol groups are rapidly formed less than 1.0000 ps, then roughly reached the constant level after 4.0000 ps for both surface.

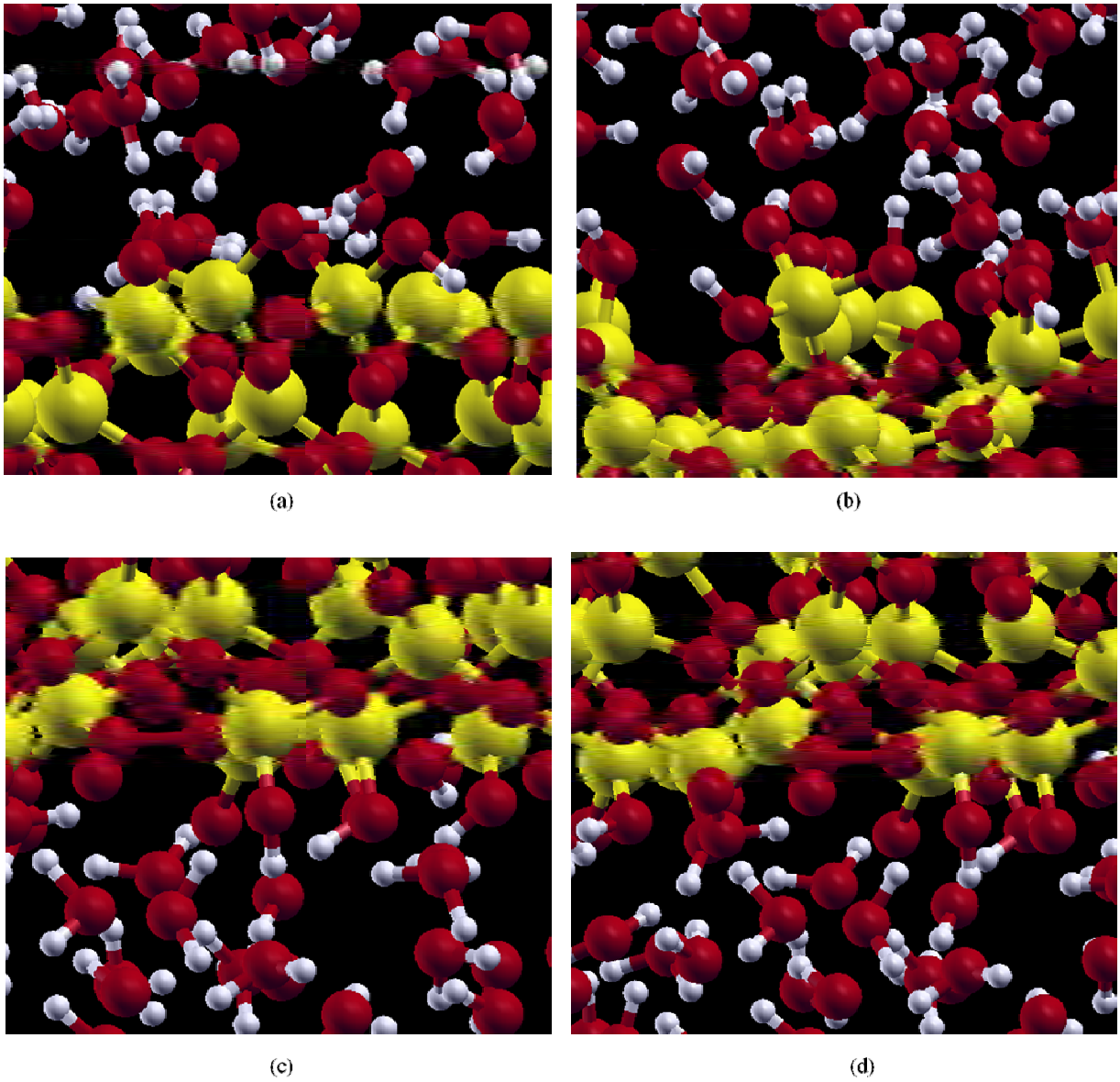

Fig. 4.5. The quartz system A structure after 6.0000ps simulation. (a) Geminal silanol group [$Si(OH)_2$]. (b) Triple silanol group [$Si(OH)_3$]. (c) Single silanol [Si(OH)]. (d) Peroxy link Si-O-O-Si.

Both quartz surfaces were predominantly terminated by geminal silanol groups [$Si(OH)_2$] as shown in Fig. 4.5(a) and Fig. 4.6(a). The single silanol groups, [SiOH], were also observed in both quartz surfaces (Fig. 4.5(c) and Fig. 4.6(b)). One triple silanol group, [$Si(OH)_3$], was formed on Si-terminated of system A as shown in Fig. 4.5(c). This type of silanol group was not found on O-terminated of system A and also system B. The triple silanol (relatively rare) was

initiated by the breaking of one Si-O bond in the bulk area. The Si atom bound other three OH^- from the water molecules and formed the triple silanol. The breaking O atom in the bulk attached to the adjacent Si surface arise the new Si-O-Si bridge. Finally, to saturate the coordination number, the adjacent Si was bound to one OH^- specie from the water molecule forming the single silanol. The other single silanol was detected at terminal Si. Similar to previous study [Adeagbo et al., 2008], we found the Si-H act as the complement of coordination number. In addition, we observed the defect of quartz surface like peroxy link, Si-O-O-Si, and peroxy, Si-O-O-H, on O-terminated system A (Fig. 4.5(d)) but not in Si-terminated system A and system B. The detailed description of peroxy link formation will be presented in the next subsection.

The unsaturated sites were found in system A and system B. In system A, we observed the presence of O and Si atoms with only one and two coordination number, respectively. The presence of unsaturated O atom at the quartz surface have been detected in the XPS measurement which has changed the position and intensities of recorded Si 2p and O 1s line [Duval et al., 2002]. Meanwhile, the two coordinated Si atom has been presumably exist as defect on quartz surface based on the luminescence polarization [Griscom, 1991; Skuja et al., 1984]. The two coordinated Si atom was observed in the environment with two or three other two coordinated Si and four or three the saturated Si either geminal, single or triple silanol. The Si-O to the bulk oxygen was found longer than the saturated site. As a comparison the unsaturated Si has Si-O distance ~1.70 Å and O-Si-O angle less than 100° which is different to the other Si-O bond distance ~1.65 Å and O-Si-O angle ~109.5°.

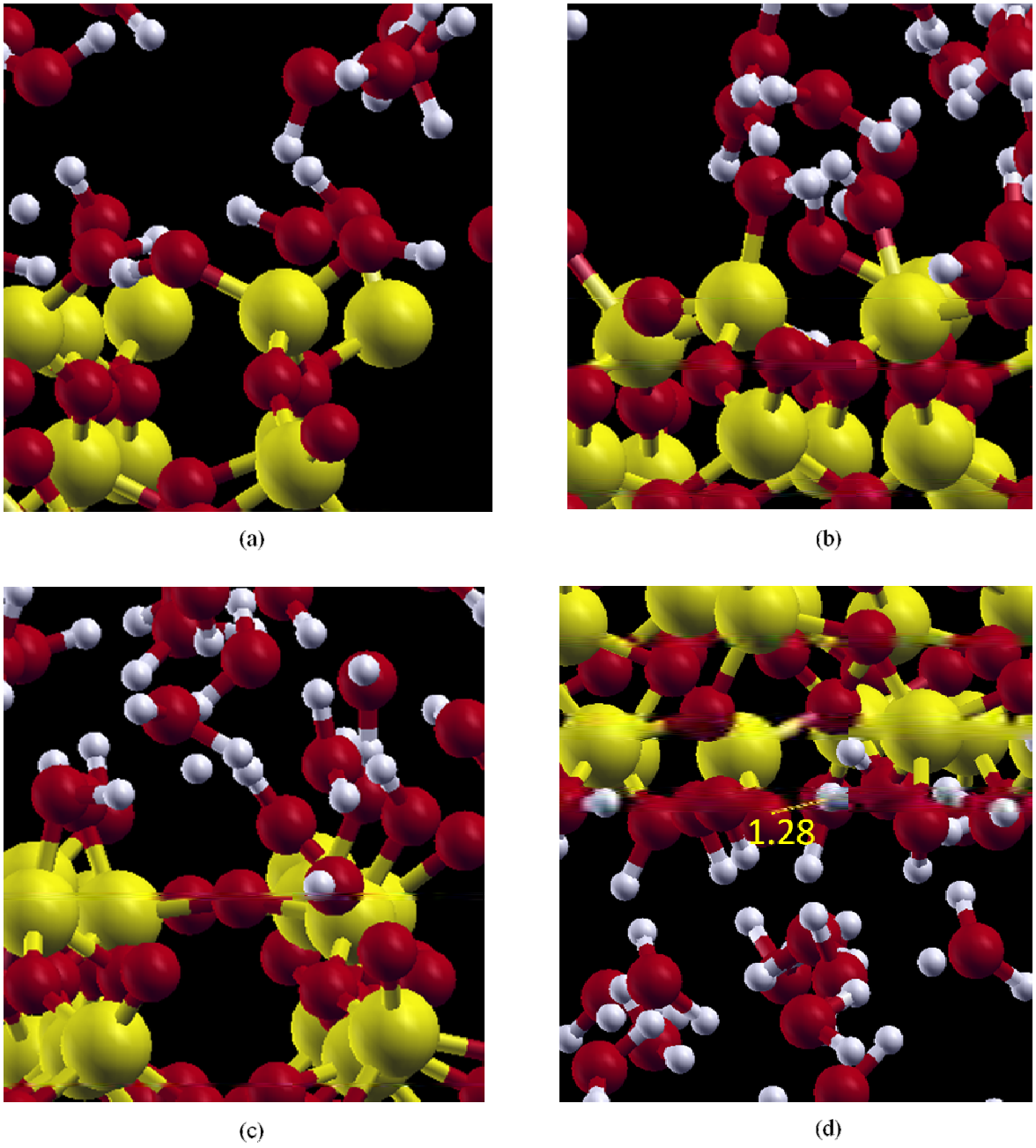

Fig. 4.6.The quartz system B structure after 6.0000ps simulation. (a) Geminal silanol group [$Si(OH)_2$]. (b) Single silanol group [Si(OH)]. (c) Siloxane bridge Si-O-Si. (d) Internal hydrogen bond.

One unsaturated site was found in system B as the one coordinated O atom. Interestingly, the unsaturated site was stabilized by the internal hydrogen bond. The internal hydrogen bond

was observed as one water molecule at the initial configuration as shown in Fig. 4.7. The dissociation was observed ~0.3 ps and each species bound to different sites. We labeled the atom into O_w for the oxygen atom which in the end of simulation act as the donor atom, H_{1w} refers to the hydrogen atom which involve in the internal hydrogen bond, and H_{2w} corresponds to the hydrogen atom which is bound to other O surface (O_2) at the last part of simulation trajectory. We found the OH group always vibrates during the simulation and interacts with other sites surround them. This interaction has induced the transfer of hydrogen atom from one site to another site. In every transition of hydrogen transfer, the distance and angle was found change significantly, as shown at ~0.3ps and ~5ps. The angle at hydrogen transfer always have value near 180° which means two oxygen atoms in the parallel position with hydrogen atom between them. The O_w-H_{2w} was found break and the other OH group was formed by H_{2w} and O_2, simultaneously. At the end of simulation, the unstable O_w started to construct the internal hydrogen bond with H_{1w}. This internal hydrogen bond is very dynamic, as shown in Fig. 4.7(a) the O_w and O_1 has almost similar distance with the H_{1w} occasionally. Moreover, at some points, we found the O_w and H_{1w} has covalent-like bond. The internal hydrogen bond is very strong with 1.504 Å of average distance (at last 0.5 ps) which is even shorter than the strong hydrogen bond in the previous first principles calculation of quartz-thin layer water interface [Yang and Wang, 2006]. The existence of internal hydrogen bond was supported by the angle of O_w-H_{1w}-O_1 which frequently 180°. This angle is important to show that the covalent bond O_1-H_{1w} is directed to the O_w.

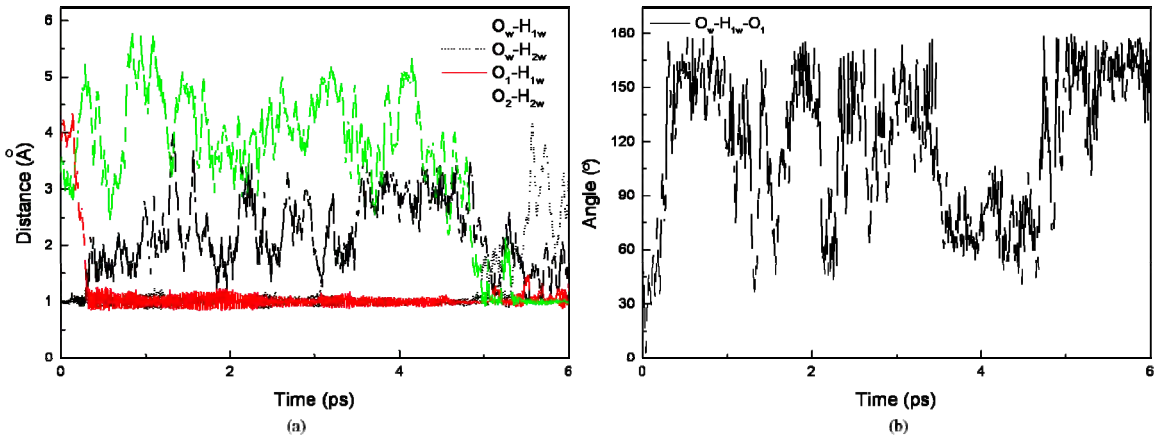

Fig. 4.7 The structure parameter during the formation of internal hydrogen bond. (a) distance as function of time. (b) angle as function of time.

4.3.2 Peroxy Link

The first peroxy link was detected at 0.20 ps of simulation. We found there are two peroxy links generated in O-terminated system A. The peroxy linkage formation was started by the slowly distance-decreasing of the adjacent =Si-$(O)_2$ on system A. The snapshot of simulation has shown the peroxy link formation did not involve water molecules directly. It was found that the precursor =Si-$(O)_2$ did not react with water molecules. These precursors did not undergo the silanol phase. They were only interacted each other, then at certain distance (~1.5 Å) the peroxy link is formed. As shown in the previous work the ≡Si-O-O specie was detected at 'dry' and "wet" environment, which means water did not involve directly to the formation of peroxy link [Friebele et al., 1979]. The mechanism of peroxy link formation step-by-step is illustrated in Fig. 4.8.

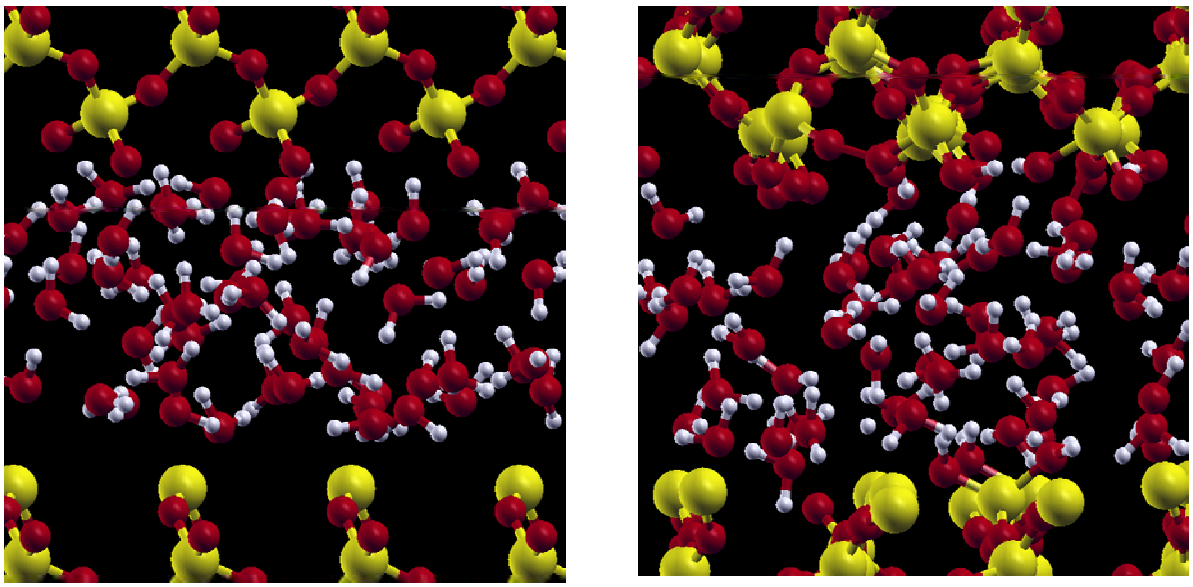

(a) 0.000 ps (b) 0.2000 ps

Fig. 4.8. The mechanism of peroxy bridge formation at 1000 K. (a) The initial structure t = 0.0000 ps). (c) The first peroxy link was formed at 0.2000 ps.

The stability of peroxy link can be seen in the temporal evolution of structure parameters (Fig. 4.9). The bond length and angle of peroxy link are fluctuated in small range. The silicon and oxygen atom of peroxy link distance has similarity with other Si-O bond. We found not much difference before and after the peroxy link formed. The significant change occurred at the O-O and Si-Si bond length. The distance of O-O and Si-Si are shorter than the other adjacent O-O and Si-Si. The distance of ordinary O-O, initially around 2.5 Å, is significantly decreased into~1.5 Å when the peroxy link generated [Ricci et al., 2001; Liang and Tse, 2009]. The shorter distance of O-O in peroxy link has influenced the Si-Si bond length by slightly decreasing from ~5 Å to ~4 Å. The decrease of Si-O-O angle is observed when the peroxy link formed. We found the peroxy link is located in the plane geometry since the dihedral angle is close to 180°. These structure parameters are in good agreement with the previous simulation [Ricci et al., 2001]. The difference was mainly detectable for the Si-Si distance and Si-O-O angle, which likely results from the different local environment. Although, the water molecules in our simulation did not influence the peroxy link formation, the environment might influence the geometry parameters. The previous optimized configuration [Ricci et al., 2001] consists of pure quartz, while our system involves the water molecules.

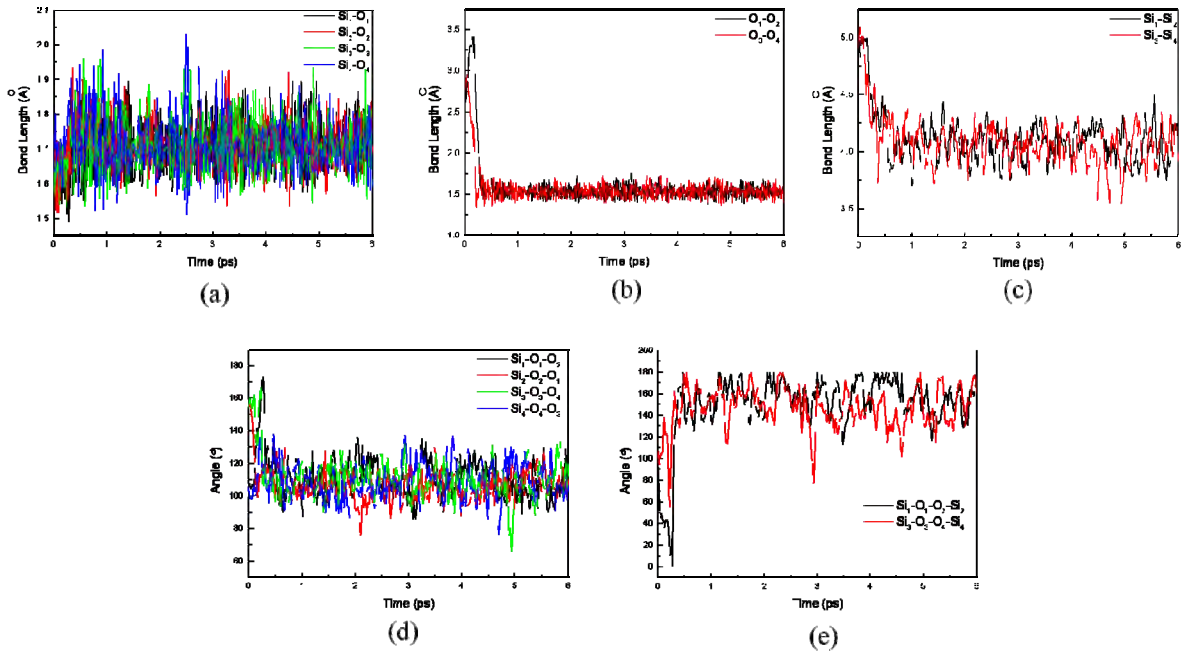

Fig. 4.9.The structure parameter of peroxy link Si-O-O-Si as function of time. (a) Si-O distance. (b) O-O distance. (c) Si-Si distance. (d) Si-O-O angle. (e) dihedral angle Si-O-O-Si.

4.3.3 Peroxy Si-O-O-H

The peroxy radical H-terminated, Si-O-O-H, was observed only in O-terminated system A. Like peroxy link, we found two peroxy radicals generated during the simulation. We have witnessed the peroxy radical with good stability at least more than 3 ps. The two peroxy radicals have different formation mechanism. The formation of first peroxy radical was initiated by the attachment of OH^- to the O surface atom. Interestingly, we found the Si atom can bind five O atoms before the Si-O-O-H group was formed. This intermediate specie has exchanged the O atom of surface with the O atom of water in the opposite order. The exchange of O atom of surface and O atom of water can be observed from the temporal evolution of structure parameters as shown in Fig. 4.10.Anotherperoxy radical was started by the binding of H atom of water to the O atom of surface. In the next step, the newly OH group is attached to other O atom of surface which finally led to the second peroxy radical. We found the structure parameters of peroxy radical (Si-O, O-O bond length and Si-O-O angle) similar to the peroxy link as mentioned above.

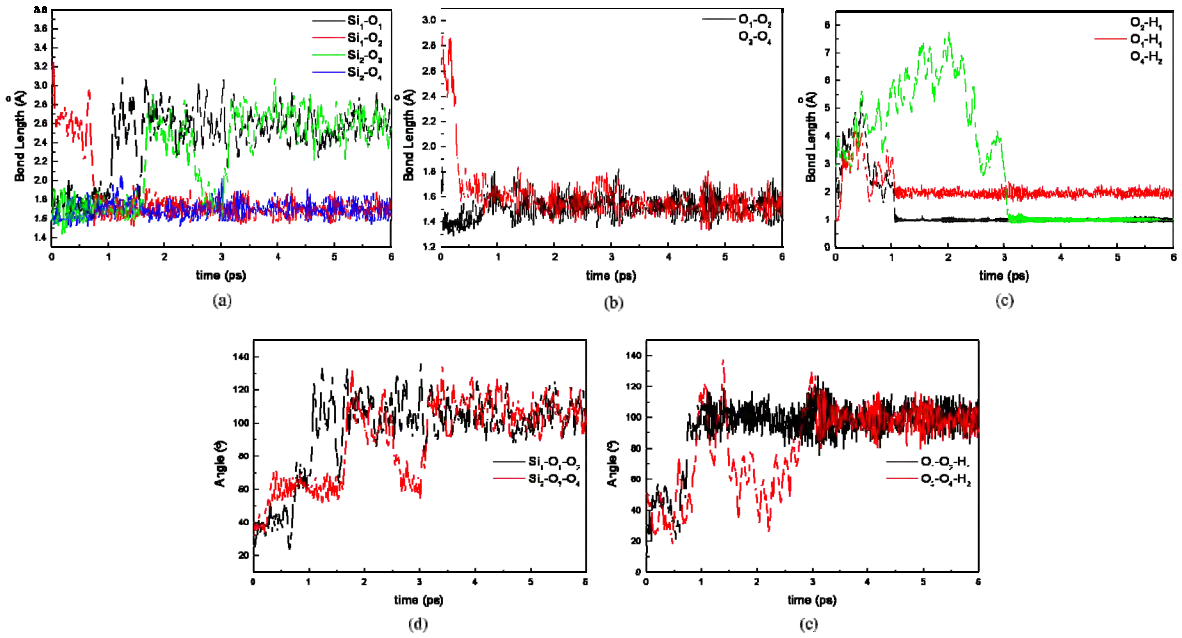

Fig. 4.10.The structure parameter of peroxy radical Si-O-O-H as function of time. (a) Si-O distance. (b) O-O distance. (c) O-H distance. (d) Si-O-O angle. (e) O-O-H angle.

4.3.4 Comparisons of Two Different Surfaces

From the energetic view, the system A was found to have enthalpy much higher than system B as shown in Fig. 4.11. In general, the formation of silanol group and other feature which saturated the quartz surface has decreased the enthalphy of both surfaces. Regarding the complexity of system A, we might assume the initial energy of system has influenced the process of quartz surface termination in aqueous environment.

The initial structure of quartz surfaces have resulted in different features on the final surface. Based on our simulation, the feature of system A (which is energetically higher) seems richer than system B. In the system B, we have only found the silanol groups in geminal and single types within the total time of our calculations. The other feature is siloxane bridge, which is common in the quartz surface. The interesting fact in the system B was that we found the unsaturated oxygen site was accompanied by an internal hydrogen bond with the new formed silanol. With distance 1.504 Å in average of last 0.5 ps which is shorter than the hydrogen bond of quartz hydrophilic surface in the previous first principles calculation [Yang and Wang, 2006]. We believe that this is a strong hydrogen bond. The angle 180° of O-H-O also has supported our investigation of internal hydrogen bond. Moreover, the Si-O bond length of unsaturated site in system B was found to be 1.639 Å which belongs to the single bond category. The unsaturated O surface in system A also exists in single bond based on the average bond length ~1.650-1.700, which is also significantly longer than Si=O double bond distance ~1.52 Å [Kageshima and Shiraishi, 1997]. No Si=O double bond was detected in our interface systems. Another interesting feature at system A is the present of Si-H which is coming from the binding OH^- and H^+ of one water molecule to the same Si terminal.

The absence of peroxy link at system B might result from the product competition of fresh quartz surface and water reaction. It seems the initial structure of system B provides more sites to the silanol formation than peroxy link. As mentioned before, the system B is covered by silanol groups more than system A. We observed the silanol groups are very stable, once formed the specie exist until the end of simulation. We did not notice reaction between two adjacent silanol which create the peroxy link as proposed by previous work [Freund, 1985]. The adjacent silanol in system A also presents the similar behavior. They are stable as silanol until 6 ps of simulation without any additional reaction. The siloxane bridge (Si-O-Si) was also present as

product of fresh quartz surface and water reaction. The nearest distance O atom at system B (~4.9 Å) is almost twice of system A (~2.5 Å). The formation of siloxane bridge is preferable, due to the shorter distance of Si surface-O surface (~3.4 Å) than the O-O distance. As the two (three)-membered ring quartz surface was believed with high local stress field and favors hydroxylation at a relatively high temperature [Mischler et al., 2005], we have also analyzed the detailed ring statistics for the quartz slab with the new formed Si-O-Si bridge and found that the newly formed rings at surface are from 4- to 7- member ring for both surfaces, and therefore 2- and 3-member rings are ruled out in this system.

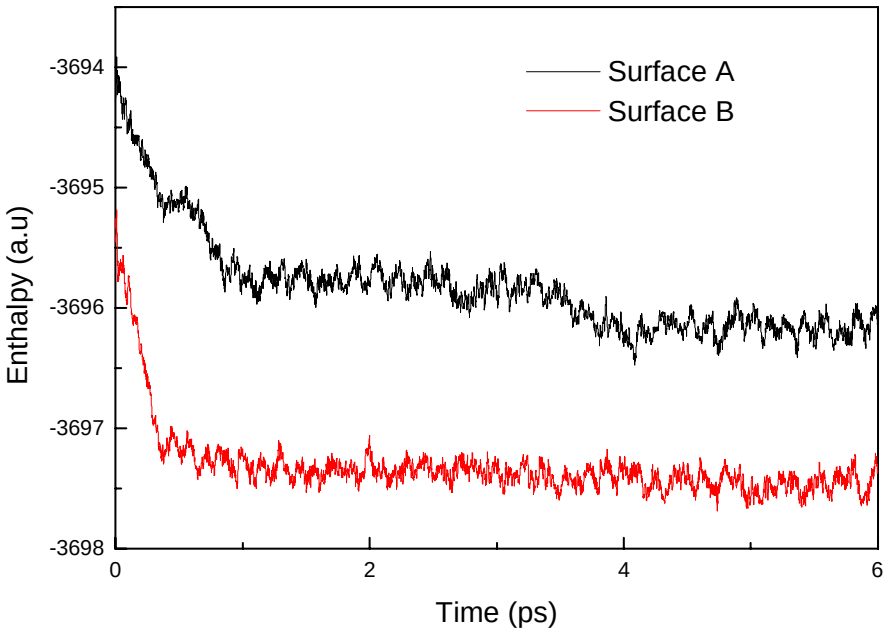

Fig. 4.11.Temporal evolution of the interface system for two different new cleaved quartz surfaces (System A and System B).

4.4 Quartz Surface in Non-aqueous Environment

Similar to simulation of quartz surface in aqueous environment, the simulation in non-aqueous environment was started by using the clean surface and liquid methane as substituent of water (Fig. 4.12). In this simulation, we only concern to system B due to the result of quartz-

water interface as shown in the previous. Methane has different behavior compare to water. If water molecules immediately dissociate into ionic species, the methane molecules were observed undissociated during the simulation. We also did not found any reaction between methane molecules and quartz surface. It seems the methane molecules only provide the atmosphere for quartz surface to arrange its structure. The final structure of quartz surface under methane atmosphere is dominated by siloxane bridge. We did not found any silanol group in this system. The methane atmosphere has generated the quartz surface as the hydrophobic surface.

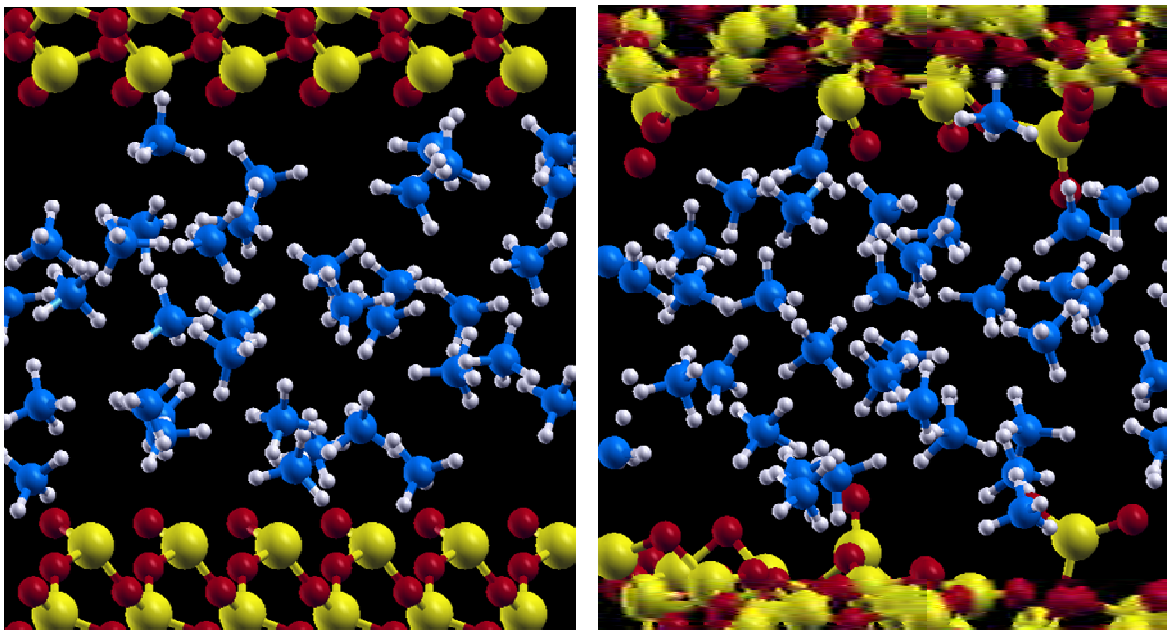

Fig. 4.12 The liquid methane in between System B. (a) Initial configuration (t= 0.0000 ps). (b) Last configuration (t= 6.0000 ps). Color legend: O: red, Si: yellow, C: blue, H: white.

The formation of siloxane bridge was found for the first time at 0.3025 ps as shown in Fig. 4.13. We define the siloxane bridge as the distance of O and S atom in the surface less than 1.85 Å, and we assumed there is no breaking in the old Si-O bond surface. The number of siloxane bridge relative constant after 4.0 ps and reach ~12 Si-O-Si at the end of simulation. This number significantly larger than the formation of siloxane bridge in the water environment which is around 4 Si-O-Si in the same quartz surface and simulation time. At the end of simulation, we still observed the unsaturated sites either three-coordinated Si or one-coordinated O atom. The

three-coordinated Si atom was found bind the one-coordinated O atom which means both atoms lose one coordination number. The distance between these atoms is ~1.55 Å in average that very close to the value of Si=O bond length [Kageshima and Shiraishi, 1997].

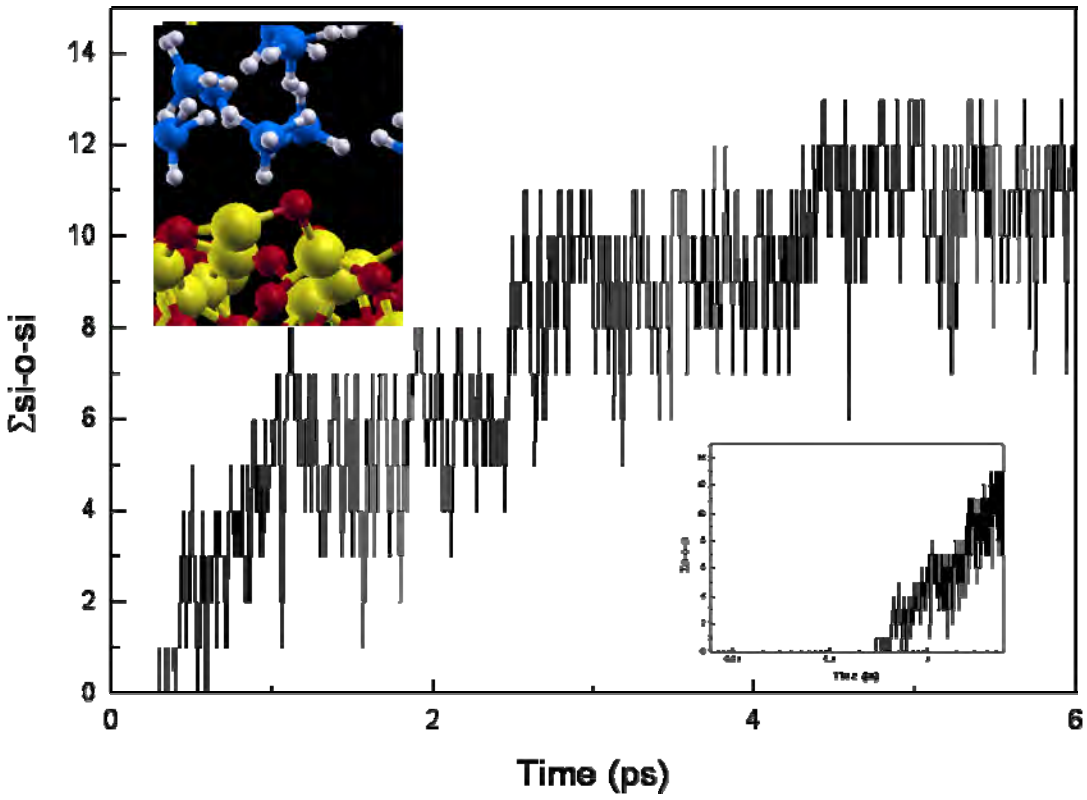

Fig. 4.13 The formation of siloxane bridge at system B (shown in the top inset). The first siloxane bridge was observed at 0.3025 ps (bottom inset).

The surface self-arrangement of quartz has generated some new ring features. We found from 2- to 9-membered ring at the final structure of quartz surface in methane environment. In the water environment, only 4 until 7-membered ring was found. The two (three)-membered ring is known as the defect of quartz surface which is reactive to water molecules. Therefore, this feature did not found in the water environment. We selected randomly one of two-membered ring to see the mechanism process and the stability by observing the distance and angle (Fig.

4.14). The selected two-membered ring was formed at 2.35 ps and still stable until the end of simulation. This ring was built from one O and Si of surface and bulk. The ring was formed by connecting the O surface to the Si bulk. The average distance Si-O and angle O-Si-O in the last 2 ps trajectory are 1.72 Å and 86.924°, respectively. These numbers are very close to the structure parameter of two-membered ring, 1.70 Å and 90° for Si-O distance and O-Si-O angle, respectively, which is optimized by the first principles calculation [Ceresoli et al., 2000]

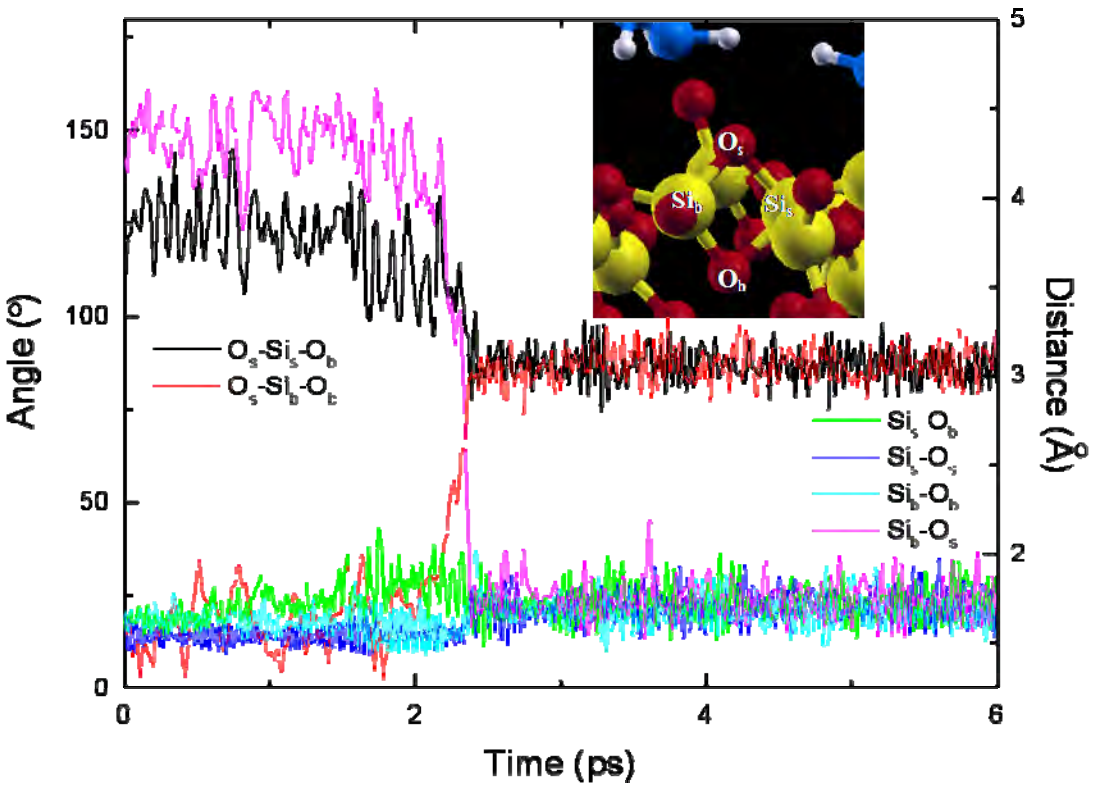

Fig. 4.14 The formation of one two-membered ring as a function of time. Note: subscript s and b represent surface and bulk, respectively.

4.5 Conclusion

This study presents the quartz surface structure in aqueous environment for two different initial fresh quartz surfaces by using first-principles molecular dynamics. The rapid hydroxylation of fresh quartz surfaces were observed in our simulation. Within 4.0 ps of simulation time, more than 50% of quartz surfaces have already been covered by silanol groups. We found system B provide more preferable site for silanol formation than system A. Until the end of simulation, system B has shown several features, such as geminal silanol, single silanol and siloxane bridge. Surprisingly, system A has more complicated structure. We found geminal silanol, single silanol, triple silanol, and some defects, i.e. peroxy link and peroxy radical. From energy point of view, the likely surface structure is System B, but the defects as observed in case of system A are definitely noteworthy.

In addition, the substitution of water by methane in system B has generated the hydrophobic quartz surface which is dominated by siloxane bridge feature. Moreover, methane molecules were found no interaction with system B, which means only provide the atmosphere of quartz surface "self-arrangement". We also observed the formation of two (three)-membered rings which is commonly occurred at dehydroxylation of hydrophilic quartz surface. We found this defect keep stable for ~4 ps. The unsaturated site in this system was found stabilized by the formation of Si=O feature which is proven by the short distance as ~1.55 Å.

The breaking and making bond process, as observed in the First Principles Molecular Dynamics, has allowed us to monitor the reaction mechanism in details. As we observed in our simulation, the reaction between fresh quartz surface (system A and system B) and liquid water has several mechanism with varies of intermediate species. We found the "dimer" water molecules during the first formation of silanol groups at O terminal system A. The other silanol formation was through the dissociation of water molecules to H^+, OH^- and H_3O^+ before each species move to the unsaturated site at the surface. The simultaneous formation of two adjacent silanol was also observed. The final structure of system A and system B would give the additional information of quartz surface variation which strongly depends on the initial structure and environment of the fresh quartz cleavage. The larger system of quartz surface may be generated from the resulting surface of our study, which may eventually be a promising model and represents the real interaction in nature.

References

Adeagbo, W. A., Doltsinis, N. L., Klevakina, K. and Renner, J. Transport processes at α-quartz-water interfaces: Insights from first-principles molecular dynamics simulations. Chem. Phys. Chem. **9**, 994-1002 (2008).

Argyris, D., Cole, D. R. and Striolo, A. Dynamic behavior of interfacial water at the silica surface. J. Phys. Chem C **113**, 19591-19600 (2009).

Balk, M., Bose, M., Ertem, G., Rogoff, D. A., Rothschild, L. J. and Freund, F. T. Oxidation of water to peroxide at the rock-water interface due to stress-activated electric currents in rocks. Earth and Planetary Science Letters **283**, 87-92 (2009).

Bandura, A. V., Kubicki, J. D. and Sofo, J. O. Periodic density functional theory study of water adsorption on the α-quartz (101) surface. J. Phys. Chem. C **115**, 5756-5766 (2011).

Becke, A. D. Density-functional exchange-energy approximation with correct asymptotic behavior. Phys. Rev. A **38**, 3098-3100 (1988).

Bunker, B. C., Haaland, D. M., Ward, K. J., Michalske, T. A., Smith, W. L., Binkley, J. S., Melius, C. F. and Balfe, C. A. Infrared spectra of edge-shared silicate tetrahedral. Surf. Sci. **210**, 406-428 (1989).

Ceresoli, D., Bernasconi, M., Iarlori, S., Parrinello, M., and Tosatti, E. Two-membered silicon rings on the dehydroxylated surface of silica. Phys. Rev. Lett. **84**, 3887-3890 (2000).

Coasne, B., Alba-Simionesco, C., Audonnet, F., Dosseh, G. and Gubbins, K. E. Adsorption and structure of benzene on silica surfaces and in nanopores. Langmuir **25**, 10648-10659 (2009).

De Leeuw, N. H., Higgins, F. M. and Parker, S. C. Modeling the surface structure and stability of α-quartz. J. Phys. Chem. B **103**, 1270-1277 (1999).

Du, Q., Freysz, E. and Shen, Y. R. Vibrational spectra of water molecules at quartz/water interfaces. Phys. Rev. Lett. **72**, 238-241 (1994).

Duval, Y., Mielczarski, J. A., Pokrovsky, O. S., Mielczarski, E. and Ehrhardt, J. J. Evidence of the existence of three types of species at the quartz-aqueous solution interface at pH 0-10: XPS

surface group quatification and surface complexation modeling. J. Phys. Chem. B **106**, 2937-2945 (2002).

Edwards, A. H. and Fowler, W. B. Theory of the peroxy-radical defect in *a*-SiO_2. Phys. Rev. B **26**, 6649-6660 (1982).

Freund, F. Conversion of dissolved "water" into molecular hydrogen and peroxy linkage. J. Non-Crystaline Solids **71**, 195-202 (1985).

Freund, F. T., Takeuchi, A. and Lau, B. W. S. Electric currents streaming out of stressed igneous rocks- A step towards understanding pre-earthquake low frequency EM emissions. Phys. Chem. Earth **31**, 389-396 (2006).

Freund, F. T., Takeuchi, A., Lau, B. W. S., Al-Manaseer, A., Fu, C. C., Bryant, N. A and Ouzounuv, D. Stimulated infrared emission from rocks: assessing a stress indicator. eEarth **2**, 1-10 (2007).

Freund, F. Toward a unified solid theory state theory for pre-earthquake signals. Acta Geophysica **58**, 719-766 (2010).

Friebele, E. J., Griscom, D. L., Stapelbroek, M., and Weeks, R. A. Fundamental defect centers in glass: The peroxy radical in irradiated, high purity, fused silica. Phys. Rev. Lett. **42**, 1346-1349 (1979).

Goedecker, S., Teter, M. and Hutter, J. Separable dual-space Gaussian pseudopotentials. Phys. Rev. B **54**, 1703-1710 (1996).

Goumans, T. P. M. Wander, A., Brown, W. A. and Catlow, C. R. A. Structure and stability of the (001) α-quartz surface. Phys. Chem. Chem. Phys.**9**, 2146-2152 (2007).

Griscom, D. L. Optical properties and structure of defects in silica glass. J. Ceramic Soc. Japan **99**, 923-942 (1999).

Iller, R. K. The colloid chemistry of silica and silicates. Cornell University Press, New York, 1955.

Kageshima, H. and Shiraishi, K. Microscopic mechanism for SiO_2/Si interface passivation: Si=O double bond formation. Surf. Sci. **380**, 61-65 (1997).

Klaus, J. W., Sneh, O. and George, S. M. Growth of SiO_2 at room temperature with the use of catalyzed sequential half reactions. Science **278**. 1934-1936 (1997).

Kokalj, A. Computer graphics and graphical user interfaces as tools in simulations of matter at the atomic scale. Comp. Mat. Sci. **28**, 155-168 (2003).

Lee, C. T., Yang, W. T. and Parr, R. G. Development of the Colle-Salvetti correlation-energy formula into a functional of the electron density. Phys. Rev. B **37**, 785-789 (1988).

Liang, Y. and Tse, J. S. Mechanism for the formation of H_2 and O_2 from x-ray irradiated dense ice. Phys. Rev. B **79**, 104105 (2009).

Liang, Y., Miranda, C. R. and Scandolo, S. Temperature-induced densification of compressed SiO_2 glass: A molecular dynamics study. High Pressure Research **28**, 35-44 (2008).

Lippert, G., Hutter, J and Parrinello, M., A hybrid Gaussian and plane wave density functional scheme. Mol. Phys. **92**, 477-487 (1997).

Liu, W.-T. and Shen, Y. R. Surface vibrational modes of α-quartz (0001) probed by sum-frequency spectroscopy. Phys. Rev. Lett. **101**, 016101 (2008).

Marians, C. S. and Hobbs, L. W. The phase structure of aperiodic SiO_2 as a function of network topology. J. Non-Crystalline Solids **106**, 309-312 (1988).

Mischler, C., Horbach, J., Kob, W., and Binder, K. Water adsorption on amorphous silica surfaces: a Car-Parrinello simulation study. J. Phys.: Condensed Matter **17**, 4005-4013 (2005).

Murashov, V. V. Reconstruction of pristine and hydrolyzed quartz surface. J. Phys. Chem. B **109**, 4144-4151 (2005).

Nose, S. A molecular dynamics method for simulations in the canonical ensemble. Mol. Phys. **52**, 255-268 (1984).

Ostroverkhov, V., Waychunas, G.A. and Shen, Y.R. Vibrational spectra of water at water/α-quartz (0001) interface. Chem. Phys. Lett. **386**, 144-148 (2004).

Parks, G. A. Surface and interfacial free energies of quartz. J. Geophys. Res.: Solid Earth **89**, 3997-4008 (1984).

Ricci, D., Pacchioni, G., Szymanski, M. A., Shluger, A. L. and Stoneham, A. M. Modelling disorder in amorphous silica with embedded clusters: the peroxy bridge defect center. Phys. Rev. B **64**, 224104 (2001).

Rignanese, G. -M., Charlier, J., -C. and Gonze, X. First-principles molecular-dynamics investigation of the hydration mechanisms of the (0001) α-quartz surface. Phys. Chem. Chem. Phys. **6**, 1920-1925 (2004).

Schlegel, M. L., Nagy, K. L., Fenter, P. and Sturchio, N. C. Structures of quartz $(10\bar{1}0)$- and $(10\bar{1}1)$-water interfaces determined by X-ray reflectivity and atomic force microscopy of natural growth surfaces. Geochim. Cosmochim. Acta **66**, 3037-3054 (2002).

Skelton, A. A., Wesolowski, D. J. and Cummings, P. T. Investigating the quartz (10-10)/water interface using classical and ab initio molecular dynamics. Langmuir **27**, 8700-8709 (2011).

Skuja, L. N., Streletsky, A. N. and Pakovich, A. B. A new intrinsic defect in amorphous SiO_2: twofold coordinated silicon. Sol. State Comm. **50**, 1069-1072 (1984).

Takeuchi, A. Positive holes flowing through stressed igneous rocks. Electrical Engineering in Japan **169**, 307-310 (2009).

Vande Vondele, J., Krack, M., Mohamed, F., Parrinello, M., Chassaing, T. and Hutter, J. QUICKSTEP: Fast and accurate density functional calculations using mixed Gaussian and plane waves approach. Comp. Phys. Comm. **167**, 103-128 (2005).

Yang, J. and Wang, E. G. Water adsorption on hydroxylated α-quartz (0001) surfaces: From monomer to flat bilayer. Phys. Rev. B **73**, 035406 (2006).

Zhuravlev, L. T. The surface chemistry of amourphous silica. Zhuravlev model. Colloids and Surfaces A: Physicochem. Eng. Aspects **173**, 1-38 (2000).

CHAPTER 5

Effect of Temperature on Quartz Structure

In this chapter, we investigate the negative (zero) thermal expansion phenomenon presented in β-quartz. By using classical and first principles molecular dynamics simulations, we found that the negative thermal expansion of β-quartz is not necessarily connected with the "repopulation" of α-states as proposed recently [Huang and Kieffer, 2005]. We also explain why the bulk modulus of β-quartz increases with temperature on basis of the structure parameters, such as Si-O-Si angle and Si-O bond length, response to pressure.

5.1 Introduction

5.1.1 Theory

The properties of material can change in the variation of temperature, due to the structure respond to this parameter. Above the absolute zero temperature, atom has thermal vibration which can improve to the macroscopic properties called thermal expansion. The fundamental of volume thermal expansion coefficient and several thermodynamics quantities relation is derived by Grüneisen in 1926, also known as Grüneisen's law [Kirchner, 1964]. In simple way, the equation is derived by using Euler reciprocity relation, as shown in Eq. (5.1).

$$\left(\frac{\partial P}{\partial T}\right)_V = \left(\frac{\partial S}{\partial V}\right)_T \tag{5.1}$$

with P is the pressure, T is the absolute temperature, V is the volume and S is the entropy. The Maxwell's relation can transform Eq. (5.1) to Eq. (5.2)

$$-\left(\frac{\partial P}{\partial V}\right)_T \left(\frac{\partial V}{\partial T}\right)_P = -\left(\frac{\partial S}{\partial T}\right)_T \left(\frac{\partial T}{\partial V}\right)_P \tag{5.2}$$

Therefore

$$K_T \alpha_v = -\frac{C_v}{T}\left(\frac{\partial T}{\partial V}\right)_S \tag{5.3}$$

with α_v is the volume coefficient of expansion $\left(\frac{1}{V}\frac{\partial V}{\partial T}\right)_P$, K_T is the isothermal bulk modulus $\left(-V\frac{\partial P}{\partial V}\right)_T$ and C_v is the heat capacity at constant volume. In the use of Eq. (5.3), the important point is the smaller electronic specific heat relative to the total. If γ is defined as

$$\gamma = -\frac{V}{T}\left(\frac{\partial V}{\partial T}\right)_S = -\left(\frac{\partial lnT}{\partial lnV}\right)_S \tag{5.4}$$

Then

$$\alpha_v = \frac{\gamma C_v}{V K_T} = \frac{\gamma C_P}{V K_S} \tag{5.5}$$

with K_S is the adiabatic bulk modulus and C_P is the heat capacity at constant pressure. The equation (5) has the same form with Grüneisen's law, as shown in Eq. (5.6)

$$\alpha_v = \frac{\gamma_G C_v \chi}{V} \tag{5.6}$$

with χ is the compressibility and γ_G is the Grüneisen's constant. The Grüneisen's law gives the information that thermal expansion will vary with temperature as does the heat capacity, C_v, and the material with strong bonds will have lower thermal expansion [Roy et al., 1989]. The α_v normally in positive value, but the experiment has shown some materials have negative value of α_v. The zero (and negative) thermal expansion of solids on heating is an anomalous phenomenon since it contradicts with the intuitive conception that atoms need more space as the vibrational amplitude increase at elevated temperature.

5.1.2 The Anomaly of Quartz Thermal and Mechanical Properties at High Temperature

Quartz, as a common rock-forming mineral component in the crust of the earth, has become one of the main objects for more than a century because of its technological and geological importance. The response of quartz to elevated temperature can trigger cracks in quartz ceramics if the heating rate is not sufficiently slow. The cracks are believed to be connected with the α-β phase transition at 573°C and the negative (zero) thermal expansion of β-quartz at higher temperature [Dolino, 1990]. While some experiments show negative thermal

expansion of β-quartz at high temperature [Jay, 1933; Ackermann and Sorrell, 1974; Kihara, 1990; Bourova and Richet, 1998; Mao et al., 2001], the others show zero thermal expansion [Carpenter et al., 1998; Hudon et al., 2002]. These two evidences have become debate among scientists [Hudon et al., 2002]. Of particular, it was pointed out in their paper [Hudon et al., 2002] that attempts by taking into account the negative thermal expansion of β-quartz had failed to produce a coherent silica phase diagram. Given the importance of the quartz in earth sciences, the thermal expansion of quartz and its underlying nature needs to be scrutinized further.

The structure parameter like Si-O bond length and bending of Si-O-Si angle gave contribution to negative thermal expansion which suggested by Kihara (2001) and Welche et al. (1998). Huang and Kieffer (2005) observed negative thermal expansion immediately after α-β transition in the case of quartz and cristobalite. They relate the negative thermal expansion to the 'repopulation' of α-phase. On the other hand, Takada et al. (2008) has shown the decreasing of α-phase concentration as function of temperature. Simulation by Herzbach et al. (2005) which applied some interatomic forces showed different trend which is zero thermal expansion. The experiment and theoretical works has shown two kinds of quartz response of temperature, but still there is no satisfied explanation for this problem. For experimental measurements, the result might be strongly affected by impurity. On the other hand theoretical studies will be varied by the suitable interatomic force field. Therefore, it is of essential importance to study the phase diagram by mapping many different temperature and pressure points using classical molecular dynamics (MD).

The mechanical properties of β-quartz remain of interest to researchers due to its peculiar behavior. Usually, the bulk modulus of material decreases with temperature. As we know at ambient pressure, the low and high temperature phases are α-quartz and β-quartz, respectively. Consider to this statement, β-quartz should be less stiff than α-quartz, but in reality β-quartz has higher bulk modulus than the α-quartz [Kammer and Atanasoff, 1942; Ohno et al., 2006; Lakhstanov et al., 2007]. Moreover, the bulk modulus of β-quartz continues to increase with temperature up to at least 1520°C [Lakhstanov et al., 2007]. This anomaly can in fact generate a measurable seismic signature [Mechie et al., 2004] and therefore offers the possibility for precisely estimating temperature and pressure of the middle continental crust from the known phase diagram of silica. However, the mechanism of such bulk modulus anomaly is still unclear.

As the bulk modulus is defined by the pressure increase needed to cause a relative decrease in volume, it is interesting to jointly consider the bulk modulus anomalies and the volume as function of temperature and pressure (namely, the zero or negative thermal expansion).

Through numerous experimental and theoretical studies, especially by the results of neutron scattering [Wright and Lehmann, 1981], NMR measurements [Spearing et al., 1992] and molecular dynamics simulations [Tsuneyuki et al., 1990; Kimizuka et al., 2003; Huang and Kieffer, 2005], it is clear now that β-quartz at ambient pressure and at elevated temperature is a dynamically disordered phase, in which the atoms in fact hop between two equivalent α_1 and α_2 structures by anharmonic motions, when average over a long time, yields an ordered structure with hexagonal symmetry. It was shown, at atomic scale, that the α-β transition involves a cooperative rotation of the Si-O-Si bonds about the Si-Si axis [Huang and Kieffer, 2005] and the Si-O-Si planes in the β phase do not remain steady at these characteristic orientations relative to those in the α-state. Further, it was concluded in their paper that the nearly zero or negative thermal expansion of the β-quartz is a consequence of the "repopulation of α-states" [Huang and Kieffer, 2005]. However, this theory didn't consider the thermal expansion of the repopulated α-states, therefore not completed. Lattice dynamics [Smirnov, 1999] on the other hand can give an explanation based on the negative Grüeneisen constant, but, it lacks an intuitive picture of the inherent large fluctuations of the atomic motion and the detailed knowledge of the dynamic structures.

5.2 Computational Detail

Molecular dynamics (MD) is employed as tool to disclose the anomalies of quartz's thermal and mechanical properties. The potential, developed by Tangney and Scandolo, which was parametrized by using the forces, stresses and energies extracted from first principles calculation and had taken account of the large polarizability of the oxygen ion [Tangney and Scandolo, 2002]. This interatomic force field has already been used in various studies and shown a very good agreement with first principles calculations as well as experiments. The simulation was started by using α-quartz with symmetry $P3_221$ consist of 24 quartz units (2x2x2 unit cell) with a time step of 30 a.u (0.72 fs). The size (72 atoms) is standard for first principles molecular

dynamics in nowadays. However, by using a parametrized potential, we are now able to study the system in several nano seconds. The "real" *ab initio* molecular dynamics is performed when the time scale is deemed not that important (say within several pico seconds) for comparisons.

We studied the quartz at different pressures from -10 to 10 GPa with interval 2 GPa and temperatures from 0 to 1650 K with interval 100 K, by using isothermal-isobaric ensemble (NPT). All the configurations were analyzed based on a 150 ps long MD trajectory. The longer time scale simulation was done because of the density convergence problem. We have also studied the convergence of our results in terms of the time scale and found that the density is only converged with a longer time scale simulation like 150 ps for the temperatures close to the α-β transition point, in the meanwhile, for the sample far from the transition point, a few ps would be fine to obtain a converged density.

For the calculation at 0K, we have also done first principles calculation by using VASP code [Hafner, 2008]. The primitive cell of quartz consists of 3 molecules SiO_2. Ultrasoft pseudopotential was used in all calculations and the exchange correlation treated by Perdew and Wang functional (PW91). The energy cut off 550 eV and the Monkhorst-Pack k-point 4x4x4 grid were used for the plane-wave basis set. The structure was optimized with the conjugate gradient method until the energy difference between two consecutive iterations below 0.04 eV. For the calculation at elevated temperatures, we have performed *ab initio* Car-Parrinello molecular dynamics calculations (CPMD) by using Quantum Espresso package [Giannozzi et al., 2009]. CPMD were executed by using NPT ensemble as what we did with TS potential, for 5 ps. Ultrasoft pseudopotential was used in all calculations and the exchange correlation treated by Perdew, Berke and Ernzerhof functional (PBE). The energy cut off 40 Ry. and Brillouin zone sampling restricted within Γ point were used for the plane-wave basis set. A fictitious electron mass of 200 a.u. and a time step of 6 a.u. were used for the integration of the ionic motions.

5.3 The α-β Quartz Transition at Different Pressure

The transition of α to β quartz was obtained by observing the slope changes of volume per unit cell response as function of temperature. As shown in Fig. 5.1, the volume increases with temperature until reach the transition point. The transition of α-β quartz was observed

around 800 K at ambient pressure (0 GPa), close to the transition temperature of experiment 846 K [Carpenter et al., 1998]. The other simulation using the same potential by Herzbach et al. (2005), the transition occurred at 712 K, which, on one side, might be dependent on the definition, and on the other hand, might stem from different calculation details, e.g. time scale they used (~30 ps). We have studied the symmetry for the averaged configuration within 150 ps, at elevated temperatures at 0 GPa. The symmetry is found to change at range 700-800 K, from $P3_221$ (α-quartz) to $P6_222$ (β-quartz).

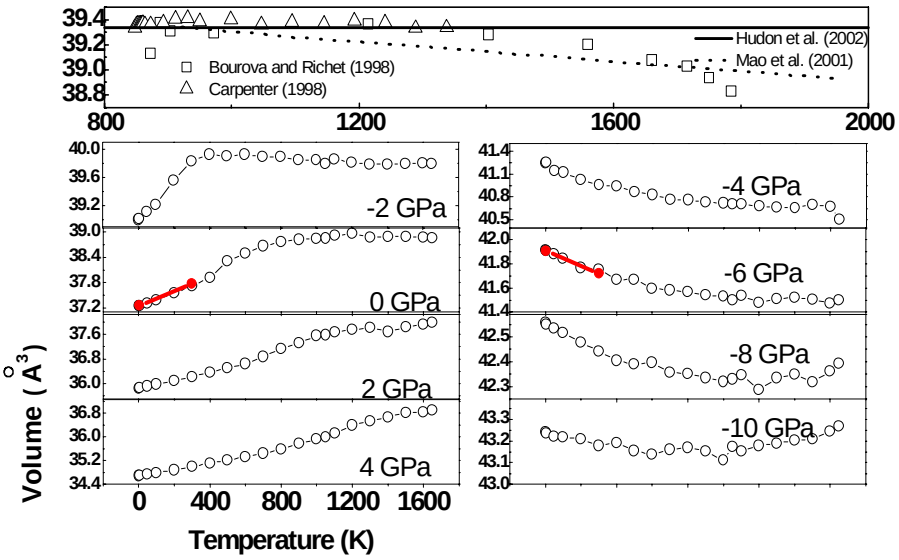

Fig. 5.1 The volume as function of temperature at -10 to 4 GPa with an interval 2 GPa. The experimental data are also included for comparisons. Experimentally, two different trends (negative thermal expansion [Bourova and Richet, 1998; Mao et al., 2001] or zero thermal expansion [Carpenter et al., 1998; Hudon et al., 2002]) have been reported for β-quartz. Interestingly, our simulation can "reproduce" two different trends at 0 GPa and –2 GPa, respectively. At –4GPa and even lower pressures a "pure" static β-phase is observed, which presents only negative thermal expansion starting from 0K to intermediate temperatures. The *ab initio* MD volumes are also shown in the corresponding panels of the figure. Generally the *ab initio* MD data is ~ 4-5% larger than those calculated from classical MD systematically and was rescaled to have the same volume at 5K for comparisons. Note: the trend and slope between *ab initio* MD and classical MD are the same.

The transition point is shifted depends on the applied pressure. If the positive pressure is applied, the transition goes to higher temperature. The opposite shifted was observed when the negative pressure is applied. The α-β transition was occurred at ~1200 K and ~1400 K when the 2 GPa and 4 GPa were applied to system, respectively. We detected no α-β transition was occurred at negative pressure, except at -2 GPa, which 400 K is indicated as the transition temperature. The symmetry of quartz at 0 K and pressure less than -2 GPa is $P6_222$ (β-quartz). It means the transition also can be induced by pressure. The detail of α-β transition pressure induced will be described in section 5.6.

5.4 The Negative (Zero) Thermal Expansion

The thermal expansion of material could be studied from the trend of volume when the material is heated up. The α-quartz is shown the positive thermal expansion as can be seen in Fig. 5.1. The same trend was observed at positive pressure, ambient pressure and -2 GPa. The lower pressures (less than -2 GPa) show different trends because quartz in these pressures have already in the β-phase. The positive thermal expansion of α-quartz in our result also observes in previous work [Jay, 1933; Ackermann and Sorrell, 1974].

The ambiguity of thermal properties in quartz is begun after the transition point. The different pressure yields different trend of thermal expansion. The constant volume after transition, namely zero thermal expansion, was observed at ambient pressure. The experimental result by Hudon et al. (2002) and Carpenter et al. (1998) support our result. Interestingly, we found negative thermal expansion at slightly negative pressure the same as Mao et al. and Bourova-Richet's works. In the experiment, slightly negative pressure might be related to the impurities of material. In order to gain more confidence on what we have found, we compare the results obtained from the classical MD to those obtained from *ab initio* MD at several selected temperature and pressure points. It is found that the trend and slope are the same, though *ab initio* MD has volume difference around 4-5% larger than classical (Fig. 5.1).

5.5 The Mechanism of Negative (Zero) Thermal Expansion of β-Quartz

We use the same approach which has done by Welche et al. (1998) and Kihara (2001) to explain the negative (zero) thermal expansion. They suggested that the Si-O bond length and bending of Si-O-Si gave contribution to the negative (zero) thermal expansion. Therefore, we investigate some structural parameter of quartz at every pressure and temperature as shown in Fig. 5.2. The range of temperature and pressure in this figure is similar to Fig. 5.1. First, we plotted the volume per unit cell as function of temperature in different pressure (Fig. 5.2(a)). This figure is similar to Fig. 5.1, which is act as the reference for the structural parameter of quartz. The distance of Si-Si (Fig. 5.2(b)) has the same trend as the volume-temperature curve. The bending angle Si-O-Si also shows the similar trend (Fig. 5.2(d)). We found different trend on Si-O bond length (Fig. 5.2(b)). In this figure, we observe the Si-O bond length always increase with temperature. Temperature seems does not have any effect on this bond length. Then, we only focused on Si-Si distance and Si-O-Si angle as the parameter to explain the negative (zero) thermal expansion.

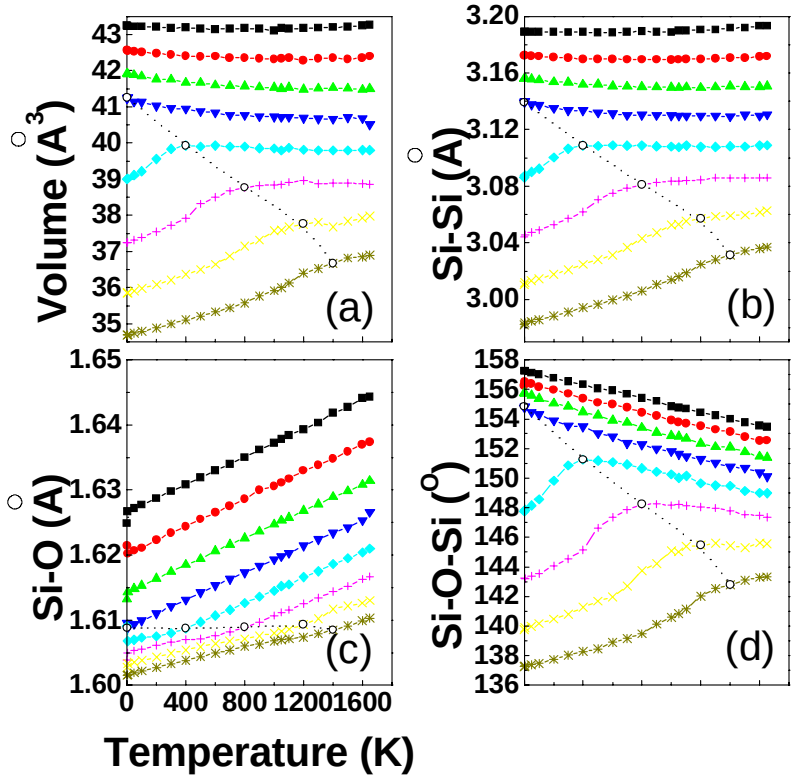

Fig. 5.2 a) Volume per SiO_2 unit, b) Si-Si bond length, c) Si-O bond length and d) Si-O-Si angle as a function of temperature at different pressures. Note: volume changes are tightly connected with varies of the Si-Si

distance, which mainly results from the changes of the Si-O-Si angle. A boundary between α and β phases is drawn according to the Si-O-Si angle and then used for all the panels. Apparently, the Si-O bond length of α phase reveals a weaker change than that of β phase with pressures, while Si-O-Si angle of α phase presents a stronger change than that of β phase with pressures.

The distance of Si-Si and bending angle Si-O-Si increases with temperature then decreases (constant) after the transition temperature. This trend exactly same with the volume-temperature curve. Due to this similarity, we propose the thermal expansion of quartz is driven by the change of Si-O-Si angle that indirectly affected distance of Si-Si, which is consistent with the previous findings [Levien et al., 1980; Bourova et al., 2000; Yamahara et al., 2001]. The calculations at negative pressure have, however, offered us a unique chance to investigate the β-quartz, which has separated the static structural origins from those reasons like dynamic disordering [Lakhstanov et al., 2007]. The contribution of Si-O-Si angle to the thermal expansion has observed in the previous work.

Recently, Huang and Kieffer (2005) suggest the 'repopulation' of α-state based on their simulation to explain the negative (zero) thermal expansion of quartz and cristobalite. The 'repopulation' of α-state is coming from the investigation of Si-O-Si bridge plane normal correlation [Huang and Kieffer, 2003; 2004; 2005]. We use the same idea to confirm the 'repopulation' α-state which is proposed by Huang and Kieffer. The two configurations were use as reference, i.e. configuration at 0 K in each pressure and 0 GPa 0 K.

For the first case, the reference phase is different in each pressure which illustrated in Fig. 5(a). At range of pressure -2 until 4 GPa, the reference phase is α-quartz, and we observe the rotating of plane at phase transition different in each pressure. For example at 0 GPa, the plane rotates ~60° when α-quartz transform to β-quartz. At negative pressure (-4 until -10 GPa), we cannot see the α β phase transition, since the reference has already in β-phase. Second case, we always use α-phase as reference (0 GPa and 0 K) for each pressure as shown in Fig. 5(b). Same as the first case the plane rotating different in each pressure, we also found the phase transition only observe at -2 until 4 GPa. The relation of plane normal correlation and pressure at 0 K has shown the plane rotate around 45° confirm with the previous work [Huang and Kieffer, 2005]. Transition occurred in negative pressure at range -2 until -6 GPa, same as the result that already

explained above. In the previous work by Huang and Kieffer, the negative thermal expansion of β-quartz related to 'repopulation' of α-states [Huang and Kieffer, 2005]. But our result did not show the plane normal back to 1, which means back to α-phase. In both cases, we observed quartz keeps in β-phase after transition.

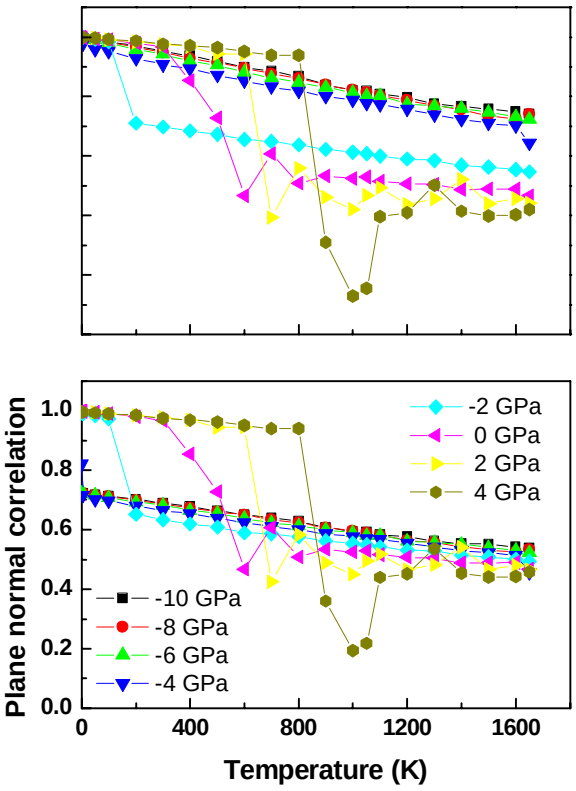

Fig. 5.3 The average plane normal correlation of quartz as a function of temperatures for two kinds of reference structure: the upper panel is at 0 K at each pressure, and the lower panel is at 0 GPa and 0 K. Note: the transition is only observed at pressures above -2 GPa, which indicates a "pure" static β-phase is retained at lower pressures.

5.6 The Bulk Modulus of Quartz

The phase transition is not only driven by temperature, pressure also can induce it, which supported by the curve of energy as function of volume taken from classical MD as shown in Fig. 5.4(a). At this figure, the curve of α-phase converges with β-phase at negative pressure,

which indicates at this pressure quartz in the same phase. Similar to the curves of bulk modulus α and β-phase at 0 K, which also converges at negative pressure, thus supported the transition induced by pressure. The Si-Si-Si distribution function at 0 K also supports our prediction. The α-quartz which has four peaks gradually reduced to three peaks which is the characteristic of β-quartz at negative pressure. The three peaks are not only similar quantitatively but also qualitatively same.

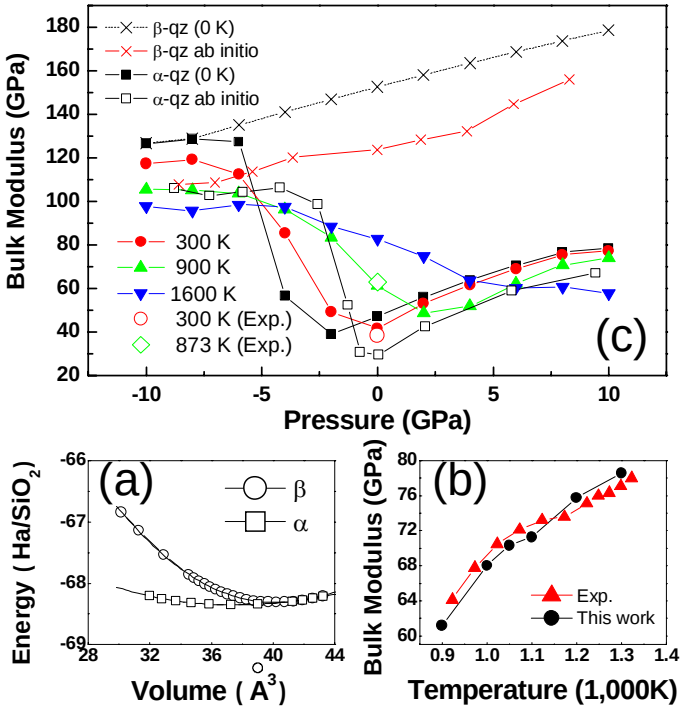

Fig. 5.4 The α-β transition induced by pressure. (a) The energy as a function of volume of α and β quartz, the two curves converge together at larger volumes. (b) The bulk modulus anomalous of quartz at high temperature. (c) Bulk Modulus of quartz at pressures ranged from -10 to 10 GPa at four different temperatures. The *ab initio* results are also included for comparisons. Note: the β quartz has higher bulk modulus than α-quartz and presents a "normal" softening with elevated temperatures. That the shift of α to β transition from low pressure (negative) to high pressure with the temperature increasing explains the β quartz at 873K (diamond) has a higher bulk modulus than α quartz (circle) at room temperature.

The anomalous of β-quartz bulk modulus can be seen in Fig. 5.4 (b), which increases with temperature. Our simulation is in a good agreement with experimental result [Lakhstanov et al., 2007]. The bulk modulus increases with temperature can be explained by the shift of the pressure-induced α-β transition at elevated temperature as shown in Fig. 5.4 (c).

Similar to thermal expansion properties, bulk modulus will have significant change at transition point. We selected some temperatures according to the phase that exist at that condition to learn more the α-β transition induced by pressure. Firstly, we choose 0 K as basic temperature for simulation work. In this temperature, the transition starts at -2 GPa and totally transform to β-quartz at -8 GPa, which proved by the hold of α and β-phase curves. At room temperature (300 K), the starting point of transition shifted to 0 GPa. The transition pressure cannot be observed clearly slightly above transition temperature (900 K), and getting unclear at higher temperature (1600 K). The decrease of bulk modulus caused by softening material can be seen at 0 GPa, the bulk modulus of quartz at 300 K lower than 0 K. We found bulk modulus of α-quartz at 0 and 300 K are 47.33 and 44.75 GPa, respectively. These values different from simulation by Keskar-Chelikowsky (1992) and experiment, which is 39 GPa and 34-37 GPa, respectively [Keskar and Chelikowsky, 1992; Demuth et al., 1999]. The anomalous observed at 900 K and 1600 K, in the same pressure (0 GPa) their bulk modulus higher than quartz at 0 K and 300 K. The bulk modulus of β-quartz measured by experiment at 873 K is 56.4 GPa, the closest condition of our calculation is 61.2 GPa occurred at 900 K.

5.7 The Mechanism of Bulk Modulus Anomaly of β-Quartz

The structural parameter may describe the mechanical properties anomaly as the explanation of negative (zero) thermal expansion previously. The anomalous of bulk modulus can be explained by the response of Si-O-Si angle and Si-O bond angle to temperature. In Fig. 5.2(c), the Si-O bond length change significant above the transition temperature when quartz exist in β-phase. In α-phase, the slope of Si-O bond length is not steep as β-phase. As we know, Si-O bond include to covalent bond type which is very strong, and required a lot of energy to change this parameter. Meanwhile, we observe the opposite trend in Si-O-Si angle. The significant change of Si-O-Si angle occurred before the transition point (Fig. 5.2(d)). We assume

bending of Si-O-Si angle easier than compression of Si-O bond length. The assumption implied to bulk modulus of α-quartz lower than β-quartz. Despite the previous explanation about anomalous of glass bulk modulus [Huang and Kieffer, 2004], we suggest the clear explanation of this problem from structural properties point of view.

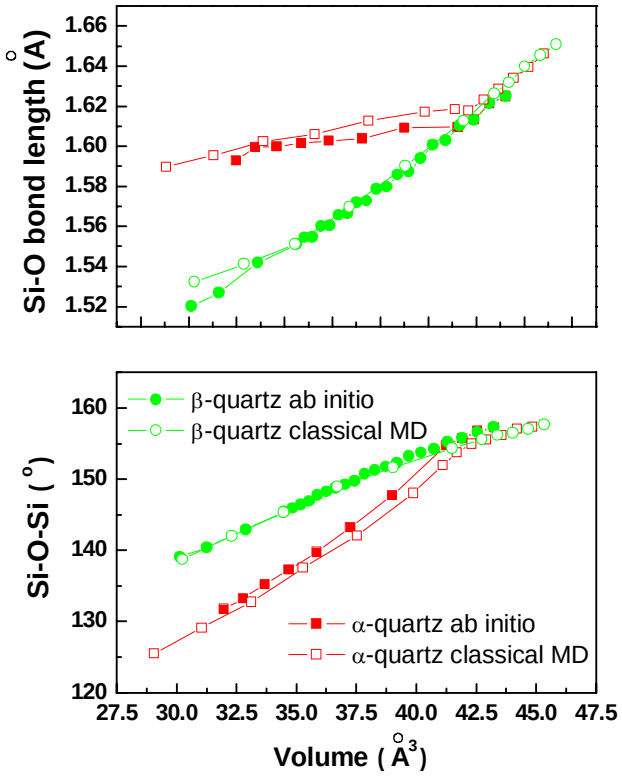

Fig. 5.5 Si-O bond length (upper panel), Si-O-Si angle (lower panel) as a function of volume from classical MD and *ab initio* calculations. Note: two phases converge together at larger volume. The α-quartz responses to pressure by the bending of Si-O-Si angle while β phase (responses to the pressure) through the compression of Si-O bond length. The harder Si-O bond than the Si-O-Si bond angle indicates a higher bulk modulus of β quartz than that of α quartz as shown in Fig. 5.4.

Beside the explanation of bulk modulus anomalous, the structure analysis of Si-O bond length and Si-O-Si angle as function of volume can prove the transition of quartz which driven by pressure. First, we analyzed Si-O bond length as function of volume (Fig. 5.5(a)) and founded

at larger volume (negative pressure), α and β-quartz curve converge. The same trend also observed in Fig. 4(b). In this figure, Si-O-Si angle of α and β has the same value at larger volume. *Ab initio* calculation and classical MD are showing good agreement. The same trend also observed in *ab initio* calculation by Demuth et al. (1999). The response of Si-O-Si to decreasing pressure same as increasing temperature, the angle tend to change significant in high pressure than low (negative) pressure. Meanwhile the opposite trends observed in Si-O bond length. These facts support our explanation about the anomalous of bulk modulus. Thus, the *ab initio* result analogous with classical MD.

5.8 Conclusion

During the last thirty years profound development in experimental techniques to measure high temperature and pressures and thermodynamic properties of minerals have occurred. But the different trend in result inhibit the systemized data base compilation which satisfies the constraints of calorimetric measurements, phase equilibrium data, measured thermophysical properties of a phase and heat capacities and entropies estimated from lattice vibrational models. We found both negative and zero thermal expansion in β-quartz which depends on the applied pressure. The zero thermal expansion occurred at 0 GPa, and the negative thermal expansion observed at slightly negative pressure. The thermal expansion can be described not necessary by the 'repopulation' of α-state, but we can explain it from structural response to temperature. From structural properties point of view, the thermal expansion analog with the changes of internal angle Si-O-Si and implied to Si-Si bond length. The negative thermal expansion of β-quartz means the decreasing of its Si-O-Si angle and Si-Si bond length. The bulk modulus anomalous of β-quartz also can be explained by structure parameter. In this case we obtained the Si-O-Si angle and Si-O bond as the key point of explanation. We noticed the bending of covalent bond Si-O in β-quartz harder than compression of internal angle Si-O-Si in α-quartz, which implied to the high bulk modulus of β-quartz. By careful adjustment of the chemical content, a zero expansion coefficient can be achieved within a desired temperature range.

References

Ackermann, R. J. and Sorrell, C. A. Thermal expansion and the high-low transformation in quartz. I. high-temperature X-ray studies. J. Appl. Cryst. **7**. 461-467 (1974).

Bourova, E. & Richet P. Quartz and cristobalite: high temperature cell parameters and volumes of fusion. Geophys. Res. Lett. **25**, 2333-2336 (1998).

Bourova, E. Parker, S. C. and Richet, P. Atomistic simulation of cristobalite at high temperature. Phys. Rev. B **62**. 12052-12061 (2000).

Carpenter, M. A., Salje, E. K. H., Graeme-Barber, A., Wruck, B., Dove, M. T., and Knight, K. S. Calibration of excess thermodynamic properties and elastic constant variations associated with the α↔β phase transition in quartz. Am. Mineral. **83,** 2-22 (1998).

Demuth, Th., Jeanvoine, Y., Hafner, J., and Ángyán, J. G. Polymorphism in silica studied in the local density and generalized-gradient approximations. J. Phys.: Condens. Matter. **11,** 3833-3874 (1999).

Dolino, G. The α-inc-β transitions of quartz, a century of research on the displacive phase transitions. Phase Transitions **21**, 59-72 (1990).

Giannozzi, P. et al. Quantum espresso: a modular and open source software project for quantum simulations of materials. J. Phys.: Condens. Matter. **21,** 395502 (2009).

Hafner, J. Ab initio simulations of materials using VASP: density-functional theory and beyond. J. Comp. Chem. **29,** 2044-2078 (2008).

Herzbach, D. Binder, K. Müser, M. H. Comparison of model potentials for molecular-dynamics simulations of silica. J. Chem. Phys. **123,** 124711 (2005).

Huang, L. and Kieffer, J. Amorphous-amorphous transitions in silica glass. I. reversible transitions and thermomechanical anomalies. Phys. Rev. B **69,** 224203 (2004).

Huang, L. and Kieffer, J. Molecular dynamics study of cristobalite silica using a charge transfer three-body potential: phase transformation and structural disorder. J. Chem. Phys. **118,** 1487-1498 (2003).

Huang, L. and Kieffer, J. Structural origin of negative thermal expansion in high-temperature silica polymorphs. Phys. Rev. Lett. **95**, 215901 (2005).

Hudon, P. Jung, I-H. and Baker, D. R. Melting of β-quartz up to 2.0 GPa and thermodynamic optimization of the silica liquids up to 6.0 GPa. Phys. Earth. Planet. Interiors **130**, 159-174 (2002).

Jay, A. H. The thermal expansion of quartz by X-ray measurements. Proc. Royal Soc. London **142,** 237-247 (1933).

Kammer, E. W. and Atanasoff, J. V. A determination of the elastic constans of beta-quartz. Phys. Rev. **62**, 395-400 (1942).

Keskar, N. R. and Chelikowsky, J. R. Structural properties of nine silica polymophs. Phys. Rev. B **46,** 1-13 (1992).

Kihara, K. An X-ray study of the temperature dependence of the quartz structure. Eur. J. Mineral **2**, 63-77 (1990)

Kihara, K. Thermal expansion in quartz: a geometrical consideration. J. Mineral. Petrol. Sci. **96,** 159-163 (2001).

Kimizuka, H., Kaburaki, H. and Kogure, Y. Molecular dynamics study of the high-temperature elasticity of quartz above the α-β phase transitions. Phys. Rev. B **67**, 024105 (2003).

Kirchner, H. P. The thermal expansion of ceramic crystals. Progress in Solid in Solid State Chemistry, Macmillan, New York (1964).

Lakshtanov, D. L. Sinogeikin, S. V. and Bass, J. D. High-temperature phase transitions and elasticity of silica polymorphs. Phys. Chem. Minerals **34,** 11-22 (2007).

Levien, L. Prewitt, C. and Weidner, D. J. Structure and elastic properties of quartz at pressure. Am. Mineral. **65,** 920-930 (1980).

Mao H., Sundman, B., Wang, Z., and Saxena, S. K. Volumetric properties and phase relations of silica-thermodynamics assessment. J. Alloys Compd. **327**, 253-262 (2001).

Mechie, J. Sobolev, S. V., Ratschbacher, L., Babeyko, A. Y., Bock, G., Jones, A. G., Nelson, K. D., Solon, K. D., Brown, L. D., and Zhao, W. Precise temperature estimationin the Tibetan crust from seismic detection of the α-β transition. Geology **32**, 601-604 (2004).

Ohno, I. Harada, K. and Yoshitomi, C. Temperature variation of elastic constants of quartz across the α-β transition. Phys. Chem. Minerals **33,** 1-9 (2006).

Roy, R., Agrawal, D. K. and McKinstry, H. A. Very low thermal expansion coefficient materials. Annu. Rev. Mat. Sci. **19**, 59-81 (1989).

Spearing, D. R., Farnan, I. and Stebbins, J. F. Dynamics of the α-β phase transitions in quartz and cristobalite as observed by in-situ high temperature ^{29}Si and ^{17}O NMR. Phys Chem Minerals **19,** 307-321 (1992).

Takada, A., Richet, P., Catlow, C. R. A., and Price, G. D. Molecular dynamics simulation of temperature-induced structural changes in cristobalite, coesite and amorphous silica. J. Non-Cryst. Solids **354,** 181-187 (2008).

Tangney, P. and Scandolo, S. An *ab initio* parametrized interatomic force field for silica. J. Chem. Phys. **117,** 8898-8904 (2002).

Tsuneyuki, S., Aoki, H., Tsukada, M., and Matsui, Y. Molecular-dynamics study of the α to β structural transition of quartz. Phys. Rev. Lett. **64,** 776-779 (1990).

Welche, P. R. L., Heine, V. and Dove, M. T. Negative thermal expansion in beta-quartz. Phys. Chem. Minerals **26,** 63-77 (1998).

Wright, A. F. and Lehmann, M. S. The structure of quartz at 25 and 590°C determined by neutron diffraction. J. Solid State Chemistry. **36**, 371-380 (1981).

Yamahara, K., Okazaki, K. and Kawamura, K. Molecular dynamics study of the thermal behavior of silica glass/melt and cristobalite. Journal of Non-Crystalline Solids **291,** 32-42 (2001).

CHAPTER 6

Summary and Future Research

6.1 Summary

In this work, we present the application of molecular dynamics in order to study more detail about the structure and properties of quartz, which is of essential importance in (Nano-) geosciences. Though many experiments and simulations have been done, some long-standing problems still remain open. Here, we have mainly focused on three aspects, i.e. the interaction of idealized quartz surfaces with heptane and toluene, the investigation of quartz surface structure in aqueous and non-aqueous environment, and the structure and properties of quartz on elevated temperature. The first principles and classical molecular dynamics were employed dependent on the system studied.

The simulation of heptane and toluene on top of hydrophilic and hydrophobic quartz surface brought important information in understanding the interfacial structure. It was found that the interfacial structure, as obtained from our simulation studies, can complement the modern sum frequency generation spectra interpretation. In details, our simulation has shown that heptane mostly lie flat and perpendicular in the first and second sub-layer, respectively. The orientation of toluene, which is perpendicular to the quartz surface with a tilted angle ~25° as detected in the experiment, was found to be located in the second sub layer. The presence of methyl group in toluene molecule has generated the asymmetric pattern of orientation with methyl group pointed away from the quartz surface. The weak hydrogen bond that occurred in the hydrophilic system same as simulation in the oil-water interface has become the driving force of toluene strongly adsorbed on quartz surface. Furthermore, only first sub-layer of toluene has weak hydrogen bond with hydrophilic quartz surface.

While quartz surface usually represented as idealized surface whatever perfectly hydrophilic or hydrophobic as shown above, could be used in order to study the effect of the polarity of quartz surface (as discussed in Chapter 3). However, the surface of quartz is not always ideal. In Chapter 4, the result of reaction between fresh quartz surface and liquid water

was simulated in order to investigate the quartz surface structure in aqueous environment, which has not yet to be fully available by experimental tools. In order to study the effects of different initial configurations, two fresh quartz surfaces were presented. The final configuration for both surfaces was dominated by silanol groups. Some defects that detected in experiment has also been observed, such as peroxy link, peroxy group, siloxane bridge, Si-O radical and Si radical. The higher initial enthalpy of one of quartz surface has indicated influence its complexity. Moreover, the environment of fresh quartz surface also determined the final structure. In addition, molecular dynamics of fresh quartz surface in non-aqueous environment (in methane) has shown that the siloxane bridge is dominant on the quartz surface. In short, we have been able to show the variety of quartz surface, which depends on the initial structure and environment.

In Chapter 5, the study of quartz structure at different temperatures and pressures was presented. We have confirmed the positive thermal expansion of α-quartz. Interestingly, we observed the negative and zero thermal expansion after the transition point at different pressures. At the ambient pressure or higher, we found the zero thermal expansion of β-quartz. Meanwhile, the negative thermal expansion can be found at tensile pressure. From structural point of view, the thermal expansion analog with the changes of internal angle Si-O-Si and is tightly connected to Si-Si bond length, namely, the negative thermal expansion of β-quartz can be explained by the decreasing of its Si-O-Si angle and Si-Si bond length. The bulk modulus anomalies of β-quartz can also be explained by structure parameters including the Si-O-Si angle and Si-O bond. For α-quartz, the response to pressure by bending of Si-O-Si angle, while for β-quartz, this response is through the compression of Si-O bond length. The harder Si-O bond compared with the Si-O-Si bond angle would implicitly explain the high bulk modulus of the β-quartz.

6.2 Future Research

There are several developments that can be done in the future based on our findings. First, the interaction of quartz surface-hydrocarbon can be developed by replacing the heptane and toluene to other heavier hydrocarbons such as asphaltene or the crude oil model. The adsorption of hydrocarbon molecules can change the wettability of quartz surface, which is of essential importance, for oil production from natural reservoirs or non-aqueous bitumen

extraction technologies for oil sands, in petroleum engineering. The presence of water molecules also should be included. Second, the final structure of quartz surface, which is built from the reaction of fresh quartz surface and liquid water, needs to be extended to a larger system for different surfaces. This new reconstructed surface can be the alternative model to learn the adsorption phenomena as we studied in Chapter 3. Third, the investigation of thermal and mechanical properties of quartz can be expanded to larger system to directly simulating the crack induced by temperature gradient and by including the aqueous environments.